THE UNIVERSITY OF CHICAGO

INACTIVATION AT THE SELECTIVITY FILTER OF A POTASSIUM CHANNEL

A DISSERTATION SUBMITTED TO

THE FACULTY OF THE DIVISION OF THE BIOLOGICAL SCIENCES

AND THE PRITZKER SCHOOL OF MEDICINE

IN CANDIDACY FOR THE DEGREE OF

DOCTOR OF PHILOSOPHY

COMMITTEE ON COMPUTATIONAL NEUROSCIENCE

BY

JARED L. OSTMEYER

CHICAGO, ILLINOIS

MARCH 2016

Without the people around me I can accomplish nothing.

TABLE OF CONTENTS

LIST OF FIGURES

LIST OF TABLES

ACKNOWLEDGEMENTS

I owe a special thanks to my mentor Dr. Benoît Roux. He took the time to personally teach me the methodology, but was wise enough to let me move the research in my own direction. We discussed my research nearly everyday, sometimes walking home from campus. He kept me motivated. I do not think I would have completed graduate school if it was not for him.

I also want to thank the remaining members on my thesis committee. First, I want to thank Dr. Deborah Nelson for providing me with her invaluable council. I see her as a voice of reason. Next, I thank Dr. Francisco Bezanilla and Dr. William Green for their contributions.

I owe a great deal of credit to the members of the Roux lab. Sometimes we cannot understand just how silly our own ideas are. Dr. Christopher Rowley, Dr. David Medovoy, and Dr. Mikolai Fajer served as a sounding board. I appreciate their time and energy in critiquing my ideas and my work. That said, I sought the assistance of every person in the lab over the course of my PhD, and I always received the help I requested.

I need to acknowledge the help I received from other laboratories. I especially need to thank Dr. Eduardo Perozo and his lab members. In particular, I need to thank Dr. Raymond Hulse and Christina Palka for their help in arranging the experiments described in Chapter 2. I also need to thank my collaborators in the laboratories of Dr. Sudha Chakrapani and Dr. Marc Baldus.

Finally, I want to acknowledge the support I received from my family. I want to thank my wife for staying with me as I completed my PhD, even when we were forced to live in different cities, and I want to thank my parents for culturing my sense of curiosity.

ABSTRACT

Potassium channels have been called Nature's transistors and diodes. These tetrameric membrane proteins act as control valves that regulate the flux of K^+ ions crossing the lipid bilayer of a cell. Sometimes the electrical signals generated by an open potassium channel will mysteriously terminate, a process that has been named inactivation. Several distinct mechanisms can underlie the loss of current, one of them being a conformational change in a part of the channel called the selectivity filter. Once the selectivity filter has become inactivated, the block will remain present for a prolonged period of time that can last for tens of seconds.

X-ray crystallographic structures of the bacterial channel KcsA have revealed both conductive and non-conductive conformations of the selectivity filter, the latter of which have been speculated to represent the inactivated state. However, only a slight $\sim$1 Å pinching motion at the center of the selectivity filter occurs in the non-conductive structures, raising the question of how such a small conformational change can explain the long timescales associated with inactivation. Using Molecular Dynamics simulations, it has been discovered that water molecules may become buried behind the selectivity filter locking the filter in the non-conductive conformation. Only when all the water molecules leave may the selectivity filter return to a conductive state. Because it would be an extremely rare event for all the buried water molecules to leave and not return, the non-conductive conformation is expected to persist for a lengthy period of time on par with that of inactivation.

To claim that the non-conductive conformation represents the inactivated state, it is necessary to recreate the conditions that favor inactivation. Two factors that destabilize the conductive selectivity filter and promote inactivation are (i) simply holding the channel open or (ii) decreasing the extracellular potassium concentration. Under either of these conditions, Molecular Dynamic simulations starting with the selectivity filter in a conductive conformation reveal it making a transition to the non-conductive state. In contrast, the selectivity filter remains conductive when the conditions are absent. Water molecules penetrating behind the selectivity filter appear to catalyze the transition. Before each spontaneous transition water molecules enter the protein behind the filter. Removing the water molecules causes the filter to immediately return to a conductive conformation.

The results reinforce the view that the non-conductive conformation of the selectivity filter represents the inactivated state and highlights the role that water molecules throughout the inactivation process.

CHAPTER 1
INTRODUCTION AND BACKGROUND

1.1 Abstract

Potassium channels play vital roles in virtually every organism on the planet from the smallest microbes to the most advanced of species [1]. The primary function of a potassium channels is to provide a passageway for K^+ ions to permeate through the cell membrane, which would otherwise be impossible for the ions to cross. The task of regulating K^+ flux across the cell membrane has placed potassium channels at the center stage of life: They have evolved to play integral roles in many cellular and physiological processes. The fact that their basic function and structure has remained the same across the tree of life testifies to their importance in living systems.

1.2 Motivation: Potassium Channel Diseases

Because they play a central role in many physiological processes, the ability of potassium channels to function properly is essential to human health. Over 80 different genes encode for potassium channels in humans, and a mutation to any one of these genes can presumably cause disease. Potassium channels are expressed throughout the Human body, and not just in the nervous system, so it is sometimes surprising which organs are effected by a potassium channel mutation. Several diseases will be listed below that afflict tissues located in the nervous system, heart, kidney, pancreas, and immune system. Each disease being the result of a mutation can be inherited. Although the list is far from complete, it illustrates what can happen when potassium channels malfunction.

Of all the diseases that afflict the nervous system, epilepsy is perhaps the most common and dramatic. About 1% of the world's population suffers from this disorder. The loss of motor control and consciousness during a seizure are believed to happen when neurons become over excited and begin firing in lock-step synchrony. While many different factors have been found that can lead to the disease, potassium channel mutations have been identified as the root problem in specific cases. For example, a case study found that specific point-mutations

in the potassium channel genes KCNQ2 (K_v 7.2) or KCNQ3 (K_v 7.3) were responsible for a form of inherited neonatal epilepsy [2, 3]. Because potassium channels regulate neuron excitability (see next section), it is not surprising that these channels play a role in epilepsy.

Episodic Ataxia is another disease that can be caused by mutations to potassium channels. The disease is characterized by a loss of voluntary motor control that may be accompanied by uncontrolled continuous muscle spasms. The primary variant of the disease, Type-1 Episodic Ataxia, has been linked to mutations on the gene KCNA1 that encodes for the potassium channel K_v 1.1 [4]. The disease first starts in adolescence and continues on through adulthood with attacks occurring during situations of duress. Although there is no cure, a small number of patients with Type-1 Episodic Ataxia respond well to acetazolamide and other drug options.

Several other neurological diseases have been linked to aberrant potassium channel behavior. It has been shown, for example, that mutations in the potassium channel gene KCNQ4 (K_v 7.4) can result in hearing loss [5]. The list of neurological disorders linked to ion channel mutations is long, but the role that potassium channels play in these types of diseases is clear.

Potassium channel mutations effecting the heart are perhaps the best studied. A repertoire of various ion channels must fire in a coordinated harmony to create the cardiac Action Potential, which should ideally last for several hundred milliseconds. Channels that open too early or to late can lead to a dangerous heart arrhythmia. Long-QT syndrome is one such example. The disease is characterized by a delayed ventricular repolarization of the heart, which can lead to sudden death. Mutations in the potassium channel genes KCNQ1 (K_v 7.1), KCNH2 (hERG), KCNJ2 (K_{ir} 2.1), KCNE1 (β-subunit), and KCNE2 (β-subunit), all of which are expressed in the heart, have been firmly linked to the disease [6]. A related disorder, Short QT syndrome, is also caused by mutations in many of the same genes [6]. The disease is characterized by spells of unexplained fainting and collapsing due to a shortening of the repolarization cycle in the ventricle.

Potassium channels are expressed in nearly every tissue of the body where they are responsible for several unrelated diseases. For example, the potassium channel gene KCNJ1 is expressed in the kidney and a mutation in the gene can result in a disease called Bartter's syndrome. The disease is characterized by metabolic acidosis (acidification of the body), hypokalemia (low potassium), and a need to urinate frequently [7]. Treatment options are limited and include trying to manage pH and K^+ levels in the bloodstream. Another example

of a potassium channel disease outside the heart and nervous system is a specific form of inherited hyperinsulinism caused by a malfunction in the K_{ATP} channel [8]. Normally these channels would close in response to ATP binding, which is the first step in a signal cascade that regulates the release of insulin from pancreatic β-cells. However, mutations have been identified that offset the channel's activity, causing an over-release of insulin. Depending on the severity of the disease, epilepsy and brain damage can ensue as a result. Many options exists for managing the disease, including removing a fraction of the insulin producing cells from the pancreas.

Potassium channels have been incorporated into signal pathways without any obvious reason as to why. The potassium channel $\mathrm{K_v}$ 1.3 is expressed on memory T-cells [9] where it is part of a signal cascade that regulates the immune response. Blocking the channel is expected to suppress T-cell activity at sites of inflammation providing a mechanism for dialing down the strength of the immune response. Such a treatment could in theory stop the progression of autoimmune disorders such as multiple sclerosis, rheumatoid arthritis, and possibly even type-1 diabetes by selectively turning off memory T-cells while leaving the rest of the immune system intact to fight off commonly occurring infections [10]. Although such a treatment sounds promising, it is unclear why potassium channels make up part of the immune system at all.

Clearly potassium channels play vital roles in many physiological processes in the human body. Although their malfunction underlies a variety of diseases, the channels are fortunately a promising drug target. This is because potassium channels are expressed on the cell surface, allowing drugs circulating in the bloodstream to reach the channels without having to permeate through the cell membrane. The goal of developing new ways to treat disease provides the motivation to better understand how these proteins work. But to understand potassium channels we must first understand the environment in which they function.

1.3 Background

1.3.1 Basic Membrane Electrochemistry

The movement of current through any channel is entirely passive—the protein simply behaves like a kitchen faucet that opens and closes. Once activated, current will rush through the channel because of a charge/concentration imbalance between the two sides of the membrane.

Table 1.1: Equilibrium values for Nernst equation

Ion Type	Intracellular Concentration	Extracellular Concentration	Reversal Potential
K^+	150mM	4mM	E_K = -96.81 mV
Na^+	15mM	145mM	E_{Na} = +60.60 mV
Ca^{2+}	0.07nM	2mM	E_{Ca} = +137.04 mV
Cl^-	10mM	110mM	E_{Cl} = -64.05mV

The direction and magnitude of the driving potential behind an ionic current is the difference between the membrane voltage and the reversal potential.

$$E_{\text{drive}} = E_{\text{mem}} - E_{\text{ion}} \tag{1.1}$$

When the membrane voltage, E_{mem}, exceeds the reversal potential, E_{ion}, current will flow out of the cell, while the opposite will happen if the membrane voltage somehow manages to fall below the reversal potential. Each type of ion will have a different reversal potential, so the diving force will not necessarily the same in each case. To determine E_{drive}, the value for E_{mem} can be measured in advance, while the value for the reversal potential of an ion can be calculated from the Nernst equation.

$$\begin{aligned} E_{\text{ion}} = \frac{RT}{zF} ln \frac{[K^+]_o}{[K^+]_i} \quad &\text{where} \\ R &= \text{Universal Gas Constant}, \\ T &= \text{Absolute Temperature}, \\ F &= \text{Faraday's Constant}, \\ z &= \text{Ion Valence} \end{aligned} \tag{1.2}$$

Notice that the reversal potential is proportional to the log ratio of the extracellular concentration of the ion over its intracellular concentration. For K^+ ions, the intracellular concentration is usually much higher, giving rise to a negative reversal potential. See Table 1.1 for typical values used in the Nernst equation.

Potassium channels have a strong influence on the steady state value of the membrane voltage. The default value, called the resting potential, is kept low by a continuous leak of potassium current [11]. Two-pore-domain potassium channels, constantly letting a small

number of K^+ ions pass through, drag the membrane voltage down until E_{drive} approaches zero, at which point the electrochemical gradient driving the current diminishes. Other types of ion channels and membrane proteins influence the resting potential, but because these channels are not constitutively open like the two-pore domain channels their contributions are smaller by comparison. If the membrane potential becomes disturbed, opening additional potassium channels will encourage the membrane voltage to return back to the resting value. A rise in the membrane voltage is called a depolarization, while a decrease in the potential is called a hyperpolarization.

The membranes of excitable cells such as neurons and myocytes undergo large, brief swings in membrane voltage called an Action Potential (AP). An AP is started when the membrane potential rises above a specific threshold value, at which point voltage-gated sodium channels respond by opening. The flux of ions drives the membrane voltage to shoot upward towards the reversal potential of sodium, E_{Na} (See Table 1.1). The potential is reset back to the resting value, a process called repolarization, once voltage-gated potassium channels respond, which terminate the spike. An AP will propagate across the surface of a cell, with each patch of membrane exciting neighboring patches like one domino knocking over another, until the signal has propagated across the entire cell body. An AP will never backtrack because once voltage-gated channels open they enter into a refractory period due to ion channel inactivation. Only after a sufficient amount of time has passed can the channels respond again.

1.3.2 Functional Behavior

Decades before the first ion channels were purified [12] and before any structural data became available, electrophysiologist had already developed an understanding of the protein's functional behavior [13]. By studying the electrical signals generated by the current flowing through an ion channel, scientists managed to narrow down what types of ions could pass through, what stimuli would trigger the protein to open, and how long it could remain in a conductive state. From this data, it became possible to predict the electrical output of a channel based on the external conditions around the protein. The channels were effectively treated as a black-box because the chemical interactions underlying molecular processes of the protein remained unknown. Although the electrical signals only revealed information about the protein's behavior, the knowledge proved useful in understanding many physio-

logical processes of the Human body.

Intracellular recordings provided a first peek at the electrical signals passing through ion channels. In a series of landmark studies published during the early 1950s, Hodgkin and Huxley showed how to record populations of ion channels moving from closed to open states in response to a gating stimuli [14, 13]. In addition to these two states, specific ion channels were also found to inactivate, which is a process where the channels enter into a non-conductive state even in the presence of an activating stimuli. By measuring the transition rates between various states, detailed mathematical models were developed that accurately captured the dynamic behavior of excitable membranes. To this day, only a handful of systems in biology can be described with the same level of mathematical precision (in the opinion of this author).

Intracellular recordings only measure the macroscopic activity of ion channel populations. The invention of single channel recordings brought about a more refined understanding of ion channel behavior. The methodology, introduced by Neher and Sakmann during the late 70s and early 80s, allowed for the first single molecule study of any kind [15]. Individual transitions between states appeared as a sudden change in the current traces. The data revealed that a single channel would spontaneously fluctuate between open and non-conductive states, favoring open conformations in the presence of an activating stimuli. The recordings beautifully demonstrated the stochastic nature of ion channel behavior—the protein could be seen visiting different states randomly according to probabilities that depend on the external conditions.

Recordings can also be used to determine a channel's permeability to different ions. The relative permeabilities of several different ions—$Tl^+ > K^+ > Rb^+ > NH_4^+$—appears to be the same in almost every potassium channel [16]. Because the ranking of ion permeabilities is conserved, it would seem unlikely that the rate liming step in ion conduction, which is highly variable, has anything to do with the mechanism of selectivity.

1.3.3 Structural Details

The core of a typical potassium channel is made up of four subunits arranged symmetrically around the permeation pathway. Little more was known about their structure until the first potassium channels were purified, which finally allowed for a determination of the protein's secondary structure. The secondary structure of the core domain contains two transmem-

brane α-helical segments that span the lipid bilayer connected together by a re-entrant loop that was named the pore region (Fig. 1.1a) [16]. The pore region contains the selectivity filter and a small α-helical segment called the pore-helix. In addition to these segments, many potassium channels are also decorated with additional transmembrane α-helical segments or form complexes with auxiliary subunits that regulate their behavior. For example, the voltage-gated potassium channels contain four additional transmembrane segments per subunit that form the voltage sensors [16]. When the membrane potential becomes depolarized, the voltage sensors respond by applying a mechanical stress that drives the channel to open.

Figure 1.1b shows a sequence alignment of several potassium channels along their core domain, revealing the degree of similarity between them. The sequence identity between the voltage-gated channels in the Human nervous system and the bacterial channel KcsA, found in the microbe Streptomyces lividans, is greater than 70% at the pore region. The selectivity filter region is even more conserved, forming a consensus sequence—TXXTXGYGD, where X is any residue—that has been used to identify whether or not a novel protein belongs to the potassium channel family. The degree of similarity between the voltage-gated potassium channels at the pore domain suggests that it is possible to draw generalizations about the protein family as a whole whenever appropriate.

At the turn of the millennium, the MacKinnon lab published a series of X-ray crystallographic structures of the bacterial channel KcsA, providing the first high resolution structural data of a potassium channel (Fig. 1.2a) [17]. This was a landmark achievement not only because crystallizing membrane proteins is fraught with difficulty, but also because very little structural data had existed to compliment the electrical signals recorded from potassium channels. Although the activation gate of the channel was closed, scientist could still infer the ion permeation pathway. It was clear that K^+ ions crossing the membrane from the intracellular side would have to pass through the activation gate of the channel before entering into a large aqueous cavity, where they would have to dehydrate to squeeze through the selectivity filter. Once through the filter, the ions could then reach the extracellular side of the membrane. The permeation pathway was confirmed after structures of open potassium channels were published [18], including some of KcsA that complimented the closed structures (Fig. 1.2b) [19, 20].

The open and closed structures of KcsA reveal the conformational change that occurs at the activation gate. When the channel is closed, the transmembrane α-helices from the four

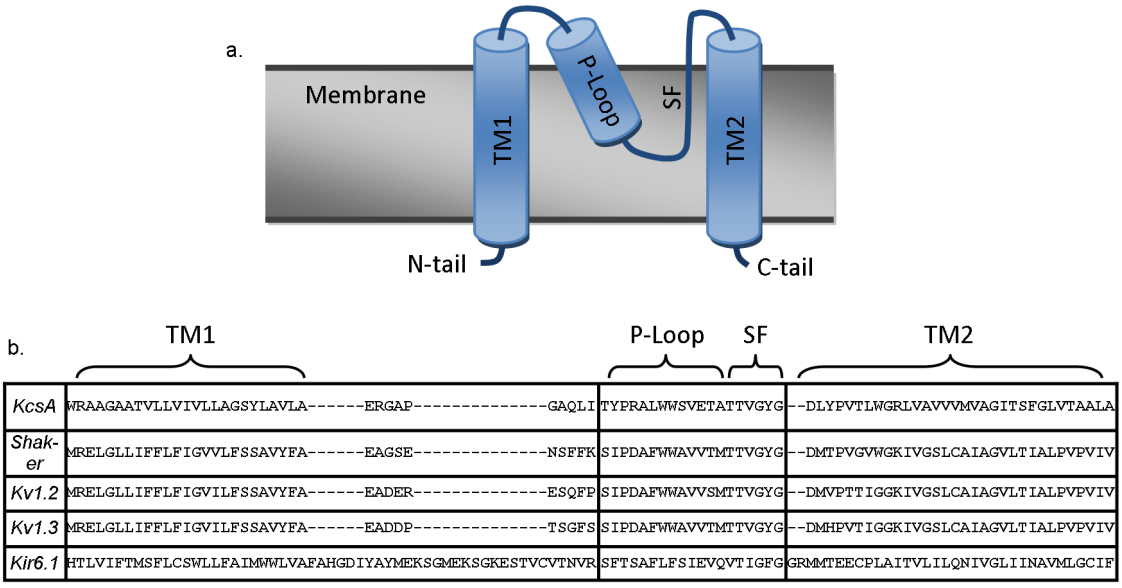

Figure 1.1: a, Secondary structure of a potassium channel subunit along the central core domain. The first and second transmembrane α-helices (TM1 and TM2, respectively) are connected together by the pore region, which includes the P-loop and selectivity filter (SF). b, Amino acid sequence alignment of several potassium channels along the central core domain. Notice that Shaker and the other K_v channels are the same length as the bacterial channel KcsA, indicating that the structure of the protein follows the same basic template. The K_{ATP} channel K_{ir} 6.1 was included because its sequence differs from that of the K_v channels.

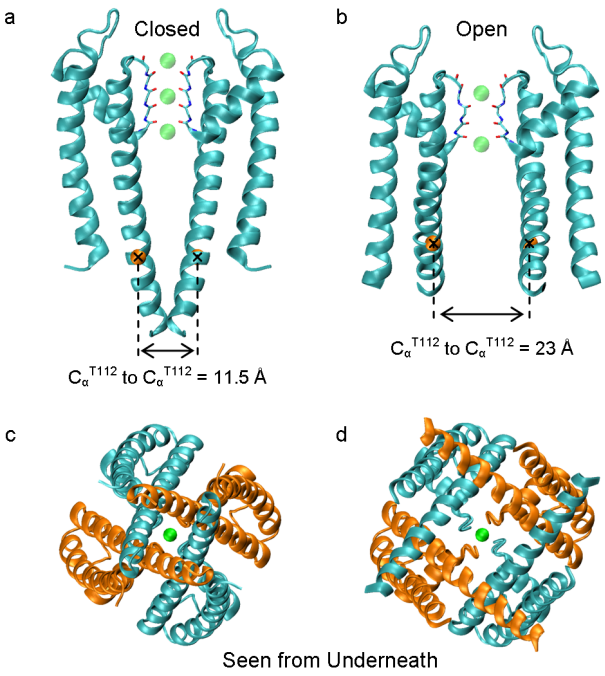

Figure 1.2: a, Representation of the left and right subunits of KcsA with the activation gate closed generated from the X-ray crystallographic structure 1K4C. b, The distance between C_α atoms of residue T112 is larger when the activation gate is open, as revealed by the X-ray crystallographic structure 3F7V (Right, helical ends modeled). c, View of all four subunits of the closed channel seen from the intracellular side. The innermost α-helical segments cross like poles on a tepee. d, The α-helical segments splay outward in the open channel allowing K^+ ions into the intracellular vestibule of the channel.

subunits cross at the intracellular side of the membrane like poles crossing at the top of a tepee, effectively blocking the permeation pathway (Fig. 1.2c). The same transmembrane segments splay outward in the open conformation to allow ions through the channel (Fig. 1.2d). Such a large conformational rearrangement is permitted because a conserved glycine residue (position 104 in KcsA) allows the innermost α-helix to bend when the channel opens [21]. Just how much the protein can open depends on the type of channel and any modifications made to it. For example, in the open structures of KcsA, the protein was truncated to keep only the core domain, which may have allowed the channel to open to a greater extent than it normally could [22].

At the heart of the channel lies the selectivity filter, which is the part of the protein that controls what ions may permeate across the membrane (Fig. 1.3a). Each of the four subunits contribute to one side of the filter, creating a narrow tunnel that allows K^+ ions to pass through in a single file. Carbonyl oxygen atoms from the backbone of the protein

line the entire passageway acting as surrogate water molecules for the ions. Eight carbonyl oxygen atoms work together to coordinate with one K^+ ion, creating a cage around it. The carbonyl oxygen atoms form a series of binding sites that allow K^+ ions to hop from one site to the next on their way through the filter [23]. Starting from the intracellular side, the four major binding sites are labeled S4 through S1. An additional binding site labeled S0 lies at the extracellular mouth of the channel, but the carbonyl oxygen atoms of the protein backbone do not form a full cage around the ion at this site.

The selectivity filter, while being the most conserved part of the channel, is the oddest feature of the protein. Although the filter lacks any secondary structure being neither an α-helix nor a β-sheet, it cannot be classified as a random coil because it clearly has a well defined shape. The backbone atoms of the selectivity filter, after making a sharp turn off the pore-helix, follow a line that points straight toward the extracellular side of the membrane (Fig. 1.3a). Normally the C_β atoms would prevent the backbone of the protein from lying in a straight line, but every other amino acid in the selectivity filter is a glycine residue, which lacks a C_β atom. It has been suggested that such unique structural constraints explain why the amino acid sequence of the selectivity filter is highly conserved [24].

Two conformations of the selectivity filter have been observed in crystal structures of wild-type KcsA. The first set of structures revealed the selectivity filter in a conductive conformation with K^+ ions appearing in every binding position from S0 through S4 (Fig. 1.3a) [17, 23]. Ions could clearly permeate through the filter by hoping from the one binding site to the next one. An alternative conformation was obtained by soaking K^+ ions out of the crystal structures using Na^+ (Fig. 1.3b) [23]. The new structure revealed that the selectivity filter had collapsed shut at the central glycine residues (position 77 in KcsA) leaving the selectivity filter too narrow for K^+ ions to fit in positions S2 or S3. The constricted state of the selectivity filter, which is sometimes referred to as the pinched conformation, appeared again in structures of KcsA with its activation gate open [19, 20]. The significance of this observation will be discussed later.

1.3.4 Dynamics of Inactivation

In all potassium channels that exhibit inactivation, current flowing through the channels will begin to taper off as soon as the protein opens. Ultimately, a conformational transition in the open channels underlies the loss of current. The only way to restore the proteins

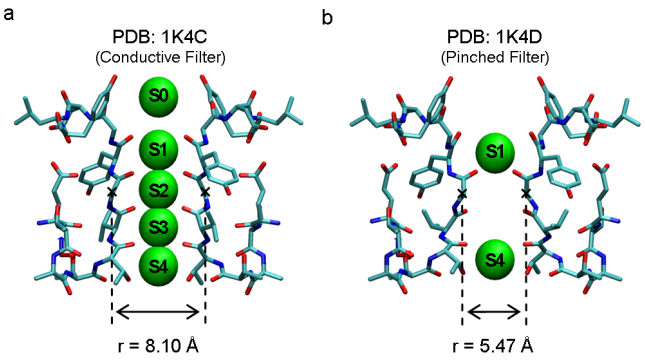

Figure 1.3: a, The conductive conformation of the selectivity filter. Potassium ions (green) coordinated by carbonyl oxygen atoms (red). Ions can permeate through the selectivity filter by hoping through the binding sites labeled S4 through S0, although the ions are expected to be separated by water molecules as they pass through in single file. Notice how the backbone atoms of the filter form a straight line. b, The pinched conformation of the selectivity filter obtained by soaking K^+ ions out of the crystal structure. Notice that the selectivity filter has collapsed to a non-conductive state. No ions in the crystal structures detected at sites S2 and S3.

back to a conductive ready state is to remove the block, a process that is called recovery from inactivation. Inactivation is an important concept in physiology because it limits both the number of available channels and the duration of their activity. Two major kinds of inactivation have been identified, which have been named N-type and C-type inactivation.

By studying the Shaker potassium channel, Aldrich and Hoshi correctly determined the molecular underpinnings of N-type inactivation [25]. The N-terminal tail of the protein was found to enter into the open channel where it would physically occlude the permeation pathway. To confirm the proposed mechanism, the N-terminus was removed and the channels tested to verify that the inactivating block was absent. N-type inactivation is analogous to a ball on a chain that can plug the entryway of the channel, a model first proposed by Armstrong and Bezanilla in the 70s [26]. Removing the N-terminus revealed the existence of a slower form of inactivation, kinetically distinct from the first kind [27]. Working off the incorrect assumption that the C-terminus was involved, this second type of inactivation was named C-type inactivation.

It is now known that a conformational transition in the selectivity filter underlies C-type inactivation—a fact supported by several lines of evidence. First, the presence of additional extracellular K^+ appears to slow down inactivation and accelerate the recovery process. The role of K^+ has been described as a "foot in the door"—the idea being that K^+ somehow binds

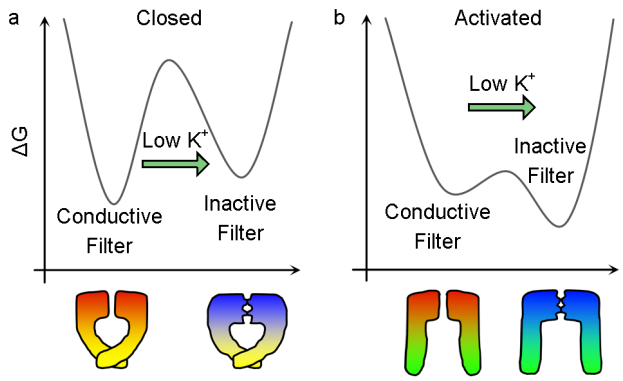

Figure 1.4: Hypothetical free energy landscape of the selectivity filter. a, When the activation gate is closed the conductive conformation of the selectivity filter is favored. b, Opening the channel changes the landscape biasing the filter toward an inactivated state. The barrier for the closed channel is drawn larger because the recovery process is considerably longer. Reducing the concentration of extracellular K^+ also lowers the relative stability of the conductive state, providing an alternative mechanism for controlling the conformation of the selectivity filter.

to the channel to keep the protein in a conductive state. The channel's only conserved binding site for K^+ lies in the selectivity filter, suggesting that it is the site of the conformational transition. Furthermore, the rate of C-type inactivation varies with the type of ion present in the same order as the channel's permeabilities. Only the selectivity filter has the ability to distinguish between different kinds of ions. Finally, mutations introduced in the vicinity of selectivity filter have been discovered that enhance or abolish inactivation, localizing the conformation change to that area [28, 29, 30]. In light of these findings, C-type inactivation has more recently been referred to as slow inactivation.

C-type inactivation begins immediately after the channels open. While the rate of inactivation can vary depending on the type of channel, the process typically takes several hundred milliseconds. After the current is blocked, the only way to recover from inactivation is to remove the activating stimuli for a prolonged period of time lasting around ten seconds or more. Somehow, closing the channels resets the protein to a conductive ready state. A hypothetical free-energy landscape summarizes this knowledge (Fig 1.4). When the channels are open, the conductive state is destabilized relative to the inactivated conformation, while the reverse holds true if the channels are closed. In other words, the activation gate is inversely coupled to C-type inactivation. The barrier for the recovery process appears much larger that the forward process into inactivation because the transition rate is much slower (Fig 1.4b).

Although it is clear that C-type inactivation is a result of a conformational change in the selectivity filter, the precise changes that take place remain a matter of debate. One of two hypothesis are possible: Either the selectivity filter becomes constricted blocking the passage of K^+ ions through the channel or the filter losses its ability to properly coordinate K^+ ions possibly because it dilates. Separate lines of evidence have been used to support each hypothesis.

1.3.5 Conformation of C-type Inactivated State: Contradictory Evidence

Yellen et al. first explored the idea that C-type inactivation is the result of a constriction in the selectivity filter [31]. Working on the Shaker potassium channel, they mutated the threonine residue located on the extracellular side of the filter (position 449) to a cysteine so that the channel could bind Cd^{2+}. Cd^{2+} bound weakly to the conductive state of the channel but the metal's presence accelerated the transition to the C-type inactivated state, after which the binding affinity for Cd^{2+} increased by ∼45,000. To explain this effect, they proposed that Cd^{2+} could only bind to one cysteine at a time while the channel was conductive, but that after C-type inactivation the extracellular mouth of the channel constricted allowing Cd^{2+} to simultaneously interact with cysteines across multiple subunits. More recently, the same experiment was repeated on the bacterial channel KcsA by Perozo and co-workers [32]. After introducing a cysteine mutation at the equivalent site (position 82) in KcsA, the rate at which the channel entered the inactivated state appeared to be accelerated in the presence of Cd^{2+}. Tandem dimer and tandem tetramer constructs of equivalent cysteine mutants in KcsA and the Shaker potassium channels demonstrate that these Cd^{2+} metal bridges are formed only between adjacent subunits. This conclusion is also supported by results from X-ray crystallography and molecular dynamic structures. All observations support the view that a conformational transition similar to that of Shaker takes place in KcsA to cause inactivation.

Structures of the selectivity filter have been obtained using X-ray crystallography under conditions that are expected to promote the C-type inactivated state. The MacKinnon lab published the first of these structures for the bacterial channel KcsA [17]. After obtaining conformations of the conductive filter, the MacKinnon lab soaked their crystals in a solution at low K^+ concentration and high Na^+ concentration, and discovered that the filter had constricted [23]. The filter constriction was characterized by a rotation of the Val76-Gly77

amide plane that moved the central glycine residues of the filter (position 77) ∼1 Å inward on each subunit. The overall distance between the C_α atoms of the glycine residues decreased from 8.1 Å to 5.5 Å. Recently, structures of KcsA obtained under a high K^+ concentration with the activation gate open, a condition expected to promote the C-type inactivated state, revealed the selectivity filter to be in the same pinched conformation [19, 20]. In addition to the wild type channel, X-ray crystallographic structures have also been obtained of KcsA with the E71A mutation, which is significant because it has been shown that the mutation removes C-type inactivation [30, 33]. In none of the crystal structures of the E71A mutation has the filter been observed to exist in the constricted conformation. When K^+ is soaked out of the crystals using Na^+, instead of constricting the filter adopted a novel conformation where the carbonyl oxygen atoms lining the filter flipped outward to accommodate Na^+ [33]. To summarize, the constricted conformation is observed when the channel is crystallized under conditions used to promote C-type inactivation, and an alternative conformation is observed when a mutation is introduced to block the inactivated state.

The crystallographic structures of KcsA are complimented by structural data obtained with Nuclear Magnetic Resonance (NMR) spectroscopy. Using both solution and solid state NMR, researchers have managed to assign peaks to Val76, a residue adjacent to the filter's central glycine residues. After lowering the K^+ concentration, the peaks shifted, consistent with the observation that the Valy76-Gly77 amide plane rotates after soaking K^+ out of the KcsA crystal structures. A similar shift in the peaks was observed after opening the KcsA channel by lowering the pH, suggesting that the filter had adopted a similar conformation. The shift was not observed in NMR recordings of the non-inactivating E71A mutation, confirming that the signature is unique to C-type inactivated state [34, 35]. Although the available results from NMR appear to be consistent with the crystallographic data, the NMR data does not provide a sufficiently complete picture to conclusively determine the conformation of the filter.

While the structural data collected on KcsA makes a compelling case that the filter constricts during C-type inactivation, efforts to reproduce these results on other channels have been inconclusive. The constricted conformation has never been observed in X-ray crystallographic structures of the potassium channels MthK, Kv1.2, and the Kv1.2/2.1 chimera under conditions designed to promote the C-type inactivated state [36, 37, 38]. The fact that the constricted filter is not observed in these channels has been cited as evidence that the selectivity filter does not constrict during C-type inactivation. However, in each structure,

the filter was always observed to exist in the conductive state, so no alternative conformation was found that could serve as the C-type inactivated state. These structures therefore provide no evidence to either reinforce or refute the claim that the constricted conformation observed in KcsA represents the C-type inactivated state. A structure would be significant if an alternative filter conformation were identified for an open channel, but so far only the conductive and constricted filter conformations have been observed in the open channels.

Observations that the relative ion selectivity shifts during C-type inactivation in the Shaker potassium channel have lead some to suggest that this reveals something about the conformation of the filter. In the complete absence of K^+, the Shaker channel (with the N-terminus removed) has been observed to weakly conduct Na^+ through the inactivated state [39]. More recently, it has been proposed that the small Na^+ current is evidence that the filter must dilate during the inactivation process. According to this argument, a dilated state would allow partially hydrated Na^+ ions through the channel while destroying the filter's ability to coordinate with K^+. However, no structural data exists to support this hypothesis—the only non-conductive conformation observed in X-ray crystallographic structures is the constricted filter conformation of the KcsA channel. As an alternative, it seems plausible that the filter constricts just enough to allow only Na^+ ions through, which has an ionic radius that is $\sim$0.5 AA less than that of K^+. In other words, the selectivity filter on the Shaker channel does not completely collapse during inactivation but instead undergoes a partial constriction that is just enough to block K^+ ions.

Although structures of the potassium channel KcsA reveal the selectivity filter in a constricted conformation under conditions designed to promote inactivation, some of these same conditions can also promote alternative states, leaving it unclear if the constricted conformation actually corresponds to the inactivated state. For example, the Shaker potassium channel is observed to enter into what has been named the "defunct state" when all the external K^+ is removed for a prolonged period of time [40, 41, 42]. Like the C-type inactivated state, the defunct state is both reversible and non-conductive. However, recovery from the defunct state can take anywhere from several minutes to hours, suggesting that the defunct state is somehow more deeply inactivated than the C-type inactivated state. That an alternative state might be reached under one of the conditions associated with C-type inactivation highlights the difficulty in assigning X-ray crystallographic conformations to specific inactivated states. Perhaps because of this difficulty, it has been proposed that the defunct state could actually correspond to the constricted conformation observed in KcsA,

although it is unclear if KcsA even exhibits the defunct state [43].

The hypothesis that the selectivity filter loses its ability to coordinate K^+ during C-type inactivation, as opposed to constricting, gained traction after the discovery that the channel still inactivates when D-alanine is substituted for the filter's central glycine residues [43]. The finding is significant because it is widely believed that the D-alanine substitution would prevent the filter from constricting. The MacKinnon lab first obtained an X-ray crystallographic structure of KcsA with the substitution, revealing the selectivity filter to be in the same conductive conformation as wild-type channel (Fig. 4.1c). After soaking the crystals in a solution at low K^+ concentration, a condition that promotes the C-type inactivated state in a wild-type channel, the selectivity filter was found to remain in its conductive form (Fig. 4.1d) [44]. The MacKinnon lab proposed that the D-alanine sidechain blocked the rotation of the Val76-Gly77 backbone amide plane, preventing the selectivity filter from making the transition toward the constricted conformation, an argument that they supported by presenting a space filling model where the D-alanine sidechains sterically clash into each other (See Fig. 3B in [44]). The observation that C-type inactivation still occurs with the D-alanine substitution is perhaps the strongest evidence against the hypothesis that the constricted conformation of the filter corresponds to the inactivated state. In Chapter 5 of this thesis, the hypothesis will be carefully evaluated.

Almost all the structural data of the C-type inactivated state comes from the KcsA channel. Two competing hypothesis have emerged: one is that the filter constricts and the other is that the filter losses its ability to coordinate with K^+, possibly because it dilates. Given the available evidence taken at face value, it is this author's opinion that some type of constricted conformation of the selectivity filter is most likely to best represent the C-type inactivated state.

1.4 Methods

Several methods are used to study potassium channels. Because of their importance to potassium channel research, the basic theory behind Electrophysiology, X-ray crystallography, Nuclear Magnetic Resonance, and Molecular Dynamics will be discussed below.

1.4.1 Electrophysiology

The first high fidelity measurements of ion channel electrical activity came from intracellular recordings. This recording method has proven popular through the years, and remains in use today. The basic idea of the technique is to incorporate the membrane of the cell into an electrical circuit. That way, when current passes through the circuit it will have to pass through the membrane. The membrane will block any current through the circuit as long as there are no open channels, but once ion channels become activated the resistance load will drop. To create a circuit around the membrane, the cell must be impaled with a micro-electrode to gain electrical access to the cell's interior. The intracellular electrode together with a grounding source outside the cell completes the circuit. A recording is made by amplifying and storing any signals through the circuit. Several variations of this method have been introduced over the years. For example, the cell can be impaled with a second electrode for injecting current, in which case the setup is said to be in a Two Electrode Voltage Clamp (TEVC) configuration. Intracellular recordings are relatively simple to carry out, but the method is limited to measuring only the macroscopic activity of the cell's entire membrane surface.

Patch clamp recordings turned out to be a major advancement over intracellular recordings, enabling electrophysiologist to observe individual ion channels for the first time. The technique requires isolating a small patch of the cell's membrane under a glass micro-electrode, which is done by placing the micro-electrode on the cell surface and gently sucking a piece of the membrane into the tip of the micro-electrode. With a bit of luck, a tight seal will form between the micro-electrode and the membrane capable of stopping current from leaking out at the interface of the seal. Once this seal forms, the setup is said to be in a "cell attached" mode, making it possible to study individual ion channels under the patch. Several variations of the patch clamp method exists. For example, the membrane under the patch can be ruptured by blowing through the micro-electrode. These leaves the micro-electrode exposed to the intracellular solution, so the electrode ends up collecting electrical signals from the whole cell.

Once an electrical circuit has been completed around the cell's membrane, two types of recording modes are possible: Voltage clamping and current clamping. During a voltage clamp recording, the membrane potential is held fixed while ion channels open and close. The current passing through channels after they open will effect the membrane potential, so

the voltage clamp must add current to counteract the activity of the channels. A recording is made by storing the amount of current supplied by the voltage clamp to hold the membrane potential constant at each point in time. Current clamping is just like voltage clamping except that the current, not the potential, is held at a stationary value. Maintaining a constant flux of net charge through the membrane when ion channels open or close requires adjusting the membrane potential. During a current clamp recording, the required changes in the membrane potential are saved at each point in time, which turns out to be useful when evaluating a cell's response to an electrical signal. Because both current and voltage clamping techniques only measure the electrical activity through ion channels, no direct information about the structure of the protein can be obtained using these methods.

1.4.2 X-ray Crystallography

Like most proteins, potassium channels are only nanometers in size, which is well below the diffraction limit of optical microscopy. Fortunately, X-ray crystallography has been used to obtain several structures of potassium channels in various conformations. The technique offers a way to collect a snapshot of the protein's conformation in its crystal form at the atomic scale.

As the name suggests, X-ray crystallography is a method for determining the chemical structure of a molecule in its crystal form. Because a crystal is nothing but a periodically repeating arrangement of molecules, the atoms in the crystal can be described as a series equally separated planes. Each time an X-ray beam passes through one of these planes there is a small chance that the beam may interact with the electron cloud of one of the atoms, which would cause the X-ray beam to scatter in every direction. The sum of the X-ray beam scattering off each plane in the crystal structure creates a diffraction pattern. If the spacing between two planes is just right then the scattered X-ray beam will constructively interfere, which will appear as a maximum in the diffraction pattern. The position of the peaks in the diffraction pattern can be related to the underlying orientation and spacing of the plane in the crystal using Bragg's law.

$$n\lambda = 2d\sin\theta \tag{1.3}$$

Here, n is the refractive index of the medium (the crystal), λ is the wavelength of the X-ray beams, d is the distance between the planes, and θ is half the angle between the incident

X-ray beam and a peak in the diffraction pattern.

Diffraction patterns are collected by placing the crystal in front of a collimated beam of monochromatic X-rays. One diffraction pattern is not enough to determine the underlying structure of the crystal using Bragg's law, so the crystal must be rotated in front of the beam to collect a series of diffraction patterns. The data is feed through a 3D Fourier transform to convert the electron densities into a function of Cartesian coordinates. The electron density map must then be used to figure out the underlying molecular structure. In other words, individual atoms cannot be detected directly—their positions must be inferred from the electron density maps. In general, if the resolution is 3Å or better then it becomes possible to correctly identify individual sidechains of the protein.

The challenge in X-ray crystallography is to obtain the protein in crystal form. Proteins tend to exists in irregular, globular conformations that would prevent them from naturally aligning into a latticework. To crystallize a protein, various conditions must be tried at random in an attempt to coax the protein to stack in a periodically tiled array. Membrane proteins are even harder to crystallize because the lipid interface of the protein is non-soluble. Despite these challenges, numerous potassium channels have been crystallized in several different conformations.

1.4.3 Nuclear Magnetic Resonance

Nuclear Magnetic Resonance (NMR) spectroscopy is a technique that can be used to study the structure and dynamics of molecules [45]. At the atomic level, each nucleus carries a small magnetic moment μ that is associated with its quantum mechanical spin S via the gyromagnetic ratio γ, with $\mu = \gamma S$. The magnetic moment can align either parallel or anti-parallel to an external magnetic field, corresponding to low and high energy states, respectively. The difference in energy between two states ΔE is directly proportional to the strength of the external magnetic field. In an equilibrium sample, most of the spins will populate the lower energy state. A pulse of radio waves parallel to the field can be used to induce detectable transitions from the lower to the higher energy state. In order for the energy of the pulse to be absorbed it must match the separation energy ΔE, so the required frequency of the radio wave, known as the resonant frequency, is given by $\Delta E = \hbar \cdot f$. Spectroscopic data is collected by measuring the amount of energy absorbed by the system, and by measuring electromagnetic signal given off as the population of spin states relax back

to the lower energy state. Because they carry a very large magnetic moment, protons yield the greatest signal and produce the highest sensitivity in NMR.

Using NMR to study the structure of protein systems is challenging because most proteins are very large and the observed spectra become spectra becomes crowded with overlapping signals. To separate individual peaks, multidimensional NMR has been developed. The protein is probed with multiple pulses using different shapes, frequencies, and lengths for each pulse. By varying the pulse sequences, additional dimensions of information are captured, and the variable time periods are used to plot the additional dimensions. To make sense of the spectra, resonance peaks must be assigned to the atoms of specific residues in the protein, which usually involves running separate NMR experiments to identify the underlying residues for each peak. Once the assignments have been made, the final step is to determine the protein structure. A technique of choice is to determine inter-atomic distances through spin-spin relaxation with the *nuclear Overhauser effect* (NOE).

1.4.4 Molecular Dynamics

Molecular Dynamic (MD) simulations augment X-ray crystallographic structures by recreating the protein's dynamical behavior. Using the atoms and their coordinates from the crystal structure as a starting point, the protein is surrounded by molecules found in its native environment. For a potassium channel, the protein would be embedded into a lipid bilayer surrounded by a bath of water molecules and ions. Once the system is built, the simulation is ready. Running the simulation creates a movie of the protein spontaneously fluctuating around its environment. Typically, every atom in the system is simulated over a period of time lasting anywhere from a few nanoseconds to several microseconds. The conditions in the simulation can be modified to match those used in an electrophysiological recording so that the results can be compared. For example, it is known that a high external potassium concentration will favor the conductive state of the channel over the inactivated conformation. A simulation would be expected to recreate this exact behavior.

Within the limits of the computational resources that exists today, as much physics and chemistry as possible are included in the simulations. All interactions between the atoms of the system are completely described by the potential energy function. There are several options to choose from when selecting a potential energy model for a MD simulation, but all of them share the same basic form.

$$U(\vec{x}) = \sum_{\text{bonds}} k_b(b-b_0)^2 + \sum_{\text{angles}} k_\theta(\theta-\theta_0)^2 + \sum_{\text{dihedrals}} k_\phi[1+\cos(n\phi-\delta)] + \sum_{\text{non-bonded}} \epsilon\left[\left(\frac{R_{i,j}^{\min}}{r_{i,j}}\right)^{12} - \left(\frac{R_{i,j}^{\min}}{r_{i,j}}\right)^{6}\right] + \sum_{\text{non-bonded}} k\frac{q_1 q_2}{r_{i,j}} \tag{1.4}$$

Here, the first three terms represent intramolecular interactions between bonded atoms. Harmonic potentials used in the first and second term maintain the correct bond length and angle between neighboring atoms. The third term is called a dihedral angle, and it maintains the correct orientation of bonded atoms relative to other bonded atoms. For the bonded interactions, separate parameters (i.e. force constants, ideal bond lengths, ect.) are used for each molecule or residue. The last two terms in the equation represent non-bonded interactions between any two atoms in the simulation. Notice that the terms depend on the distance $r_{i,j}$ between the atoms. The first non-bonded term represents the Van der Waals interactions, while the last term represents the electrostatic interactions. Separate parameters exists for each type of atom for the non-bonded cases.

Given the potential energy function, all that is needed to start running a simulation is an initial configuration of the protein, its surrounding molecules, and the velocities chosen in accord with the Maxwell distribution at a temperature T. The force acting on each atom can then be computed from the negative gradient of the potential energy function, $\vec{F} = -\nabla U(\vec{x})$. Using the forces from the potential energy function and Newton's laws of motion, the acceleration acting on each atom can be calculated and used to update the atom's velocity and position. By numerically integrating Newton's laws of motion over time, a trajectory is generated for each atom in the system. The numerical schemes to integrate Newton's dynamical equation of motion with a finite time-step have the typical form (Leapfrog integration).

$$\begin{aligned} x_{t+\Delta t} &= x_t + v_t \cdot \Delta t + \frac{1}{2} a_t \cdot \Delta t^2 \\ v_{t+\Delta t} &= \frac{1}{2}(a_{t+\Delta t} + a_t)\Delta t \end{aligned} \tag{1.5}$$

Simulations following this approach are not with limitations—many types of biochemical reactions cannot be simulated. The force-fields in equation 1.4 do not allow for the breaking

and formation of covalent bonds during a simulation. All bonds between atoms on the same molecule must be pre-specified at the beginning of the simulation. Although the total number of covalent bonds are fixed, the forces from each bond are included in the simulation. What is possible is to accurately model a protein undergoing a conformational transition where the bonded atoms are simply rearranging themselves relative to one another. Another limitation of the force-fields in equation 1.4 is that they do not capture the effects of polarizability on individual atoms (although recent advancements are overcoming this limitation). Atoms are simply treated as point charges, which can become problematic when highly charged particles interact with each other over short distances. Despite these limitations, MD simulations using these force-fields have proven surprisingly accurate. For example, simulations of the potassium channel KcsA show ions permeating through the protein, demonstrating that the simulations capture the protein's basic function.

MD simulations generate the dynamics of a protein by sampling over a distribution of the molecule's different possible conformations. However, the sampling is often limited because the protein will spend long periods of time in the same conformation, never transitioning to other states within the timescales allowed by today's current computers. That is why enhanced sampling methods have been developed, which can greatly improve our ability to sample between two structural endpoints. A set of simulations running in parallel divide up the space between the endpoints into a series of intermediate steps. Biasing potentials act to hold the protein's conformation at each intermediate step, enhancing the sampling over a restricted regime. At the end of the calculation, the results are unbiased to produce a set of correctly distributed samples.

CHAPTER 2
RECOVERY FROM INACTIVATION

Jared Ostmeyer, Sudha Chakrapani, Albert C. Pan, Eduardo Perozo and Benoît Roux

Reprinted (adapted) with permission from Nature, 501(7465), pp 121-124.

2.1 Abstract

Application of a specific stimulus opens the intracellular gate of a K^+ channel (activation), yielding a transient period of ion conduction until the selectivity filter spontaneously undergoes a conformational change towards a non-conductive state (inactivation). Removal of the stimulus closes the gate and allows the selectivity filter to interconvert back to its conductive conformation (recovery). Given that the structural differences between the conductive and inactivated filter are very small, it is unclear why the recovery process can take up to several seconds. The bacterial potassium channel KcsA from Streptomyces lividans can be used to help elucidate questions about channel inactivation and recovery at the atomic level. Although KcsA contains only a pore domain, without voltage sensing machinery, it has the structural elements necessary for ion conduction, activation and inactivation [30, 29, 46, 47, 34, 48, 49]. Here we reveal, by means of a series of long molecular dynamics simulations, how the selectivity filter is sterically locked in the inactive conformation by buried water molecules bound behind the selectivity filter. Potential of mean force calculations show how the recovery process is affected by the buried water molecules and the rebinding of an external K^+ ion. A kinetic model deduced from the simulations shows how releasing the buried water molecules can stretch the timescale of recovery to seconds. This leads to the prediction that reducing the occupancy of the buried water molecules by imposing a high osmotic stress should accelerate the rate of recovery,which was verified

experimentally by measuring the recovery rate in the presence of a 2-molar sucrose concentration.

2.2 The Problem

Available X-ray structures of the KcsA channel provide an atomic view of the four most important functional states in which the intracellular gate is either closed or open, and the selectivity filter is either conductive or inactivated [23, 19, 20]. These are (in terms of their Protein Data Bank entries): the closed-conductive (1K4C), open-conductive (3FB7), open-inactivated (3F5W), and the closed-inactivated (1K4D) states (Fig. 2.1a). When the filter is in the conductive state (1K4C and 3FB7), it is occupied by several K^+ ions arranged in single file over five binding sites (S0 to S4); ion occupancy is considerably reduced when the filter is in the non-conductive inactivated state (1K4D and 3F5W) because it is 'pinched' at the central glycine residue of the signature sequence TTVGYGD. The conductive conformation of the filter is virtually unchanged when the gate is closed (1K4C) or open (3FB7). The pinched non-conductive conformation of the filter is similar in the open-inactivated conformation (3F5W) and in the closed structure (1K4D) crystallized at low-K^+ concentration, indicating that the latter provides a realistic representation of the KcsA channel in the closed-inactivated state.

Although available X-ray crystal structures reveal the conformations of the functional states, they do not explain the experimentally observed timescales. Recovery from inactivation is an extremely slow, ion-dependent process [50]. Macroscopic current measurements show that the KcsA channel inactivates within 1–3s and that recovery takes place in 5–20 s (Fig. 2.1b, c), depending on the external K^+ concentration [29, 46]. However, the structural difference between the conductive and non-conductive filter is less than 1Å root mean square deviation (r.m.s.d.), barely larger than the thermal fluctuations of proteins under ambient conditions (Fig. 2.1d). According to a naive Eyring rate theory argument, the long timescale corresponds to an activation free energy barrier of about 15–20 kcal mol^{-1}, a value that is difficult to reconcile with the very slight structural difference between the conductive and inactive filter (see Appendix 2.7, Fig. 2.5). Explaining the molecular origin of the extra-ordinarily long timescale of the recovery process is an unresolved issue.

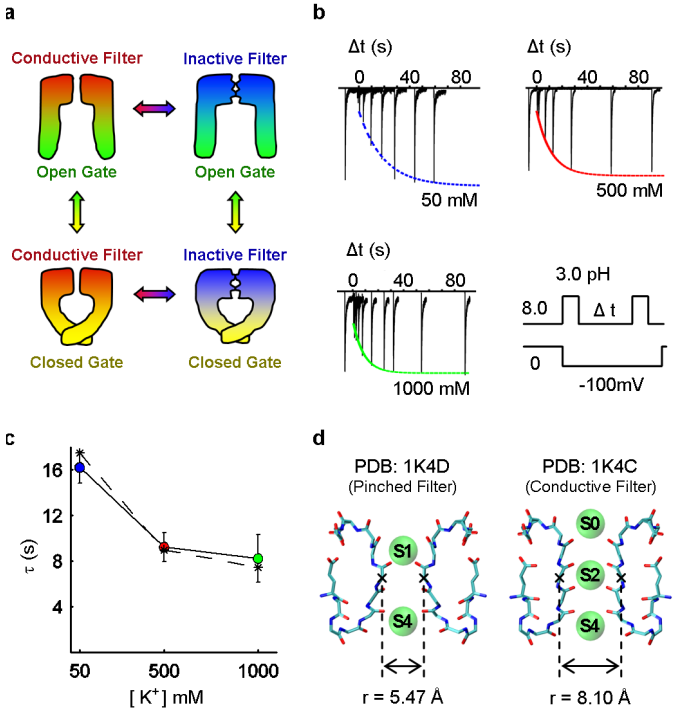

Figure 2.1: Gating, inactivation and recovery in KcsA channels. a, Schematic depiction of the four dominant functional states. b, Recovery of the selectivity filter from slow-inactivation measured from inward K^+ current during a double pulse protocol that cycles the intracellular gate from open (inactivating the filter) to closed (promoting filter recovery) to open (for measuring the extent of recovery). Currents were measured at indicated symmetrical K^+ concentration. The fraction of recovered channels increases as a function the inter-pulse duration (Δ) in each of the three patches, and may be fit to a single exponential function. c, The fit time constants for recovery for various symmetric pot concentrations demonstrate that K^+ accelerates recovery. Results based on a kinetic model are shown as a dashed line with asterisks (error bars denote standard deviation with $n = 3$). d, The conductive state of the selectivity filter compared to the pinched state is characterized by a relatively small increase in the minimum inter-subunit distance between backbone atoms of the filter and an increase in ion occupancy.

2.3 Theoretical Model

To identify the rate limiting step opposing recovery, a molecular dynamics simulation of KcsA with the non-conductive filter and the closed gate was carried out in the presence of a high K^+ concentration. Although these conditions were designed to favor a spontaneous transition of the filter towards the conductive state, the filter remained in the non-conductive state during the 17-ms-long simulation (Fig. 2.2a). Throughout the simulation, the selectivity filter stayed near the crystallographic conformation 1K4D and no ion translocation event was observed (see Appendix 2.7, Fig. 2.6). The stability of the non-conductive filter over this long timescale indicates that the simulation captured the rate-limiting step opposing a rapid recovery of the filter.

Examination of the 17 ms trajectory led us to focus on three buried water molecules in an approximately 8Å-long cavity located behind the selectivity filter of each subunit. Whereas water molecules bound near the protein surface are expected to undergo rapid dynamical fluctuations and exchange easily with the bulk [51], the buried waters maintained distinct positions and orientations throughout the entire simulation. The buried waters are stabilized by a network of water-water and water-protein hydrogen bonds (Fig. 2.2b), displaying long residence times (see Appendix 2.7, Fig. 2.9). The buried water molecules thereby become an integral part of the protein structure when the selectivity filter is in the pinched conformation. On average, a given subunit cavity is occupied by three buried water molecules, 99% of the time as each cavity releases its waters into the bulk no faster than 10–15 ms and refills in 80–100 ns (see Appendix 2.7, Fig. 2.10). The Tyr 82 side chain acts as a lid, controlling access to the cavity. In the cavity, the buried water molecules remain near the location observed in the structure with the pinched non-conductive filter (1K4D), which is also consistent with nuclear magnetic resonance (NMR) data [34, 52]. The outermost water molecule is observed in the X-ray structure of the conductive filter (1K4C), whereas the two others are absent. Structural modeling shows that the latter would clash with the backbone C_α of the central glycine residue (Gly 77) if the filter adopted a conductive conformation (Fig. 2.2c). These results indicate that the presence of the buried water molecules bound behind the filter locks its conformation into the pinched non-conductive state and prevents a spontaneous transition towards the conductive state.

To demonstrate that these 'inactivating water molecules' prevent recovery, additional molecular dynamics simulations were carried out in which they were removed (Fig. 2.2d).

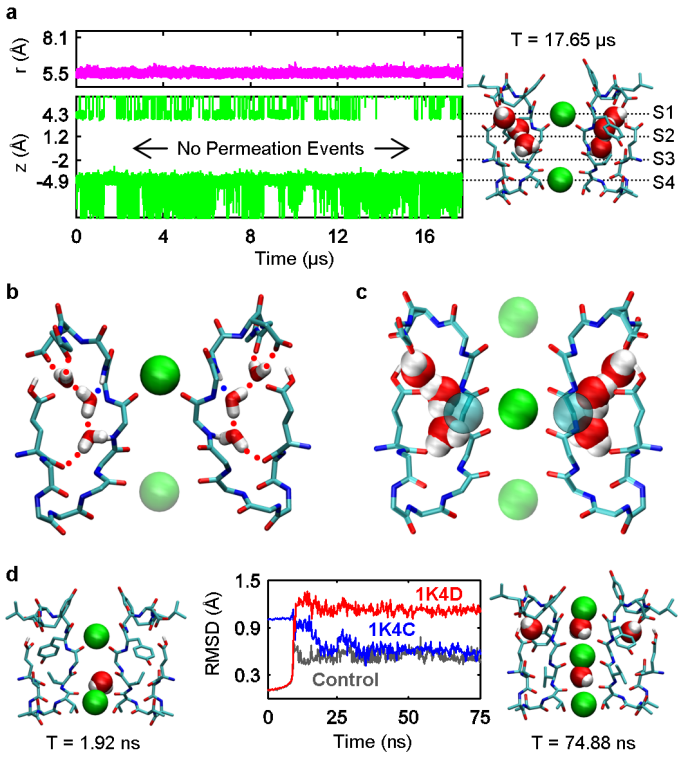

Figure 2.2: Molecular dynamics simulations reveal mechanism of recovery from inactivation. a, Results from a simulation of the pinched filter show that the width of the filter remained near $r = 55.5$Å where r is defined as the cross subunit pinching distance between the C_α atoms of Gly 77 (magenta line, top plot). Plot of the height of K^+ ions, z, above the center of mass of the selectivity filter (green traces, bottom plot). Projection of the aforementioned plot onto a snapshot of the selectivity filter taken at time $T = 517.65$ms at the end of the simulation (right). b, Network of hydrogen bonds matches each water with two donors and an acceptor, keeping water molecules trapped behind the selectivity filter throughout the simulation. c, Water positions behind the pinched filter of 1K4D sterically clash with the conductive filter 1K4C. Rendering both water positions from 1K4D and the Ca glycine atoms from 1K4C as Van der Waals spheres reveals that unfavorable steric clashes of approximately 1Å in magnitude would exist between the protein and water molecules. d, In simulations without water behind the filter, the r.m.s.d. distance of the pinched filter relative to its original crystallographic coordinates (red) increases as the r.m.s.d. distance to the conductive filter in 1K4C (blue) decreases. The r.m.s.d. distance versus 1K4C falls to approximately 0.6Å, comparable with a control simulation (dark grey) starting from the conductive filter 1K4C. Snapshots taken at time $T = 1.92$ and 74.88ms are shown.

Within a few nanoseconds, the filter made a transition towards the conductive conformation (1K4C). The recovery transition was accompanied by K^+ ions translocating inward towards the filter from the extracellular side and the binding of water molecules behind the filter at the positions observed in 1K4C. While one K^+ ion moved to the site S2 of the filter, another entered the site S0 from the extracellular bulk. These two K^+ ions, combined with a third K^+ ion in S4 that remained present at its initial location during the entire simulation, resulted in a 'S0–S2–S4' ion configuration in the filter. The involvement of K^+ ions is expected, as the timescale of recovery increases at low extracellular K^+ concentration. To clarify the role of the ions further, molecular dynamics simulations were carried out with no free K^+ ions in solution. In all cases, the filter remained in the pinched non-conductive conformation, consistent with the experimental observation that low extracellular K^+ inhibits recovery (Fig. 2.1c). In contrast, additional simulations in 1M KCl showed that whether or not a K^+ ion was initially bound in the site S4 or in the intracellular cavity of the channel, a K^+ ion entered the filter from the extracellular side to bind to the site S2. Additional molecular dynamics experiments were carried out to determine the outcome from different intermediate starting conditions (see Appendix 2.7, Fig. 2.11), indicating that the most likely pathway leading to recovery requires the absence of all three inactivating water from all four subunits to permit the binding of an external K^+ ion to the filter.

To characterize the free energy landscape controlling the recovery process, we calculated the two dimensional potential of mean force (PMF) as a function of the pinched glycine C_α–C_α distance of the filter r and the position of the external K^+ ion Z (see Appendix 2.7, Fig. 2.12), with and without the inactivating water molecules (Fig. 2.3). These two states illustrate the coupling between the inactivating waters and the external K^+ ion on the recovery process. When the inactivating water molecules are present (Fig. 2.3a), no significant free energy barrier is encountered to move a K^+ ion from the bulk to the binding site S1 of the pinched filter pinched filter (snapshot i), but the subsequent transition of this external K^+ to the binding sites S2 or S3 is energetically forbidden; the free energy landscape rises sharply, up to 30 kcal mol^{-1} relative to the local minimum, as the K^+ is brought deeper into the filter towards the site S2 along the Z coordinate. There is a large energy barrier because the non-conductive filter is too narrow for a K^+ ion to fit through. The energy barrier to gradually open the filter to a conductive conformation is also highly unfavorable, rising by, 25 kcal mol^{-1} when an ion is in the site S1 (snapshot j). Opening the pinched filter by moving along the r coordinate is opposed by a large free energy barrier because

the backbone of the filter clashes with the buried inactivating waters. The PMF with the inactivating waters removed is markedly different (Fig. 2.3b). Once a K^+ ion reaches the site S1 (snapshot k), the recovery process becomes energetically downhill. A free energy basin guides the recovery process as the free energy decreases (snapshot l). The filter first makes a transition from the pinched to the conductive conformation, the ion in S1 then permeates down to the site S2 (snapshot m), ending in a conformation that is highly similar to the 1K4C structure. In the absence of inactivating waters, the channel will spontaneously and rapidly recover to a conductive conformation upon the binding of a K^+ ion from the extracellular solution. But the filter remains locked in the non-conductive state, even with an incoming external K^+ ion, as long as the inactivating waters are present.

These computational experiments suggest that two factors control the conformational transition of the selectivity filter from the non-conductive pinched state to the conductive state: the release of the inactivating water molecules and the binding of an external K^+ ion. The buried inactivating waters act as gatekeepers, locking the filter in the pinched non-conductive conformation; the binding of an external K^+ ion cannot lead to recovery if they are present. The external K^+ ion binding to the filter acts as a catalyst for the final step; releasing the inactivating water molecules does not lead to recovery without the binding of an external K^+ ion. The inactivating waters must first be released to unlock the pinched state, and an external K^+ ion must then bind to the filter to catalyze the final step to recovery.

Although these simulations suggest a plausible mechanistic scenario, a complete and spontaneous recovery from an inactivation event was not observed during these experiments. The recovery process, which occurs over a timescale of, 10 s, is longer than what can be achieved with state-of-the-art computing technologies. Despite these limitations, it is important to bridge the results from molecular dynamics experiments to the extremely long timescales of the recovery process observed in macroscopic current measurements. For this purpose, we rely on a kinetic model (Fig. 2.4a) based on the assumption that occupancy of the cavity of each of the four subunits by inactivating waters is independent and uncorrelated, and that recovery can proceed to its final stage through the binding of an external K^+ ion only after all of the inactivating water molecules have been released. Although it is possible that recovery might occur very infrequently under different circumstances (see Appendix 2.7, Fig. 2.11), these constraints capture the dominant mechanism of recovery. Occupancy changes take place with forward and backward rates of k_f and k_b, followed by a final concerted step corresponding to the binding of an external K^+ ion to the selectivity filter. By virtue of

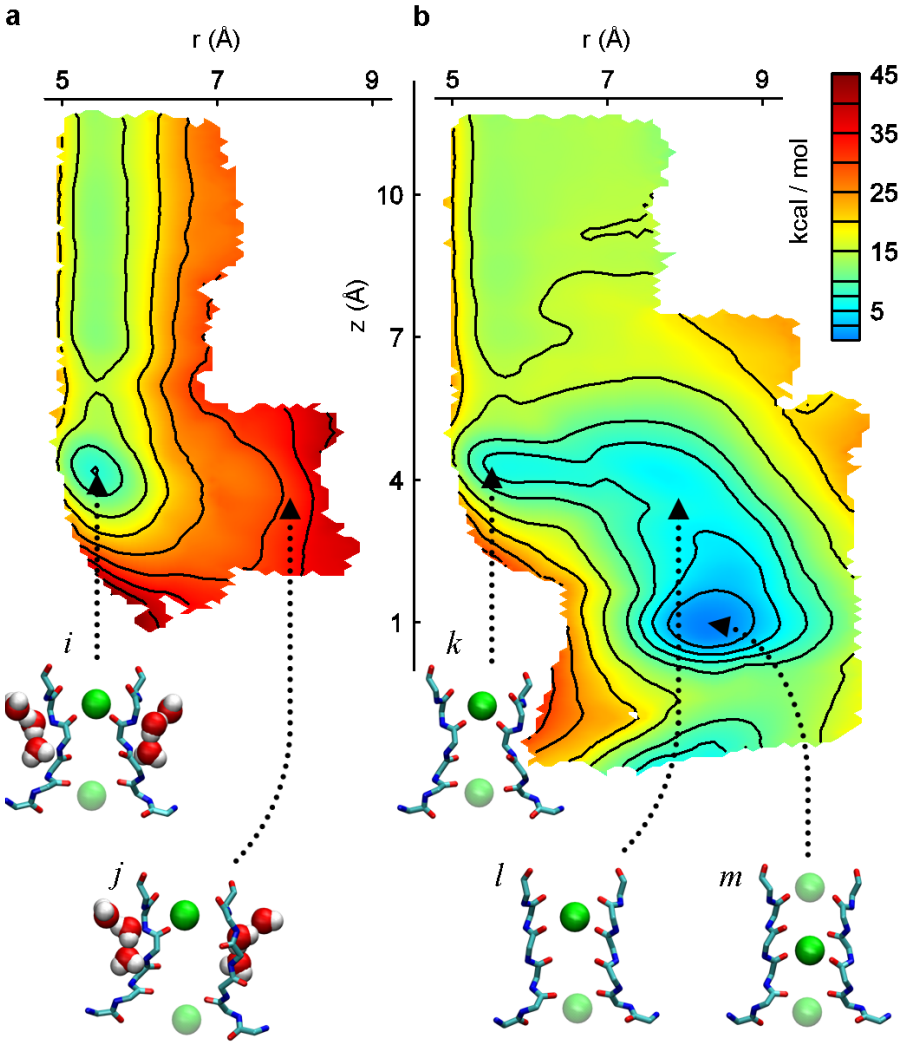

Figure 2.3: Two-dimensional free energy landscape of the recovery process. The horizontal reaction coordinate r describes the width of the selectivity filter and is defined as the cross-subunit pinching distance between the C_α atoms of Gly 77. The vertical reaction coordinate z is the height of a K^+ ion relative to the center of mass of the selectivity filter. a, PMF calculated with inactivating water molecules present behind the selectivity filter. The pinched filter rests in a free energy minimum with a K^+ in position S1 (snapshot i). The transition from a pinched to a conductive conformation (snapshot j) of the selectivity filter is impeded by an approximate 25 kcal mol^{-1} free energy barrier relative to the local minimum, resulting in an unstable conformation of the conductive filter. b, PMF calculated with the inactivating water molecules absent. The pinched filter with a K^+ ion in position S1 (snapshot k) recovers spontaneously, following the downhill slope of the free energy landscape. The filter recovers to a conductive conformation by moving first to an open conformation (snapshot l) before ions in the filter adopt a conductive configuration (snapshot m).

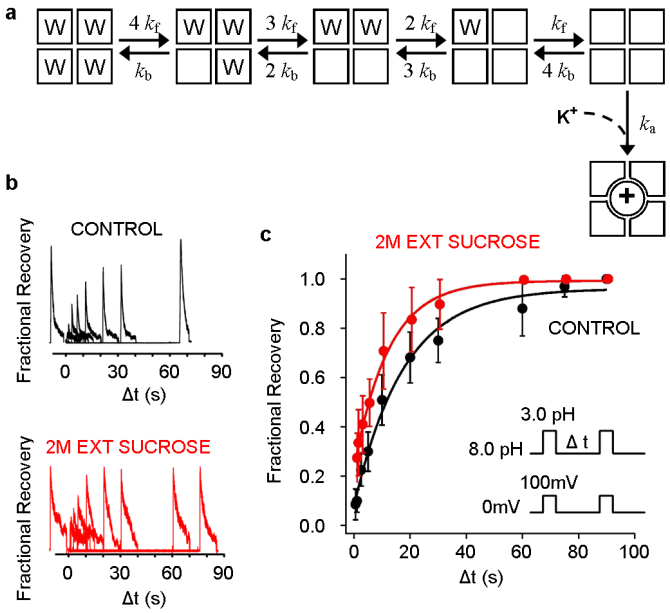

Figure 2.4: Impact of water molecules on recovery process. a, Kinetic scheme incorporating the main findings of the molecular dynamics simulations. The model was used to produce the simulated recovery times as a function of [K^+] shown in Fig. 2.1c (dashed line) using the rate constants $1/k_f$ = 511 μs, $1/k_b$ = 579 ns, $1/k_a$ = 58.3 x (150mM/[K^+]). When starting the kinetic model in the state with no inactivating water molecules (W), the channel reaches the active conductive state rather than the fully inactive state with a probability of approximately 0.5 at 50mM of [K^+]. This probability rises to approximately 0.7 at 150mM of [K^+]. b, c, Effect of external sucrose on the time course of recovery. b, Outward currents recorded with external 5 K^+/145mM NMG and internal 150mM K^+ in the absence and presence of 2M external sucrose. c, Fractional recovery averaged from eight patches plotted as a function of the inter-pulse interval. Error bars denote standard deviation.

the stoichiometric constraint posed by the four subunits, the timescale of recovery predicted by this model is tens of seconds (Fig. 2.1c, dashed line) using microscopic rates that are consistent with the current molecular dynamics simulations (Fig. 2.4). Moreover, the model displays the correct sensitivity to the external concentration of K^+, becoming slower at low concentration and reaching a plateau at high concentration.

2.4 Experimental Validation

This mechanism predicts that lowering the occupancy of the subunit cavities by inactivating water molecules should accelerate the rate of recovery from inactivation. This is consistent with the experimentally observed hydrostatic pressure dependence of recovery for the Shaker potassium channel [53], which indicates that, eight water molecules must be released from

the inactivated state to return to the conductive filter. An alternative approach to vary the occupancy of the cavities is to apply a high osmotic stress to the external solution [54]. Increasing the osmotic stress from the external solution should accelerate the process of recovery; the stability of the inactivating waters in 2 M sucrose would decrease due to the high osmotic stress, which should lead to a more rapid time of recovery (see Appendix 2.7, Fig. 2.13). To test this prediction, we measured the rate of recovery of wild-type KcsA channel in the presence of 5 mM of K^+ and 2 M sucrose in the external solution (Fig. 2.4b). In the absence of sucrose, the average recovery time is 17.06 ± 4.75 s, and in the presence of sucrose it decreases to 12.21 ± 3.73 s, consistent with our prediction (mean $\pm$ s.d.; see Appendix 2.7, Fig. 2.13). Although the overall effect is small (the waters bound to one subunit are destabilized by only, 0.7 k_BT, where k_B is Boltzmann's constant and T is the temperature), protein dynamics and the diffusion and binding of an external K^+ ion to the selectivity filter that is critical to catalyze recovery are expected to considerably slow down in a viscous environment [55]. The fact that the recovery process is accelerated in 2 M sucrose—despite a viscosity that is 30 times that of pure water—is strong evidence that the applied osmotic stress decreased the occupancy of the gatekeeper inactivating water molecules locking in the non-conductive state of the selectivity filter.

2.5 Concluding Remarks

Our molecular dynamics simulations and macroscopic current measurements suggest that the selectivity filter of K^+ channels functions as a ligand-gated pore through a built-in osmometer, where water molecules from the external solution are the 'ligands' responsible for the gating stimulus. It is unlikely that such a mechanism could have an important physiological role in higher organisms, as there are negligible variations in internal osmotic strength; however, it is possible that such a mechanism could regulate bacterial K^+ channels, as microorganisms are often exposed to widely varying external conditions. Examination of homology models of various K^+ channels indicates that the subunit cavities are conserved structurally and in terms of the hydrogen bonding interactions that they could provide through the peptide backbone (see Appendix 2.7, Fig. 2.7), indicating that the role of inactivating waters acting as gatekeepers of the pinched non-conductive filter is likely to be conserved in the K^+ channel superfamily. The present analysis may provide a basis to understand the wide range of inactivation and recovery phenotypes arising from point

mutations in the neighborhood of the selectivity filter [30, 47, 49, 19, 56].

2.6 Methods Summary

Initial coordinates for the molecular dynamic simulations were taken from the crystal structures 1K4C and 1K4D. Crystallographic water molecules around the single subunit in each of the two crystal structures were placed around all four subunits in the tetramer. Residues were assigned their standard protonation state at pH 7.0, except for residue Glu 71, which was protonated. The channel was embedded in a bilayer of POPC lipids and solvated in 1M KCl using the web service CHARMM-GUI (total number of atoms, 45,898). All-atom simulations were run using the CHARMM PARAM27 force field [57] under constant NVT conditions at a temperature of 310 K. Molecular dynamic simulations were carried out on the special purpose computer Anton [58] on loan to the Pittsburgh Supercomputer Center (PSC). A total of 114 molecular dynamic simulations were carried out starting from different initial conditions with respect to the inactivating water molecules, for an aggregate total time of 29.5 ms of molecular dynamics.

The two-dimensional PMFs (Fig. 2.3) with respect to the two coordinates r and z (see Appendix 2.7, Fig. 2.12) were calculated using NAMD 2.9 [59], which were carried out on the petaflop supercomputer Jaguar, located at the National Center for Computational Sciences (NCCS). The region of interest in the (r, z) space was covered by a grid of equally spaced umbrella sampling (US) windows. To improve the statistical sampling, the US calculations were performed using Hamiltonian Replica Exchange MD (US/H-REMD) simulations (also called US window swapping)[60]. Initial coordinates for the US windows were taken from the unbiased trajectories carried out on Anton. Initial coordinates for the missing windows were obtained by gradually dragging neighboring windows along the reaction coordinates to the center of each of the missing windows. Initial coordinates for the first PMF came from the 17-ms-long unbiased molecular dynamics simulation of the stable, pinched filter (Fig. 2.2a). Windows taken from this trajectory already contained three inactivating water molecules lodged behind the selectivity filter in the cavities of each of the four subunits. A series of flat-bottom harmonic distance restraints were added between channel atoms and the water oxygen of the inactivating waters to ensure that they remained present behind the filter. The flat portion of the restraints spanned 8Å above the pore helix of the channel—providing the water molecules freedom to move around a region of space purposefully designed to be larger

than the overall size of the cavity. The initial coordinates for the second PMF came from the molecular dynamics trajectory of the recovery process (Fig. 2.2d), providing windows spanning the conformational transition from the pinched to the conductive filter. Windows taken from this trajectory lacked all inactivating water molecules behind the filter. To maintain the system in this occupancy state during the US/H-REMD simulations, dummy atoms (no non-bonded interactions with the channel) positioned above the pore helix were introduced to repel any water molecule trying to enter into the cavities behind the filter from the bulk region. The first PMF comprised 137 windows whereas the second PMF consisted of 226 windows spanning the complete recovery process. All windows were equilibrated $\geq$ 0.5 ns before starting REMD. Exchange attempts were made every 1,000 steps (or 1 ps of simulation of time), and neighboring windows were swapped if the Metropolis Monte Carlo exchange probability was satisfied. US/H-REMD simulations for the two PMFs were run for more than 1 ns. The total aggregate simulation time used to produce the two US/H-REMD calculations is more than 800 ns. Windows were unbiased using the Weighted Histogram Analysis Method (WHAM) [61, 62], which only required that the umbrella sampling windows were generated according to Boltzmann statistics.

Electrophysiological measurements were made by patch-clamp recordings in channel-reconstituted liposomes prepared as described earlier [63, 64]. Purified protein was reconstituted in asolectin vesicles (in 1:100 (mass:mass) protein to lipid ratio) by dilution with 200mM KCl and 10mM MOPS buffer at pH 7.0. Residual detergent was further removed by incubation with biobeads (Bio-Rad Laboratories). Channel-incorporated liposome suspension was then centrifuged for 2 h at 100,000g and the pellet was re-suspended in 60 ml of KCl/MOPS buffer. A drop of the proteoliposome was placed on a glass slide and dried overnight in a desiccator at 4 μC. The sample was then rehydrated with 20 ml of buffer, which yielded giant liposomes. This preparation was suitable for patch-clamp recordings after approximately 2 h. Currents were recorded in 10mM MOPS buffer with indicated salt concentration. For measurements under KCl gradient, *N*-methyl-*D*-glucamine was used to replace KCl in the pipette. Recording pipettes were pulled from thin-walled borosilicate glass and heat polished such that they had a bath resistance of 1-2MV when filled with 200mM KCl, 10mM MOPS solution. All measurements in this study were conducted in the inside-out configuration of the patch clamp technique. Experiments were performed at room temperature (20-22 °C). Currents were elicited in response to pH jumps from 8.0 to 3.0 using an RCS-160 fast solution exchanger (Biologic) fed by gravity. Macroscopic currents

were sampled at 5kHz using Axon 200-B patch-clamp amplifier. For each experiment in the absence or presence of sucrose, the fractional recovery was measured at different inter-pulse intervals. There are eight sets of experiment without sucrose, and eight with sucrose. For the two conditions, the average recovery curve and its standard deviation was determined from the eight different sets, and the time constant was determined from a single-exponential least-square fit. To determine if the recovery time constant in the absence and presence of sucrose is significantly different, we fitted each of the eight individual data sets (for the two conditions) by a single exponential and determined the recovery time constant for each experiment. The two sets of eight values were subjected to an unpaired Students t-test (degrees of freedom = 4), which yielded a P value of 0.03969.

2.7 Appendix: Supplementary Figures

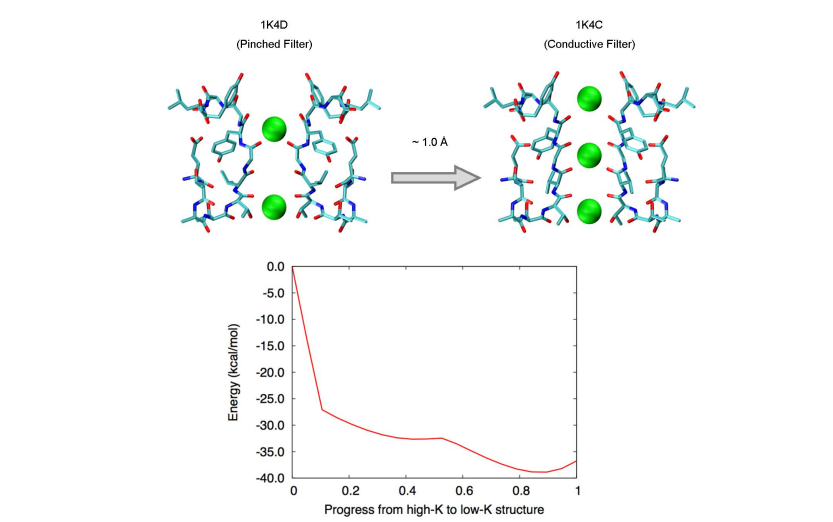

Figure 2.5: There is no structural energy barrier in going from the high-K (1K4C) to the low-K (1K4D) conformations. The energy profile was obtained by energy minimization of the KcsA structure in vacuum held by a root-mean-square-deviation (rmsd) restraint between the 1K4D and 1K4C X-ray structures using the CHARMM program.

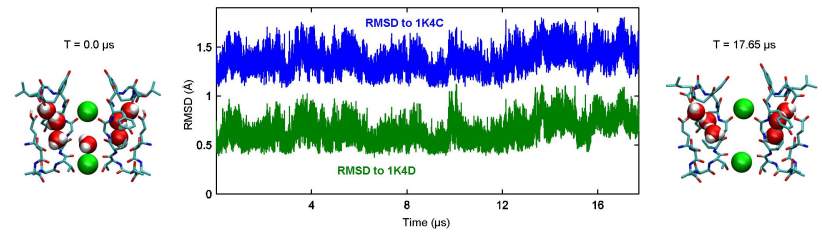

Figure 2.6: The pinched conformation of the selectivity filter is extremely stable for multiple microseconds.

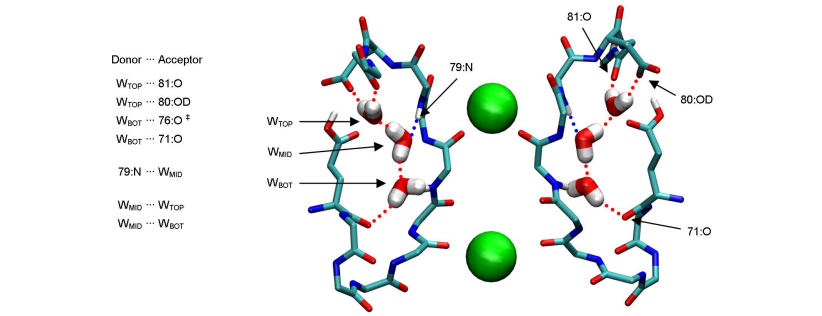

Figure 2.7: The hydrogen bonding network and 3 inactivating water molecules (top, middle, bottom). Only two subunits are shown and cross-subunit hydrogen bonds are not depicted.

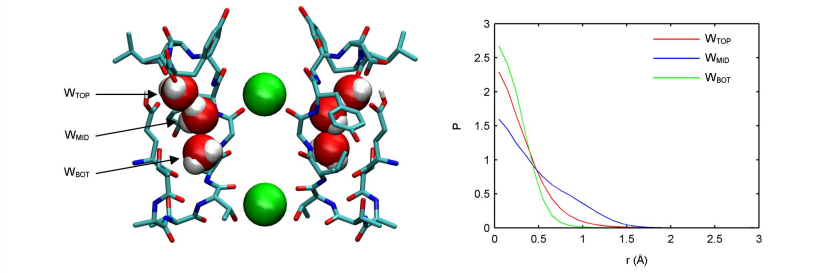

Figure 2.8: Radial distribution and position of the three inactivating water molecules (top, middle, bottom) bound to the subunit cavities behind the selectivity filter relative to the position in the X-ray structure 1K4D.

Occupancy:	W_{TOP} W_{MID} W_{BOT}	- W_{MID} W_{BOT}	W_{TOP} - W_{BOT}	W_{TOP} W_{MID} -	- - W_{BOT}	- W_{MID} -	W_{TOP} - -	- - -
Probability:	0.97	0.020	0.0011	0.0063	0.0001	0.0001	0.00001	0
Free Energy (kcal/mol):	0.0	2.4	4.2	3.1	5.6	5.7	7.1	-

Figure 2.9: Occupancy of the subunit cavities by the 3 inactivating waters (top, middle, bottom) in the 17μs MD simulation.

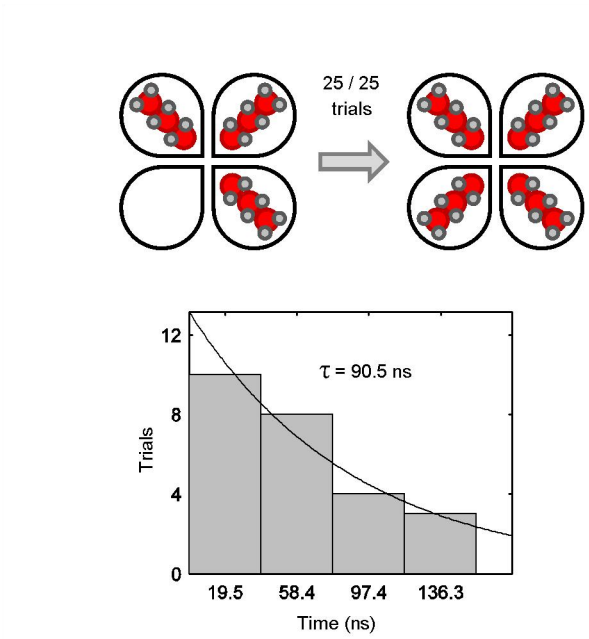

Figure 2.10: Distribution of the time for the re-entry of the 3 inactivating water molecules into one empty subunit cavity determined from 25 independent MD simulations. Each simulation, ran until it was clear that the inactivating waters formed a stable network of hydrogen bonds as described in Figure S2.7, required between 100ns to 200ns.

Observation	Starting Configuration	Ion Concentration	Configurations observed at the end of the simulation		Simulation Length (ns)[a]
			Pinched	Conductive	
Pinched filter is very stable with all inactivating waters present	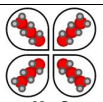 N = 3	1M KCl	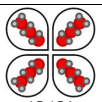 (3 / 3)		17727, 860, 502
Recovery does not occur if starting with one cavity empty of inactivating waters	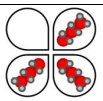 N = 25	1M KCl	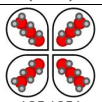 (25 / 25)		215, 197, 196, 195, 157, 136, 120, 119×4, 118, 117, 116, 116, 99×4, 98×4, 97, 39
Recovery does not occur if starting with two cavities empty of inactivating waters	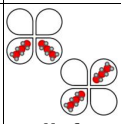 N = 6	1M KCl	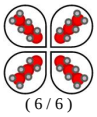 (6 / 6)		157, 115, 115, 77, 77, 39
Recovery rarely occurs if starting with three cavities empty of inactivating waters	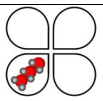 N = 33	1M KCl	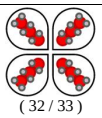 (32 / 33)	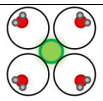 (1 / 33)	191, 190, 156, 154, 115, 77, 77, 76×3, 57, 40, 39×19, 38, 38
Recovery can occur if starting with all the inactivating waters removed	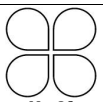 N = 26	1M KCl	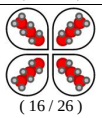 (16 / 26)	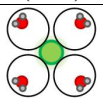 (10 / 26)	508, 267, 115, 39×8, 38×15
Recovery does not occur if starting with top inactivating waters	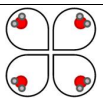 N = 4	1M KCl	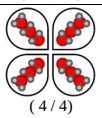 (4 / 4)		39, 39, 19, 18
Recovery requires the binding of K^+ from extracellular side	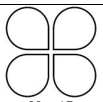 N = 15	5 mM KCl	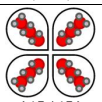 (15 / 15)		192, 191, 157, 156, 156, 154, 118, 117, 116, 116, 114, 77, 77, 76, 58
Conductive filter stable with K^+ bound inside filter	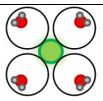 N = 2	1M KCl 5 mM KCl		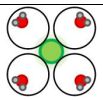 (2 / 2)	510, 399

[a]Total number of simulations:114, total aggregate simulation time: 29.5 μs.

Figure 2.11: Results of simulations starting under different conditions.

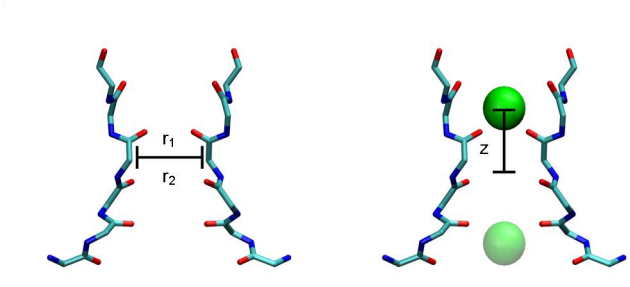

Figure 2.12: Definition of the two coordinates for the umbrella sampling simulations to compute the potential of mean force $W(r, z)$ as a function of ion re-binding (z) and the un-pinching of the filter (r). The distance z is the position of the K^+ ion relative to the center-of-mass of the backbone atoms in residues 75 to 78 of the selectivity filter and the distance r is the average C_α-C_α distance (r_1 and r_2) for the two diagonally-opposed subunits.

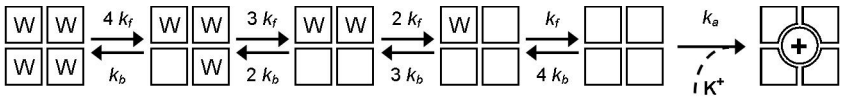

Figure 2.13: Analysis of the Markov state kinetic model. A simple analysis treating the binding of the three water molecules as completely cooperative is helpful. The probability of finding the cavity of one subunit empty is $P\{\emptyset\} = 1/(1+c^3 K_{eq}^{(3)})$, where c is the concentration of water in the system, and $K_{eq}^{(3)}$ is the equilibrium binding constant for 3 waters to the cavity of one subunit. Based on the long MD simulation, the probability $P\{\emptyset\}$ is estimated to be around 1% (the precise value is unimportant for the argument). Using this value and the concentration of bulk water, 55M, yields an equilibrium binding constant $K_{eq}^{(3)}$ on the order of about $5.95 \cdot 10^{-4}$ M^{-3}. Defining the corresponding standard binding free energy for the 3 waters as $-k_B T \ln[K_{eq}^{(3)}]$ leads to a positive value of about 4.42 kcal mol^{-1}, or about 1.47 kcal mol^{-1} per water molecule. Thus, the standard binding free energy of the inactivating waters is not favorable; it is only because of the high concentration of bulk water that the probability $P\{\emptyset\}$ is equal to 1%. Experiments show that the recovery time is about 17.6 seconds with no sucrose, and about 12.2 seconds at high osmotic stress with 2M sucrose (see Appendix 2.7, Fig. 2.10). It should be noted that the overall depth of inactivation differs if it occurs during inward versus outward current flow. The high osmotic stress is expected to affect both timescale and equilibrium for the water occupancy. The high osmotic stress cannot alter the k_f, the rate for releasing the waters. But it can alter the k_b, the rate for refilling the cavity. Furthermore, the high viscosity due to sucrose will slow down k_a the rate of binding the K^+ ion in the last step. It is assumed that the binding rate of the external K^+ ion to the selectivity filter is decreased a factor of 30 (the viscosity of 2 M sucrose is about 30 times larger than that of pure water). Using the kinetic model of Figure 2.4 to fit the experiments from Figure 2.10 (in Appendix 2.7), it is found that the rate of refilling one cavity k_b goes from 0.0126 ns^{-1} without sucrose to 0.00526 ns^{-1} with sucrose (mean times go from 79 ns to 190 ns). Therefore, the rate k_b for refilling the cavity goes down by a factor of about 2 with sucrose. Thermodynamically, this implies that one cavity goes from being empty about 1% of the time to about 2% of the time. In free energy terms, the high osmotic stress has destabilized the buried waters by about 0.7 $k_B T$ according to the kinetic rates fitted from the electrophysiological data. This value can be compared with the free energy change expected from a simple ideal gas approximation for the osmotic pressure, with $\Delta G = \Pi \cdot \Delta V$, where Π is the osmotic pressure for 2 M sucrose ($1.21 \cdot 10^{-3} k_B T/\mathring{A}^3$) and ΔV is the volume of 3 water molecules ($90\mathring{A}$). This approximation yields a ΔG equal to $0.1 k_b T$. While the ideal gas treatment underestimates the osmotic pressure and the associated ΔG, the magnitude of the free energy change is consistent with the kinetic rate constants extracted from the electrophysiological data, in support of the present mechanism. These considerations explain why the rate of recovery is accelerated in 2 M sucrose.

CHAPTER 3
QUANTITATIVE ANALYSIS OF THE WATER OCCUPANCY AROUND THE SELECTIVITY FILTER

Markus Weingarth, Elwin A. W. van der Cruijsen, Jared Ostmeyer, Sylke Lievestro, Benoît Roux, and Marc Baldus

Reprinted (adapted) with permission from Journal of American Chemical Society, 2014, 136 (5), pp 20002007.

3.1 Abstract

Recovery in K^+ channels, that is, the transition from the inactivated non-conductive selectivity filter conformation toward the conductive conformation, occurs on a time scale of the order of seconds, which is astonishingly long, given that the structural differences among the filter conformations are faint (< Å). Computational studies and electrophysiological measurements suggested that buried water molecules bound behind the selectivity filter are at the origin of the slowness of recovery in K^+ channels. Using a combination of solid-state NMR spectroscopy (ssNMR) and long molecular dynamics simulations, we sketch a high-resolution map of the spatial and temporal distribution of water behind the selectivity filter of a membrane-embedded K^+ channel in two different gating modes. Our study demonstrates that buried water molecules with long residence times are spread all along the rear of the inactivated filter, which explains the recovery kinetics. In contrast, the same region of the structure appears to be dewetted when the selectivity filter is in the conductive state. Using proton-detected ssNMR on fully protonated channels, we demonstrate the presence of a pathway that allows for the interchange of buried and bulk water, as required for a functional influence of buried water on recovery and slow inactivation. Furthermore, we

provide direct experimental evidence for the presence of additional ordered water molecules that surround the filter and that are modulated by the channel's gating mode.

3.2 Introduction

Potassium (K^+) channels share a common pore architecture for catalyzing the diffusion of ions across membranes [65, 17]. Ion passage is controlled by two coupled gates [19, 66, 34, 67]. They are located at either end of the channel pore and called the activation and inactivation gates. The inactivation gate is also known as the selectivity filter. Activation gating is associated with relatively large hinge-bending and rotational motions of the inner helix bundle, dilating the pore by about one nanometer upon channel opening [22]. In contrast, inactivation gating is accompanied by angstrom-scale local structural changes within the selectivity filter [19, 68, 30, 69, 70]. Crystal structures of KcsA from Streptomyces lividans obtained at low (3 mM, PDB: 1K4D) and high (200 mM, PDB: 1K4C) K^+ concentration [K^+]([23]) are commonly considered as representative for the closed-inactivated and closed-conductive channel gating modes, respectively [19, 71]. According to these conformations, rearrangements within the selectivity filter upon inactivation are confined to a partial flip of the V76–G77 peptide plane, pinching the filter shut. The small structural differences between the conductive and inactivated selectivity filter, however, stand in sharp contrast to the remarkably long time scale of seconds on which recovery from slow inactivation, that is, transition from the inactivated toward the conductive filter state, occurs. Recent molecular dynamics (MD) simulations[72] showed that this apparent discrepancy could be explained by the dynamics of buried water molecules bound in the back of the inactivated selectivity filter, which lock the filter in the inactivated state. MD simulations further predicted that conversion to a dewetted conductive state could only occur upon release of the inactivating water to the bulk, which was indirectly corroborated by the measurement of an accelerated recovery rate at high osmotic stress.

In a broader sense, such buried water molecules can be considered as an inherent part of the channel structure. Nevertheless, many unanswered questions remain regarding the mechanism by which the water modulates the free energy landscape associated with the conformational space of the selectivity filter, and how the distinct water occupancies are correlated with different filter conformations [48]. Previously, we have demonstrated that solid-state nuclear magnetic resonance (ssNMR) is a powerful technique to study the structural

and dynamical properties of membrane-embedded KcsA variants before and after channel inactivation [67, 68, 70]. Here, we combined ssNMR studies with long MD simulations to provide a high-resolution spatial and temporal arrangement of buried water in the rear of the conductive and the inactivated filter of membrane-embedded KcsA, which corroborates that buried water is at the molecular origin of the slowness of recovery. Moreover, we demonstrate the use of high-resolution ^{1}H detected ssNMR on a fully protonated membrane protein to dissect in atomic detail a pathway that allows the interchange of buried and bulk water, as it was suggested to be required for recovery and slow inactivation. Finally, we provide direct experimental evidence for the presence of other sources of ordered water that surround the filter and that are modulated by the states of the activation and inactivation gates.

3.3 Results and Discussion

Spatial Distribution of Ordered Water around the Selectivity Filter before and after Inactivation. In general, ssNMR experiments can report on water proximities by making use of the distinct ^{1}H chemical shift of the water resonance and the fact that polarization transfer schemes such as cross-polarization (CP) or longitudinal mixing report, in the initial rate regime, on local proton-proton proximities [73], and chemical exchange with bulk water can be neglected [68]. For $^{1}\mathrm{H} \rightarrow \mathrm{X}$ transfer, we used short CP times that restrict polarization transfer to the nearest neighbor (i.e., bonded) X nucleus [73]. Thus, ^{15}N edited experiments probe proximities around NH protons, whereas ^{13}C edited experiments are sensitive to water located close to aliphatic carbons. Note that all amino protons of the selectivity filter that we use as magnetization receptors in the ^{15}N detected experiments point directly toward the back of the filter, while aliphatic protons may be oriented toward the pore and the lower channel cavity.

First, we recorded 2D ssNMR $^{1}\mathrm{H}(^{1}\mathrm{H})^{15}\mathrm{N}$ spectra of membrane-embedded KcsA (see Experimental Section for a detailed description of the ssNMR setup) before and after channel inactivation. Using ^{13}C and ^{15}N resonance assignments obtained previously [68, 70, 74], these data provided clear evidence for higher water occupancy behind the inactivated selectivity filter (with an open activation gate) in comparison to the conductive filter conformation (with a closed activation gate). In the closed-conductive state (Figure 3.1a, red), only the upper part of the filter (G79N) showed an intense correlation with the water resonance, while such correlations were weak or entirely absent for residues of the middle and lower parts of

the filter (T78N–T74N). In the open-inactivated state (Figure 3.1b, blue), buried water is distributed along the entire rear of the filter (G79–T75), with the exception of the lowest part of the filter (T74N) that is right above a large water-filled cavity. The slightly different ^{1}H shifts of water in Figure 3.1b may indicate the presence of several water molecules behind the inactivated filter. Taken together, these ssNMR findings for the conductive and inactivated, membrane embedded channel state are hence in excellent agreement with the spread and content of buried water molecules in the low [K^+] and high [K^+] crystal structures [23], respectively (Figure 3.1c).

To characterize the distribution of buried water around aliphatic protons, we carried out a 3D ^{1}H(^{1}H)^{13}C^{13}C experiment. For open-inactivated KcsA, this experiment (Figure 3.1d) revealed clear signals in the ^{13}C–^{13}C plane at the ^{1}H water resonance for residues Y78, V76, and T75, while T74 was absent. These findings are in line with our ^{1}H(^{1}H)^{15}N data (Figure 3.1b) and confirm that buried water is confined to the upper and the middle passages behind the inactivated filter. Interestingly, ^{13}C–^{13}C cross-peaks of T75, that is located close to the dewetted residue T74, were more intense than for V76. This is not inferable from the low [K^+] crystal structure in which buried water is closer to V76 than to T75. The apparent closer proximity in the inactivated filter conformation of T75 to ordered water in comparison to V76 observed by our ssNMR data could be confirmed in a series of 2D ^{1}H(^{1}H)^{13}C experiments with varying ^{1}H–^{1}H mixing time (Figure 3.1e-g). These results suggest that cross-peak intensities correlate to differential exposure to ordered water and that they are not modulated by the ^{13}C–^{13}C PARIS spin diffusion step. The same set of ^{13}C detected experiments performed on a sample in the closed-conductive state showed an exposure to ordered water that increased toward the large water-filled cavity (T75 and T74). Notably, a few protons such as T74H$_\beta$ and T75H$_\beta$ of the selectivity filter that are monitored in our ^{13}C detected experiments point toward the selectivity filter pore and the large water-filled cavity (vide infra).

These results suggested that the ^{13}C detected experiments are, in addition to water behind the selectivity filter, sensitive to the presence of other ordered water molecules. We therefore calculated the nearest distances of water to the residues that we monitor in ^{13}C detected experiments over long MD simulations for both conductive and inactivated filter conformations (Figure 3.2a,b). For the conductive filter, the simulations clearly showed (Figure 3.2a) that water behind the filter is too distant ($\geq$ 8.0 Å) to transfer magnetization to T75 or T74, raising the question of what causes the high water access in ^{13}C detected experiments for these two residues. Ordered water within the conductive filter pore is unlikely,

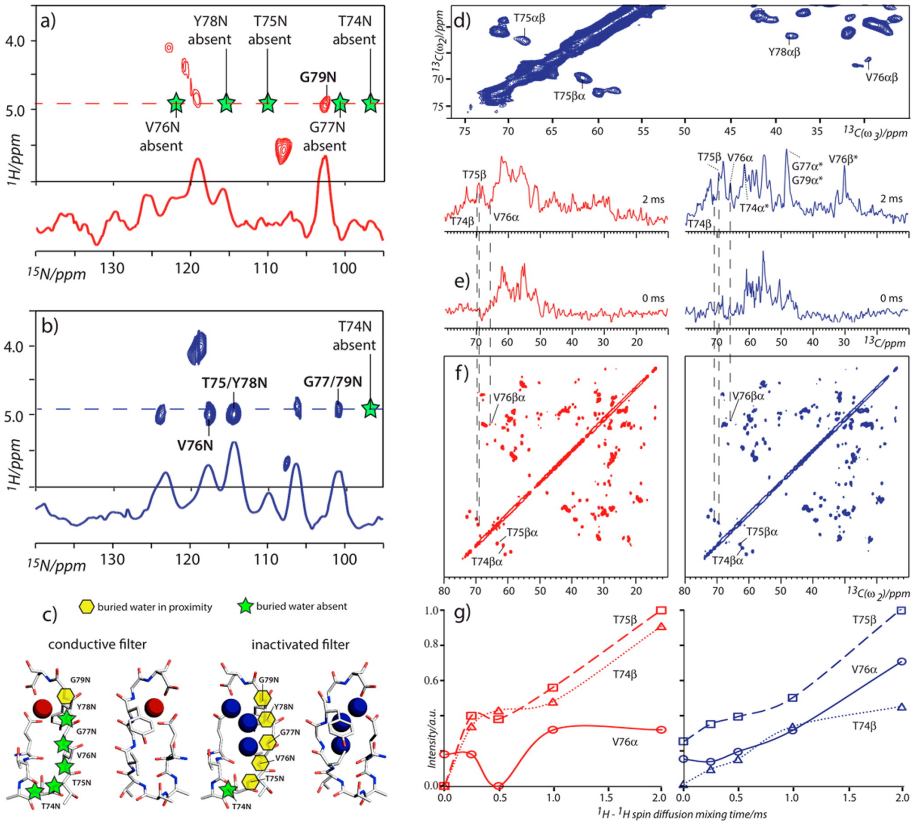

Figure 3.1: a, b, 2D ^{1}H(^{1}H)^{15}N ssNMR spectra of membrane-embedded KcsA in the closed-conductive and (top panel) the open-inactivated state (lower panel), measured at 52 kHz MAS. Cross sections along ω_2 at the ^{1}H water resonance are shown for both channel states. c, The spatial distribution and content of crystal water behind the conductive (left, PDB: 1K4C) and inactivated (right, PDB: 1K4D) selectivity filter are consistent with our ^{1}H(^{1}H)^{15}N ssNMR data. Yellow hexagons and green stars indicate ^{15}N nuclei for which ssNMR experiments suggest the presence and the absence of buried, nearby water molecules, respectively. d, ^{13}C–^{13}C plane at the ^{1}H water resonance of a 3D ^{1}H(^{1}H)^{13}C^{13}C spectrum measured on open-inactivated KcsA. e, Cross sections, extracted from a series of 2D ^{1}H(^{1}H)^{13}C measurements with varying ^{1}H spin diffusion time (2 and 0 ms from top to bottom), along ω_2 at the water resonances for both the conductive (red, left panel) and the inactivated (blue, right panel) state. Signals that are ambiguous due to spectral overlap are marked with asterisks. f, T74, T75, and V76 resonances can be retraced in PARIS [75, 76] ^{13}C–^{13}C spin diffusion spectra for conductive (red, left) and inactivated filter (blue, right) conformation. g, Build-up curves at the ^{1}H water resonance in the conductive (red, left) and inactivated (blue, right) conformations, extracted from a series of 2D ^{1}H(^{1}H)^{13}C experiments. Signal intensities were deduced from peak heights (T74C$_\beta$ in dotted lines and triangles, T75C$_\beta$ in dashed lines and squares, and V76C$_\alpha$ in continuous lines and circles). For each panel, the plots were normalized with respect to the most intense cross peak.

because water has to transverse the filter within nanoseconds to ensure fast ion flux. We hypothesize that the increased water access stems from ordered water in the closed large cavity forming a hydration complex to help K^+ to overcome the high dielectric barrier of the bilayer and to position K^+ optimally to the filter [23, 77]. Our ssNMR data suggest that both T75 and T74 are in proximity of such ordered cavity water, presumably stabilizing it with their hydroxyl functions (Figure 3.2c). Because the inner helix is supposed to stabilize ordered cavity water and moves outward upon channel opening, dilating the cavity [22], water order is presumably influenced by the mode of the activation gate and therefore attenuated in the open cavity. Indeed, in the open-inactivated state, residue T74 shows weak water access in ^{13}C detected experiments (Figure 3.1d,g). It is interesting to think about a functional role of the close proximity of the first or second ion-hydration layer to the entrance of the selectivity filter, bearing in mind that Na^+ and K^+ feature hydration shells in the cavity that are different in shape and order and also bind there with different affinities [23, 78].

The computational analysis also confirmed that water behind the inactivated filter is closer to V76H_α than to T75H_β (Figure 3.2b), which means that buried water alone is unlikely to account for the high water access of T75H_β. Remarkably, an ordered water molecule was also co-crystallized in the inactivated filter at the S3 position [23]. Such water, as shown by simulations, is very close to T75H_β (Figure 3.2b,d), often closer than 3.0 Å, and would account for its high water access in the ^{13}C detected experiments. This water in the filter featured residence times around the microsecond range in the simulations (Appendix 3.6, Figure 3.4,3.5), which will be longer at the temperatures used in our ssNMR experiments (283 K).

Taken together, our ^{13}C and ^{15}N detected ssNMR data, in reference to simulations, provide a high-resolution map of the spatial distribution of ordered water around the selectivity filter. Buried water is spread all along the inactivated filter's rear with the exception of T74, and our data suggest ordered water at the S3 position in the inactivated filter (Figure 3.2d). In the conductive filter, only the upper, extracellular part (G79) is in direct contact to buried water, while the rest of the filter is devoid of it. Moreover, with a closed activation gate, T75 and T74 seem to be in close proximity to the ordered hydration shell of cavity ions (Figure 3.2c).

High-Resolution ^1H ssNMR To Probe Water Dynamics Behind the Selectivity Filter. As an alternative and more direct means to probe the presence of buried water molecules, we resorted to high-resolution ^1H ssNMR that can be obtained by using very fast

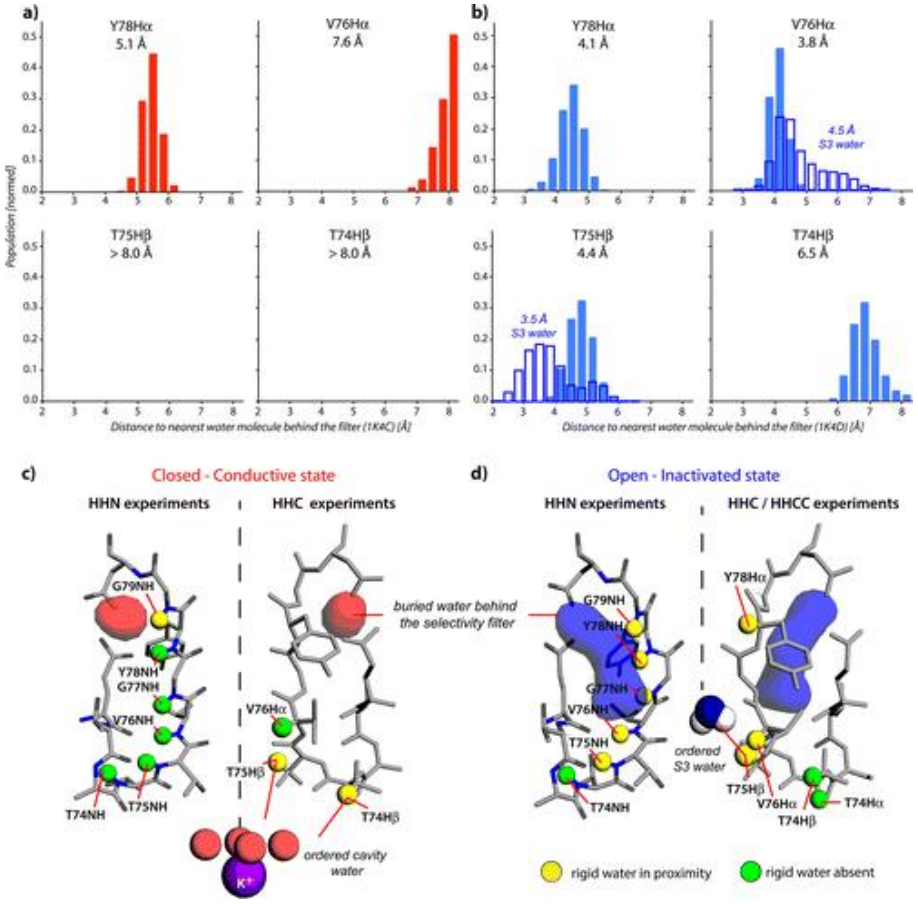

Figure 3.2: a, The distribution of nearest distances to protons of water bound behind the selectivity filter (filled columns), averaged over a long MD simulation of closed-conductive KcsA (starting with crystal structure 1K4C), calculated for filter residues resolved in $^{1}H(^{1}H)^{13}C$ ssNMR experiments. The mean distances, estimated from MD simulations, are indicated. b, Same as described in (a) for the closed-inactivated channel (starting with 1K4D). For residues V76 and T75, the nearest distances to protons of S3 water are superposed (open columns). Notably, during about 15% of the trajectory, S3 water is closer than 3.0 Åto $T75H_{\beta}$, which would pronounce spin diffusion transfer that exhibits a r^{-6} dependence on the internuclear distance r. c, Snapshot of a 1K4C simulation, representative for the distribution of buried water behind the conductive filter. The ordered K^{+} hydration shell of cavity water that was resolved in crystal structure 1K4C is illustrated below the filter. d, Snapshot of a 1K4D simulation, representative for the distribution of buried water behind the pinched filter and the water molecule at the S3 position of the filter pore. The protons used as magnetization receptors in $^{1}H(^{1}H)^{13}C/^{15}N$ ssNMR experiments are highlighted with spheres. Protons for which we observed in ssNMR experiments the proximity and the absence of buried water are color-coded in yellow and green, respectively.

MAS rates (see, e.g., refs [79, 80]) and/or by perdeuteration [81, 82]. In the latter case, ^{1}H ssNMR requires the re-protonation of protein sites via exchange with H_2O. For membrane proteins, this process is significantly slower for residues that are not solvent exposed and shielded by the lipid bilayer [83]. This property provided us with a unique opportunity to directly track residues that become protonated due to buried water on the time scale of channel recovery from C-type inactivation.

To ensure the identification of water-accessible and non-accessible amino-protons (^{1}HN), we first acquired ^{1}H detected 2D ^{15}N–^{1}H experiments at 60 kHz MAS with fully protonated open-inactivated and closed-conductive KcsA. As compared to previous work on microcrystalline proteins [84, 85], these experiments resulted in remarkably narrow ^{1}HN line widths of 0.3–0.5 ppm (Appendix 3.6, Figure 3.6) for a membrane-embedded ion channel. Spectrally well-separated ^{15}N chemical shifts of filter residues T74, G77, and G79 allowed us to identify their ^{1}HN both in indirectly and directly ^{1}H detected spectra (Figure 3.3a-d). To our knowledge, these assignments present the first ^{1}H site-specific analysis of a fully protonated membrane protein by ^{1}H detected biomolecular ssNMR. The resolution in our ^{15}N–^{1}H spectrum of fully protonated closed-conductive KcsA opened the possibility to monitor structural changes in reference to function in the canonical GYG motive of the K^+ channel superfamily. Crystal structures [23] showed G77NH to flip upon inactivation, and G77HN indeed exhibited a stark ssNMR resonance shift ($+\Delta$1.8 ppm) to low-field in the inactivated filter conformation (Figure 3.3a,c). As revealed by a computational analysis, the chemical shift change of G77HN may reflect the rotation of G77NH away from the filter's rear, where G77HN is less exposed to the shielding ring-current effect of Y78 (Appendix 3.6, Figure 3.3). Moreover, the shift of T74HN toward high-field ($-\Delta$0.5 ppm) upon opening of the activation gate is in line with a flip of the F103 ring-plane, facing T74, which was shown to be critically involved in the coupling of activation gate and selectivity filter [19, 56]. Note that such investigations of proton chemical shifts are precluded when using perdeuterated samples, because T74HN and G77HN are not exposed to water in all filter states (Figure 3.1a,b).

Next, we sought to characterize the water dynamics behind the filter by ssNMR, which is essential to convey a functional importance to buried water. Simulations demonstrated the necessity of an interchange from buried to bulk water to initiate recovery and implied long residence times for buried water to be at the molecular origin of recovery. We intended to study water dynamics by exploiting the exchangeable character of amino protons. For

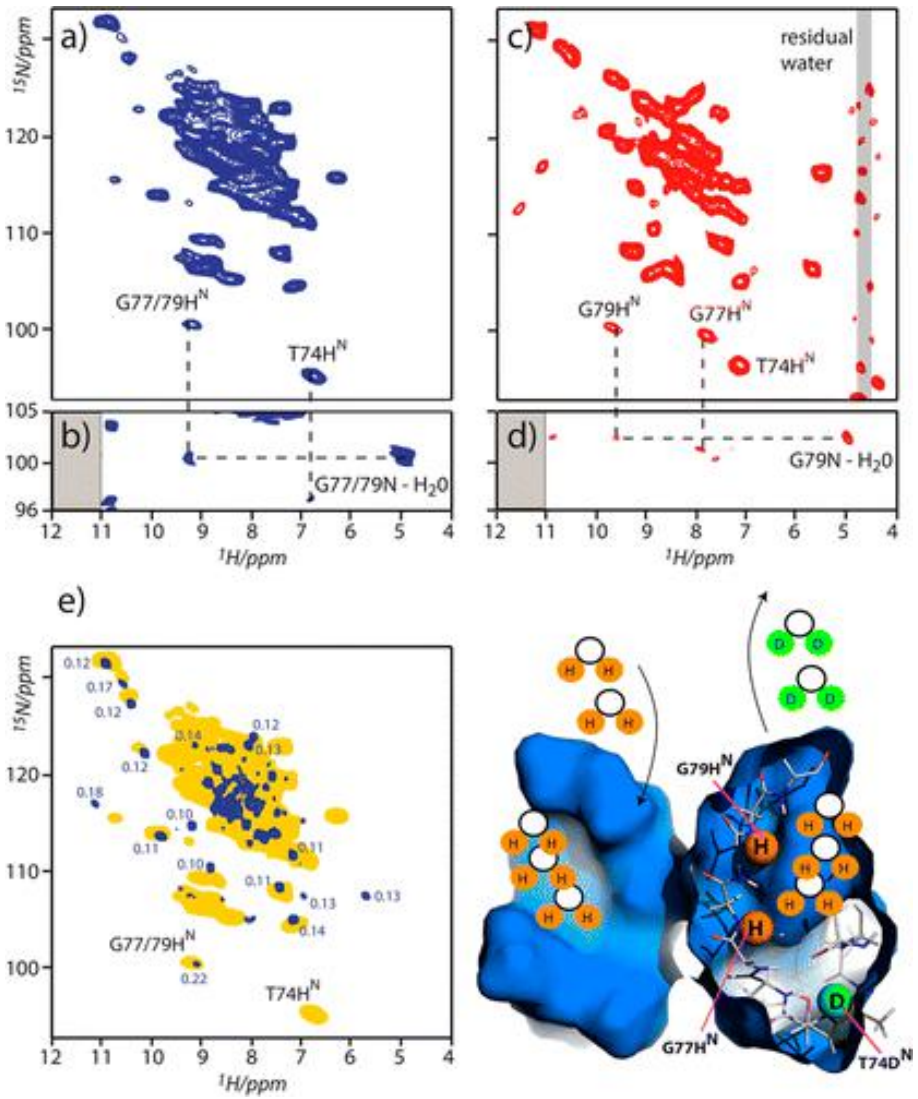

Figure 3.3: a, c, 2D ^{15}N-^{1}H spectrum of fully protonated open-inactivated and closed-conductive KcsA, respectively, measured at 60 kHz MAS and 18.8 T static magnetic field (800 MHz ^{1}H frequency). b, d, Cutouts of ^{1}H(^{1}H)^{15}N ssNMR spectra of open-inactivated and closed-conductive KcsA, respectively. The gray boxes indicate the limits of the spectral width, and the adjacent signal intensity is spurious. e, (right) Comparison of 2D NH data on (^{1}H, ^{13}C, ^{15}N; in yellow) membrane-embedded KcsA in the open-inactivated state to an equivalent (^{2}H, ^{13}C, ^{15}N; in blue) sample after washing in acidic H_2O buffer. The blue numbers represent the ^{1}H line width at half-height (in ppm) of resolved cross-peaks and the G77/G79 signal extracted from the spectrum of the back-exchanged deuterated channel.

this purpose, we acquired 2D ^{15}N-^{1}H experiments on a membrane-embedded perdeuterated (^{2}H, ^{13}C, ^{15}N) KcsA sample, which was washed in an acidic (pH 3.5) H_2O buffer solution. We compared our data to results obtained on the fully protonated channel, which allowed straightforward identification of ^{1}HN of G77/G79 as water accessible and the ^{1}HN of T74 as non-accessible (Figure 3.3e). Importantly, protonation of G77 and G79 confirmed the presence of a pathway from bulk to buried water that is restricted to the upper part of the filter. An analysis of the ^{1}H line width showed that the G77/G79 ^{1}HN signal exhibits a much larger (0.22 ppm) line width than other resolved cross-peaks (0.10–0.13 ppm), suggesting that both G77/G79 amino deuterons exchanged to ^{1}H (Figure 3.3e). These results provide direct experimental evidence that bulk water can occupy the cavity behind the selectivity filter, as it was shown to be required for slow inactivation, and also suggest the possibility of the reverse process, release of inactivating water to the bulk, as required for recovery. Importantly, the ^{1}HN assignments also hint at the nature of the water hydrogen-bonding network behind the inactivated selectivity filter [77]. While we observe (Figure 3.3e) that the ^{1}HN of G77/G79 are water-exposed, and according to simulations [72] directly hydrogen bonded to buried water, we simultaneously observe sharp G77/G79 ^{15}N–^{1}HN and ^{15}N–$^{1}H^{H_2O}$ correlations (Figure 3.3b). Hence, these experiments suggest that buried water resides behind the filter on the NMR time scale (and possibly beyond, which is in line with computational studies [72], in which buried water remained bound behind the inactivated filter during a 17 μs MD simulation).

3.4 Conclusions

Our study demonstrates the presence of several ordered water molecules surrounding the selectivity filter of membrane-embedded K+ channels and that these water molecules are directly correlated with the channel gating cycle. By combining ssNMR experiments and computational data, we could sketch a high-resolution map of the spatial and temporal distribution of buried water behind the filter that clearly shows a plus of water with extended residence times behind the inactivated filter and corroborates the notion that buried water governs recovery kinetics. Moreover, we demonstrated the presence of a pathway that allows for the interchange of buried water and bulk water, as required for recovery and slow inactivation, and we find spectroscopic evidence for conformational changes of the GYG signature sequence that accompany inactivation. We want to emphasize that many of these experi-

mental results were only possible by ^{1}H detection in fully protonated membrane proteins, an approach that bears the capacity to monitor protons of all protein sites irrespective of their access to water. Such studies may have far-reaching advantages to investigate exchangeable protons of the inner core of membrane and fibril proteins, which have been shown to be exceptionally stable [83, 86, 87].

In general, our study illustrates the correlation between selectivity filter conformational space and the exposure to ordered water consistent with the notion of water acting as an inherent part of the gating mechanism that steers the sampling of selectivity filter conformational space. Such processes may be of general importance to the regulation of potassium channels, for instance, by heterogeneous channel opening kinetics, referred to as modal gating [48, 88]. In this study, we discovered additional ordered water molecules that are located in and below the filter that could potentially act as regulatory elements of channel function. Moreover, ordered water molecules may enhance the coupling of the selectivity filter to the rest of the channel, acting as mediators that transmit conformational changes in the pore helix and turrets, which are both sensitive to the membrane environment, to the inactivation gate [70, 89].

We have demonstrated the great potential of solid-state NMR to investigate buried water molecules as an intrinsic part of ion channels in a native-like environment with the prospect of studies in native environments [90]. Such studies are of general relevance for membrane proteins, and sources of buried water as structural or functional modulators have been reported for transporters [91], G protein coupled receptors [92], and enzymes of the respiratory chain [93], to name only a few examples. As it was shown by solution NMR [94, 95], such buried water molecules may be further exploited as potential probes of intrinsic protein dynamics and the underlying energy landscape.

3.5 Experimental Section

Solid-State NMR Spectroscopy. SSNMR experiments were performed using NMR spectrometers (Bruker Biospin) at magnetic fields of 16.4 and 18.8 T with 52 and 60 kHz magic angle spinning (MAS), respectively. The sample temperature was 283 K (52 kHz MAS) and 300 K (60 kHz MAS). We used 2D ^{1}H(^{1}H)^{15}N/^{13}C and 3D ^{1}H(^{1}H)^{1}3C^{1}3C experiments (Appendix 3.6, Figure 3.8) to probe buried water molecules, transferring magnetization from rigid protons to protein heteronuclei ^{13}C or ^{15}N by a short cross–polarization step (200 μs

for ^{13}C, 600 μs for ^{15}N). The slightly longer ^{1}H–^{15}N contact time was chosen to compensate for local backbone dynamics of the selectivity filter [96]. To facilitate transfer from buried water molecules to the protein, a short ^{1}H–^{1}H spin diffusion step (1.2 ms in ^{15}N and 0–2 ms in ^{13}C detected experiments) was added prior to cross-polarization. Our experimental setup is close to those used to relate membrane protein bulk water-accessibility to membrane protein conformation [68, 97, 98], with the difference that a T_2 filter to suppress rigid sample components was omitted to avoid relaxation of possibly buried and rigid water molecules. Our experimental setup is sensitive to water that is immobilized on the time scale of microseconds and beyond. Note that the application of very fast MAS in this study allows the observation of ordered water molecules without the necessity of ^{1}H homonuclear dipolar decoupling during the ^{1}H evolution time. ^{13}C–^{13}C spin diffusion mixing at 52 kHz MAS was carried out using PARIS [75, 76], with the standard pulse length = $0.5\tau_{rot}$ (N = 0.5) and 30 kHz recoupling amplitude over 200 ms. Heteronuclear high [99] (pulse length $0.9\tau_{rot}$) and low power [100] PISSARRO decoupling was applied during all heteronuclear and proton acquisition periods, respectively. The MISSISSPI solvent suppression scheme [101] was used in ^{1}H detected experiments. ^{13}C and ^{15}N resonance assignments were taken from refs [70, 74].

Sample Preparation. Expression, purification, and reconstitution in asolectin of protonated uniformly ^{13}C, ^{15}N labeled KcsA followed earlier work (refs [70, 102]). The perdeuterated KcsA sample was expressed for 12 h to an OD600 of 1.3 in a medium containing 100% D20, uniformly ^{2}H, ^{13}C labeled glucose, and $^{15}NH_4Cl$. Uniformly ^{2}H, ^{13}C, ^{15}N labeled KcsA was washed two times for 1.5 h in 0 mM K^+/ 150 mM Na^+/10 mM H_2O citrate buffer. Purification steps where done in neutral H_2O buffers. As in refs [68, 70], samples at pH 3.5 were prepared by washing proteoliposomes with 100 mM citrate buffer, yielding the same ionic strength as the phosphate buffer used for pH 7.5 samples. All reconstitution was performed at a 100/1 lipid/protein molar ratio.

Molecular Dynamics Simulations. Initial coordinates for the Molecular Dynamics simulations of the both the conductive and the pinched selectivity filters were taken from the crystal structures 1K4C and 1K4D, respectively [23]. Crystallographic water molecules for each of the four subunits of the channel were included at the start of the simulations. With the exception of Glu71, which was protonated, all residues were assigned their standard protonation state at pH 7.0. The channels were embedded in a bilayer of POPC lipids and solvated in 1.0 M KCl using the web service CHARMM-GUI (total number of atoms, 45898). All-atom simulations were run at a temperature of 310 K under constant NVT

conditions using the CHARMM PARAM27 force field. Simulations of the conductive filter were run for 510 ns, while simulations of the pinched selectivity filter were run for 17.7 μs. All simulations were carried out on the special purpose computer Anton on loan to the Pittsburgh Supercomputer Center (PSC) [58].

3.6 Appendix: Supplementary Figures

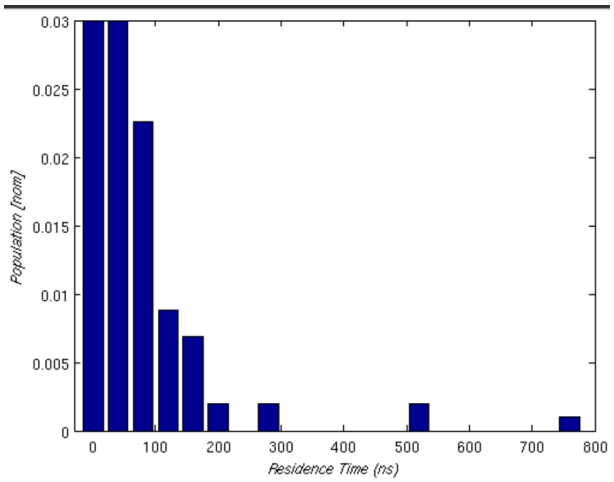

Figure 3.4: Distribution of the residence times of water in position S3 of the pinched selectivity filter calculated from the Molecular Dynamics simulation. The residence time is defined as the amount of time between when an individual water molecule first enters the position S3 to when that same water molecule leaves S3, which occurs when the water molecule is displaced by another molecule or when the position is left vacant. The mean residence time is 13.8 ns, the longest residence time we observed was about 750 ns. The major factor determining the residence time is whether or not a K^+ ion is present in S4. When an ion is present, the water molecule is trapped giving rise to the long residence times observed. However, during the simulations the K^+ ion present in S4 frequently exited the selectivity filter, which was likely the result of starting the simulation without any other K^+ ions inside the inner cavity. Hence, the presence of additional ions in the cavity is likely to result in extended water residence times at the S3 position (see Figure S1b).

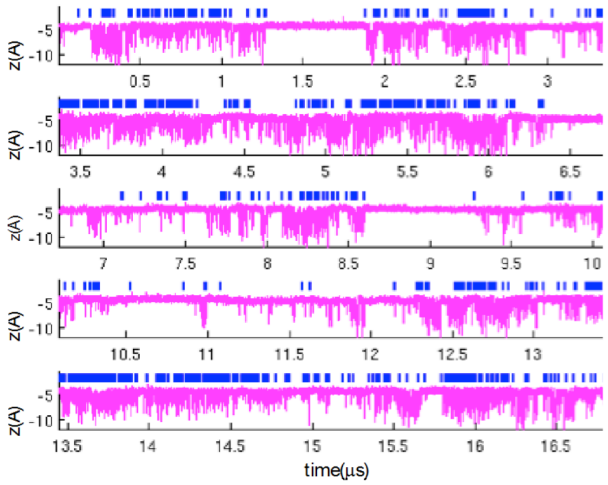

Figure 3.5: (Magenta) Plot of the height of the K^+ ion along the pinched selectivity filter as it repeatedly exchanges between position S4 of the selectivity filter and the inner cavity. (Blue Bars) Raster plot shows events where the water molecule leaves its position in S3 of the selectivity filter. These events correspond to times when the K^+ ion is not stably bound into the site S4.

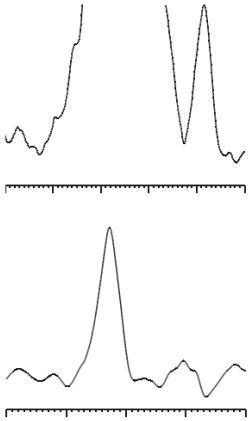

Figure 3.6: Examples for the ^{1}H-resolution in the 2D ^{15}N–^{1}H experiments measured at 60 kHz MAS and 800 MHz static field (^{1}H-frequency) with membrane-embedded KcsA in the open-inactivated (top) and closed-conductive (bottom) state. The ^{1}H-line width was measured at half-height.

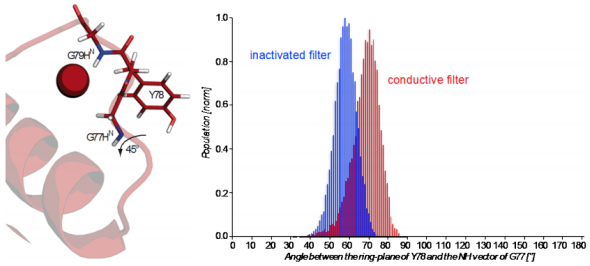

Figure 3.7: (right) Crystal structures (PDB code 1K4C and 1K4D) showed G77NH to flip upon inactivation, and G77HN indeed exhibited a stark ssNMR resonance shift (+1.8Δ ppm) to low-field in the inactivated filter conformation (see Figure 3.3a,b of the main text). (left) A computational analysis shows that G77HN moves away from the shielding effect of the Y78 ring-plane if the filter adopts the inactivated conformation. The angles were measured over the course of the Molecular Dynamics simulations between the vector normal to the plane of Y78 and the vector spanning from G77HN to the center of the ring of Y78.

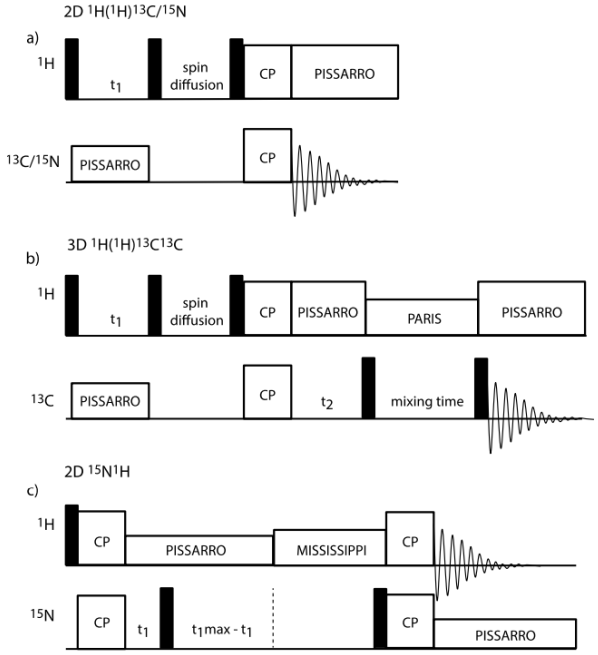

Figure 3.8: a, b, c, Schematic representation of 2D ^{1}H(^{1}H)^{15}N/^{13}C, (top panel) 3D ^{1}H(^{1}H)^{13}C^{13}C and (middle panel) ^{1}H-detected 2D ^{15}N^{1}H experiments (bottom panel). 90° pulses are indicated by filled rectangular boxes. The MISSISSIPI scheme (with = 10 ms and L = 2) for solvent suppression was applied over a total of 80 ms. Low power (LP) PISSARRO decoupling was carried out using standard parameters (decoupling amplitude $v_{LP-decoupling} \approx {}^{1}/_{4}v_{rot}$; pulse length $tau_p \approx {}^{15}/_{16}v_{LP-decoupling}$).

CHAPTER 4
ENTRY INTO INACTIVATION

4.1 Abstract

Two factors have been experimentally identified to destabilize the conductive conformation of the potassium channel selectivity filter and promote entry into C-type inactivation: Prolonged activation and low extracellular K^+ concentration. The influence of these two factors on the selectivity filter is investigated using molecular dynamic simulations of the bacterial channel KcsA in a solvated lipid membrane. Under the presence of either factor, the conductive conformation of the selectivity filter is destabilized, driving the filter to transition to a constricted conformation. Systematically, the transition is preceded by the entry of water molecules behind the selectivity filter. Removing these waters from behind the constricted filter results in the transition back to a conductive conformation. In contrast, almost no water molecules are observed behind the filter when the conditions that promote C-type inactivation are absent, allowing the filter to remain in a conductive state. These results support the view that the constricted filter conformation observed in X-ray crystallographic structures represents the C-type inactivated state.

4.2 Introduction

The bacterial potassium channel KcsA can serve as a useful prototype for studying C-type inactivation. While it lacks the complex gating machinery of a proper voltage sensing domain and is instead activated by the low pH, the sequence homology of the pore region is greater than 70% and the amino-acid composition of the selectivity filter—TTVGYG—is identical [103] [104, 105]. Macroscopic current recordings of the bacterial channel reveal telltale signs of C-type inactivation: Current decreases after the channels are opened, the precise rate of inactivation is sensitive to the external K^+ concentration, and the timescale required for the channels to return to a conductive ready state is on the order of tens of seconds [29]. Furthermore, mutations introduced in the vicinity of the selectivity filter have been found

to either enhance or abolish inactivation, localizing the underlying conformational change to the selectivity filter [30].

During C-type inactivation, current passing through the channel will decrease over time after application of an external activating stimulus that opens the channel. It is well known that the activation gate, located on the intracellular side, will remain open and that the loss of current is mediated by a conformational transition taking place in the selectivity filter. Allowing the activation gate to close by removing the external stimulus somehow resets the selectivity filter back to a conductive ready state. Together, the activation gate and selectivity filter form two distinct, inversely coupled gates. A hypothetical free-energy landscape summarizes this knowledge (Fig. 4.1a). When the channel is opened the selectivity filter inactivates, and when the channel is closed the selectivity filter spontaneously returns to conductive ready conformation. Reducing the concentration of extracellular K^+ also lowers the relative stability of the conductive filter state, providing an alternative mechanism for controlling the conformation of the selectivity filter [50, 106].

X-ray crystallographic structures of KcsA have been captured under conditions that may promote specific conformations of the selectivity filter. The initial structures published by the MacKinnon lab revealed the activation gate (Fig. 4.1b) in its closed state with the selectivity filter in the conductive conformation (Fig. 4.1c) [107]. After soaking K^+ out of the crystals to destabilize the conductive conformation of the selectivity filter, the C_α atoms of the central glycine residues (position 77) were found to have moved inward by $\sim$1Å on each subunit leaving the filter pinched shut (Fig. 4.1c) [107]. Recently published structures of KcsA obtained under a high K^+ concentration with the activation open, a conformation expected to promote the C-type inactivated state, (Fig 4.1b) revealed the selectivity filter to be in the same constricted conformation (Fig 4.1c) [19]. This in addition to structural data of KcsA obtained using solution and solid state nuclear magnetic resonance (NMR) supports the view that the pinched conformation of the filter represents the C-type inactivated state [34, 35].

Despite this body of evidence, objections have been raised as to whether the constricted conformation of the selectivity filter actually corresponds to the C-type inactivated state. Conditions designed to promote inactivation, which appear only transiently during C-type inactivation, are immutably present in the crystal structures, which leaves open the possibility that the pinched conformation is a relaxed state inaccessible during normal channel operations. Reports of a long-lived defunct state of the selectivity filter, observed in the com-

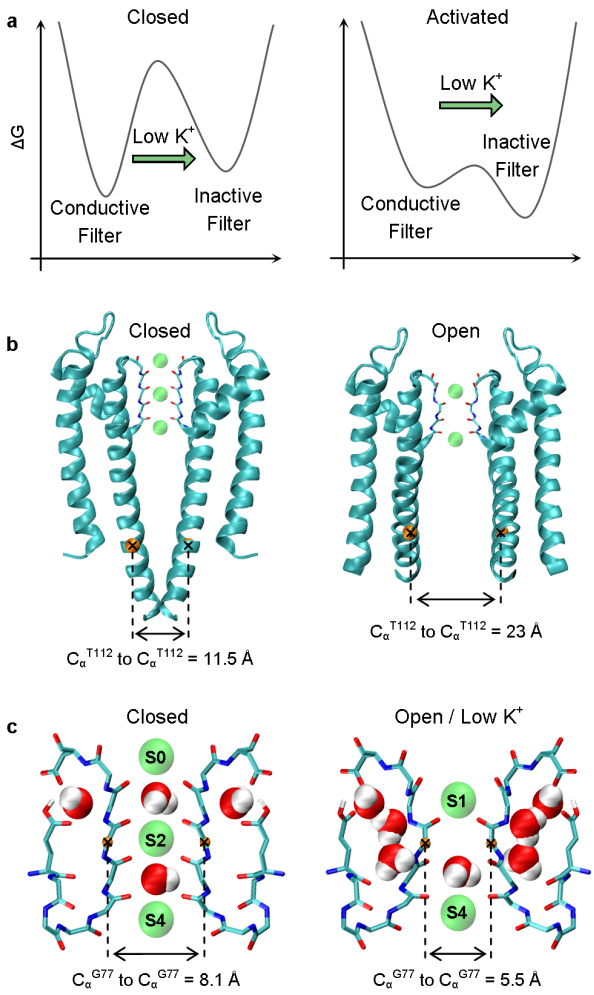

Figure 4.1: a, Hypothetical free energy landscape of the selectivity filter for both the closed (Left) and activated states (Right) of a potassium channel. b, Representation of the left and right subunits of KcsA with the activation gate closed generated from the X-ray crystallographic structure 1K4C (Left). The distance between C_α atoms of residue T112 is larger when the activation gate is open, as revealed by the X-ray crystallographic structure 3F7V (Right, helical ends modeled). c, Close up of the KcsA selectivity filter (Hydrogen atoms and water molecules modeled). The selectivity filter is observed to be in a conductive state when the activation gate is closed (Left). The distance between the C_α atoms of the central glycine residues decreases under conditions of low-K^+ and in some X-ray crystal structures of an open channel, leaving the filter too narrow for K^+ permeation (Right).

plete absence of external K^+, have been cited to support this hypothesis [108]. According to this viewpoint, the true C-type inactivated state could possibly be an intermediate step to the constricted conformation of the filter, which would represent a more deeply inactivated state of the channel [43]. To help resolve this debate, Molecular Dynamic (MD) simulations are used to study the two factors that promote C-type inactivation: Low-K^+ conditions and an open activation gate. Observations from these simulations might be relevant to several types of potassium channels because the conditions that promote C-type inactivation appear to be conserved in all of the channels that share the same selectivity filter sequence.

4.3 Results

4.3.1 Simulation of channel with closed gate under low-K^+

It has been previously reported that during Molecular Dynamic simulations of Kcsa, the selectivity filter will constrict in the complete absence of K^+ [109, 110]. In our preliminary study, we replicated these results on a channel with a closed activation gate. The selectivity filter was initially placed in a conductive conformation with only water molecules occupying each of its K^+ binding sites (see Appendix 4.7, Fig. 4.12a). After several hundred nanoseconds, the selectivity filter collapsed to a four-fold symmetric state that measures approximately the same distance across at the central glycine residues as the constricted state (see Appendix 4.7, Fig. 4.12b). The final conformation of the filter closely matched the observed crystallographic structures with one subtle exception: The Val76–Gly77 amide plane was rotated out of place by $\sim$180°.

Starting a simulation without any cations to counter-balance the electronegative carbonyl oxygen atoms places the conductive selectivity filter in a highly unstable initial configuration. To ascertain the outcome under a more appropriate setting, a simulation of the closed channel starting with a conductive filter properly coordinated by K^+ ions is carried out (Fig. 4.2a). The external K^+ concentration is equivalent to only 5 mM KCl to promote the inactivated state of the channel. After nearly 800 ns, the selectivity filter grossly dilates before undergoing a final conformational transition to a constricted state (Fig. 4.2b). In the selectivity filter the K^+ binding sites are designated S0 through S4, with S0 being the most extracellular binding site. A plot of the K^+ ions along the permeation pathway reveals that as the filter dilates the K^+ ion in S2 exits, leaving only a single K^+ ion in S4 (Fig.

4.2c). With most of the K^+ binding sites vacant, the filter enters the pinched conformation like in the preliminary results. By the end of the simulation the Val76–Gly77 amide plane settles to the same orientation seen in X-ray crystallographic structures of the constricted conformation on two of the four subunits.

Previous studies have shown that water molecules buried behind the selectivity filter play a critical role in stabilizing the pinched filter [72, 111]. To track the movement of water molecules behind the filter, we plot their distance to the C_α atom of residue 74, which is located underneath where the water molecules are found to bind (see Appendix 4.7, Fig. 4.11c). The plot shows water molecules penetrating behind the selectivity filter of the first subunit well before the conformational transition begins (see Appendix 4.7, Fig. 4.2d). However, the three remaining subunits remains empty of water until after the transition starts. The filter never undergoes a reverse transition back to a conductive state, presumably because the presence of water molecules behind the filter of all four subunits stabilizes the constricted conformation, locking the filter in the constricted conformation during the rest of the simulation.

To verify that the constriction of the filter is due to the low external K^+ concentration, it is necessary to simulate the channel in a high-K^+ environment as a control. The simulation of a closed channel starting with a conductive filter is shown in Figure 4.3. The selectivity filter remains in a conductive conformation throughout the entire simulation as expected (Fig. 4.3b). A plot of the K^+ ions along the permeation pathway of the filter reveals it is always properly coordinated by ions (Fig. 4.3c). Water molecules rarely visit behind the filter and remain their only transiently (Fig. 4.3d) in contrast to the simulation obtained under a low external K^+ concentration. The fact that water molecules precede the transition to a constricted conformation but are largely absent when the filter remains conductive suggests that water may play an active role in destabilizing the conductive filter.

4.3.2 Simulation of channel with open gate

Like other potassium channels, the activation gate of KcsA is made of two transmembrane α-helices per subunit. The transmembrane helices from the four subunits cross like poles on a tepee to form a tight bundle when the channel is closed and splay away from each other as the channel opens. Electrostatic interactions at the intracellular side of KcsA keep the activation gate shut [112]. Positive charges located on residues Arg117, Arg121, and

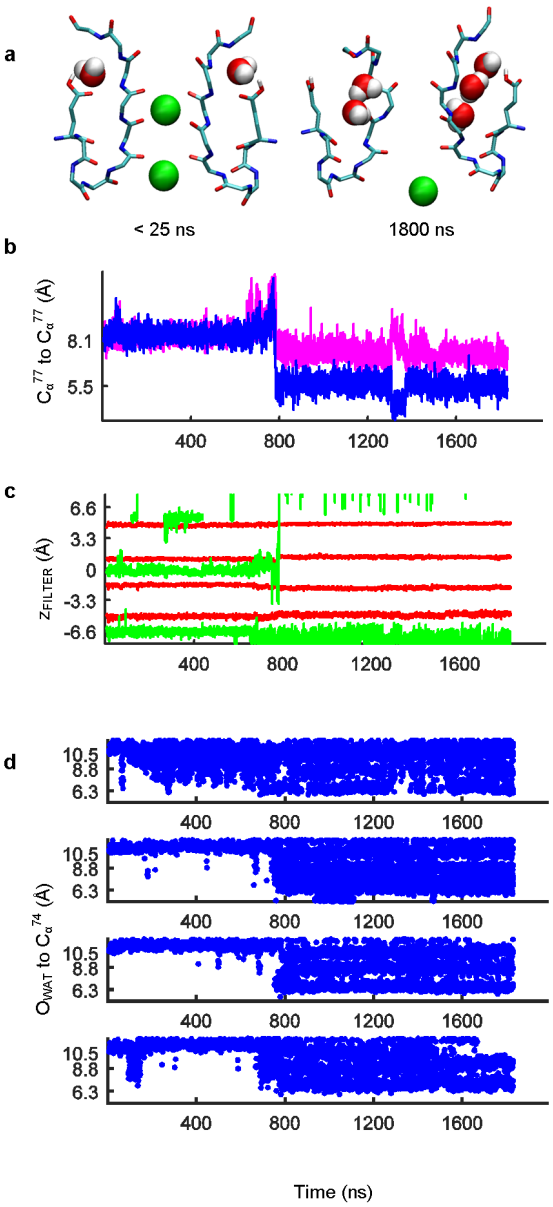

Figure 4.2: Simulation of KcsA with its activation gate closed under low-K^+ conditions. Initial coordinates taken from the crystal structure 1K4C. a, Snapshots of the filter at the beginning and end of the simulation. b, Width of the selectivity filter plotted along the reaction coordinates r_1, r_2 (see Appendix 4.7, Fig. 4.11). The filter remains conductive until about 800 ns into the simulation, at which point the filter dilates and then collapses shut. c, Position of the K^+ ions (green) in the selectivity filter plotted along the reaction coordinate z superimposed over the position of the carbonyl oxygen atoms that line the filter (red). Ions can be seen leaving the selectivity filter at 800 ns. d, The penetration of water molecules behind the filter is plotted along the reaction coordinate p (see Appendix 4.7, Fig. 4.11). Water molecules observed penetrating the first subunit before it underwent a conformational transition.

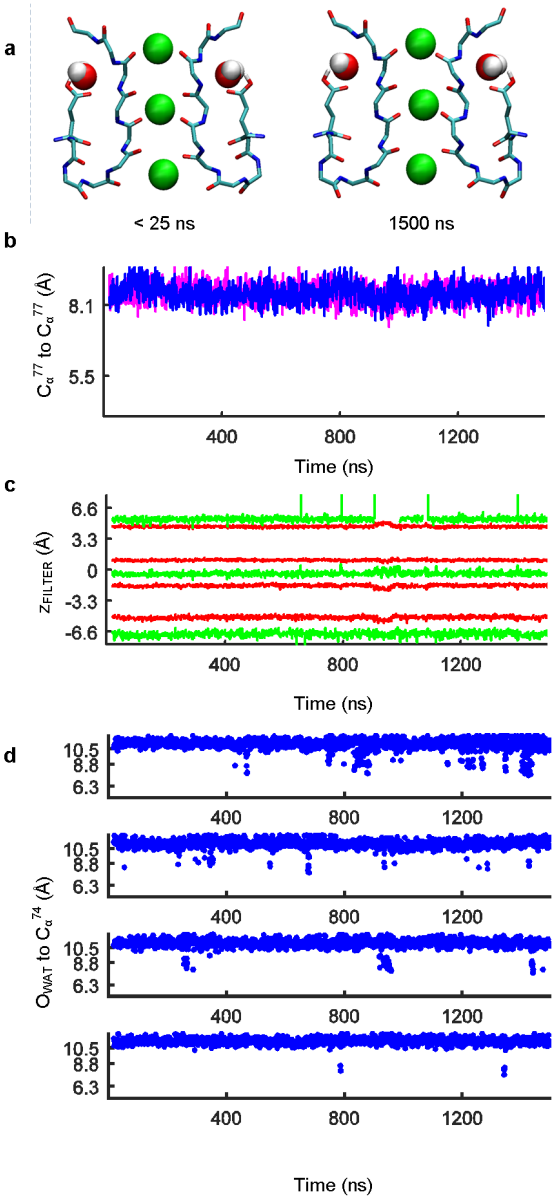

Figure 4.3: Simulation of KcsA with its activation gate closed under high-K^+ conditions. Initial coordinates taken from the crystal structure 1K4C. a, Snapshots of the selectivity filter at the beginning and end of the simulation. b, Width of the selectivity filter plotted along the reaction coordinates r_1, r_2 (see Appendix 4.7, Fig. 4.11) reveals that the filter remains conductive. c, Position of the K^+ ions (green) in the selectivity filter plotted along the reaction coordinate z superimposed over the position of the carbonyl oxygen atoms that line the filter (red). Ions remain present throughout the entire simulation d, Few water molecules observed to penetrate behind the selectivity filter along the reaction coordinate p (see Appendix 4.7, Fig. 4.11).

Arg122 are believed to attract negative charges located on residues Glu118 and Glu120 on the neighboring subunits [112]. The electrostatic balance is disrupted by lowering the pH, allowing the channel to open. By protonating the channel, residues at the bottom of the activation gate pick up an extra positive charge, masking the negative charges from the glutamic residues. Several residues could potentially become protonated including Glu118 and Glul20 as well as His25 and His124. By systematically mutating these residues to cysteines, the Perozo lab determined that the residues at position 25 and 118 make the largest contribution to activation [112].

The X-ray crystallographic structures of KcsA deposited in the PDB provides an opportunity to study the coupling of the activation gate to the selectivity filter. The KcsA structure reported to have the most open conformation of the activation gate, which the PDB identifies as 3F5W, represents the most extreme opening of the channel [19]. However, preliminary simulations revealed that the activation gate is unstable and actually begins to close even though residues His25 and Glu118 are protonated. Protonating different residues along the activation gate makes to difference to the outcome—the activation gate appears to be unstable in these simulations as well. In each simulation, the instability in the structures appears to occur around residue Phe103. Plotting the mean cross-subunit distance between opposing C_α atoms of this residue reveals the activation gate collapses shut in each case (Fig. 4.4a). By the end of each simulation, the distance measurement is no difference than that of a closed channel (Fig. 4.4c). To ascertain if another open structure of KcsA might remain stable, we turned to the crystallographic structure 3F7V, which is the second most open structure of KcsA [19]. Simulations reveal that the activation gate is stable when either residues His25 and Glu118 or residues His25, Glu120, and His124 are protonated (Fig. 4.4b). A comparison of the two crystal structures reveals why the second structure 3F7V is stable when the first one 3F5W is not. The α-helix at Gly104 skips a turn in 3F5W completely disrupting the intramolecular hydrogen bond network of the α-helix at that site (see Appendix 4.7, Fig. 4.13a). Although the presence of a glycine residue also disrupts the hydrogen bond network at the same spot in 3F7V, the α-helix does not skip a turn, preserving some of the intramolecular hydrogen bonds (see Appendix 4.7, Fig. 4.13b). Therefore, the structure 3F7V is used in the rest of this study.

To test whether the open activation gate destabilizes the conductive conformation of the selectivity filter, four independent MD simulations of the KcsA channel were carried out (341 ns, 1588 ns, 1130 ns, 450 ns). In each simulation, the selectivity filter makes a

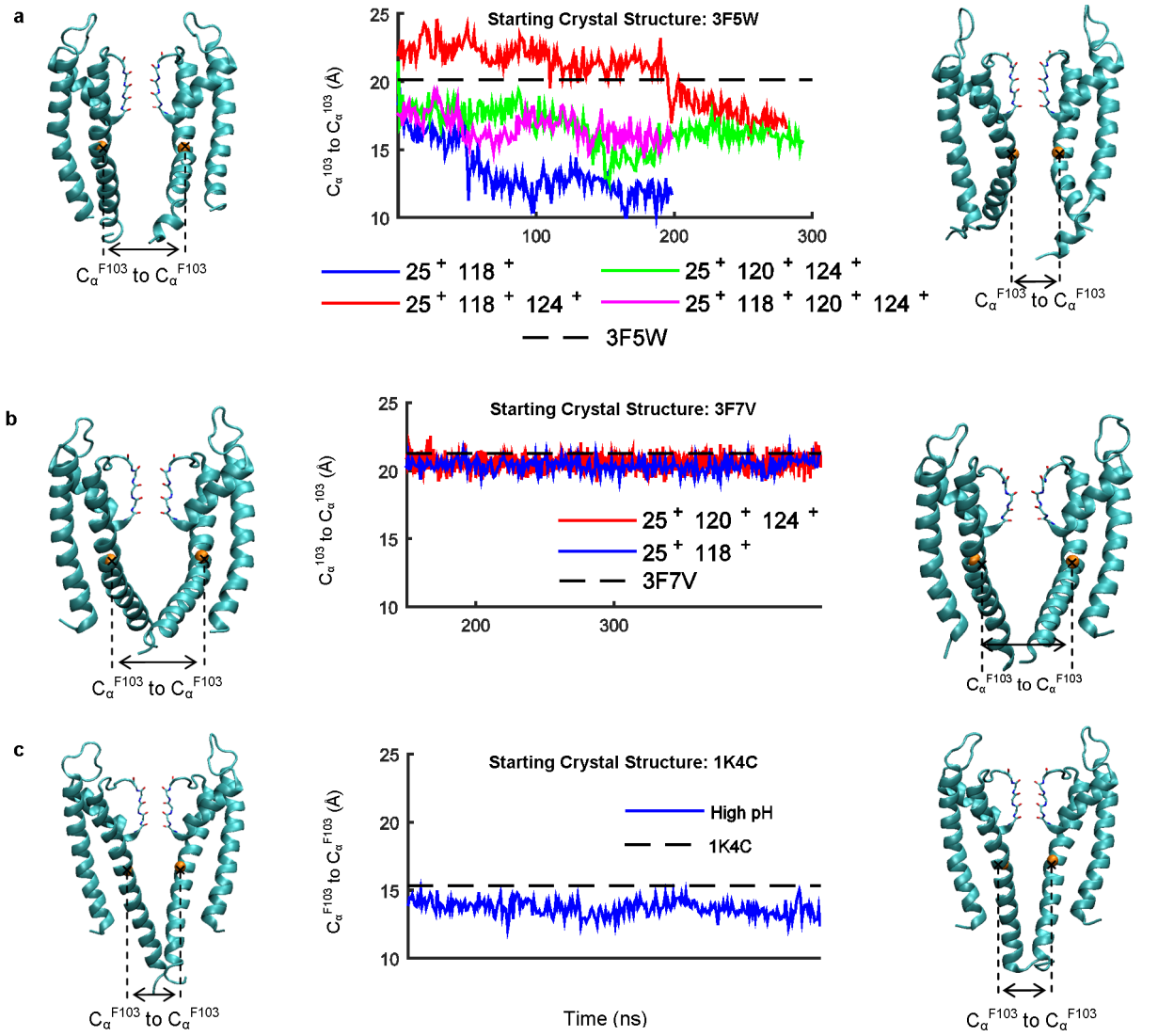

Figure 4.4: Stability of the activation gate in the open state. a, Initial coordinates were taken from the crystal structure 3F5W. Cross-subunit distance between the C_α atoms of residue Ph103 averaged for each pair of subunits reveals that activation gate is unstable for all protonation states tried. Snapshots taken and the beginning and end of the simulation (His25, Glu118, His124 protonated) reveal how conformation of the activation gate changed. b, Initial coordinates taken from the crystal structure 3F7V. The same measurement between residues Phe103 reveals that the activation gate is stable when either residues His25 and Glu118 or residues His25, Glu120, and His124 are protonated. Snapshots taken at the beginning and end of the simulation show the open activation gate is stable (His25, Glu118 protonated). c, Initial coordinates taken from the crystal structure 1K4C. The same distance measurement between residues Phe103 is plotted for a closed channel to serve as a point of comparison. Simulations starting from the crystal structures 3F5W have the same final values.

spontaneous transition from the conductive to the constricted conformation (Fig. 4.5-4.8). The average RMSD between the backbone atoms (residues 74 to 79) of the constricted state and the final frame in each simulation is 0.64 Å. In each case, the final conformation was four-fold symmetric and the Val76–Gly77 amide plane had the same orientation observed in X-ray crystal structures of the constricted conformation (Fig. 4.5-4.8a). Plotting the width of the selectivity filter measured at the C_α atoms of the central glycine residues reveals that the conductive conformation remains stable in each simulation for several hundred nanoseconds before suddenly undergoing a transition to the constricted conformation. The transition occurs abruptly without stopping at an intermediate conformation, although in some simulations the different subunits make the transition independently of each other in a step-wise fashion. After the transition, the selectivity filter does not deviate considerably from the constricted conformation (Fig. 4.5-4.8b). The transition cannot happen without K^+ ions first exiting the filter, a process which appears to occur the same way in each of the 4 simulations. Before the transition, the K^+ ions move to positions S1 and S3, kicking out the K^+ ion in S0 if present. The K^+ ion in position S3 then moves to position S4 leaving the center of the filter empty, which allows enough space for the filter to constrict (Fig. 4.5-4.8c). The transition is always preceded by water molecules entering behind the selectivity filter of at least one of the subunits, which would suggest that water molecules are an initiating factor of the transition. After the transition has occurred, water molecules become buried behind the filter of the remaining subunits (Fig. 4.5-4.8d).

4.3.3 Role of Water Molecules

In a previous study, water molecules were found to bind behind the filter at three specific sites along each subunit. The water molecules were stabilized by a network of hydrogen bonds between themselves and the protein backbone [72]. The presence of the water molecules appeared to be an integral structural element of the constricted conformation, locking the filter in a non-conductive state for a prolonged period of time consistent with that of C-type inactivation. Each time the filter spontaneously constricted in the study, water molecules entered behind all four subunits, which would suggest that the reverse transition would take several seconds to occur spontaneously.

Two-dimensional maps of the distribution of water molecules behind the selectivity filter are shown in Fig. 4.9. The position of each water molecule is binned in cylindrical coordi-

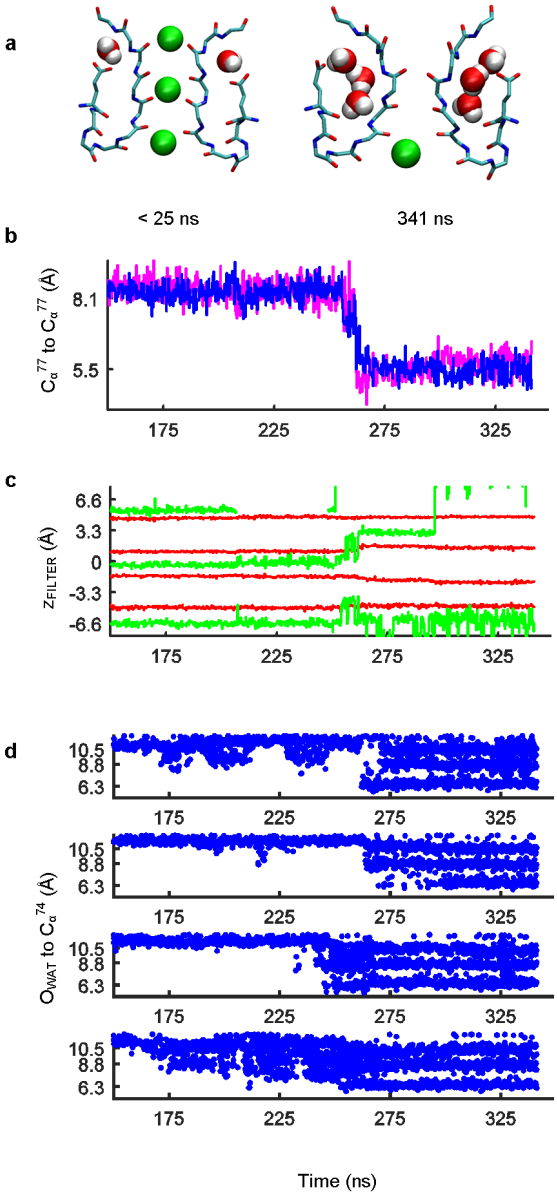

Figure 4.5: Simulation of KcsA starting with an open activation gate and a conductive filter. Initial coordinates were taken from the crystal structure 3F7V. a, Snapshots of the filter at the beginning and end of the simulation. b, The width of the selectivity filter plotted along the reaction coordinates r_1, r_2 (see Appendix 4.7, Fig. 4.11). Just after 250ns the selectivity filter spontaneously transitions to the constricted state. c, Position of the K^+ ions (green) in the selectivity filter plotted along the reaction coordinate z superimposed over the position of the carbonyl oxygen atoms that line the filter (red). The K^+ ions in S2 and S4 transition to S1 and S3 right before the filter pinches shut. After pinching, the ion in S3 moves down to S4. d, Penetration of water molecules behind the filter plotted along the reaction coordinate p reveals waters present before the filter collapsed. After the conformational transition, three distinct traces can be seen that match the water binding sites (see Appendix 4.7, Fig. 4.11).

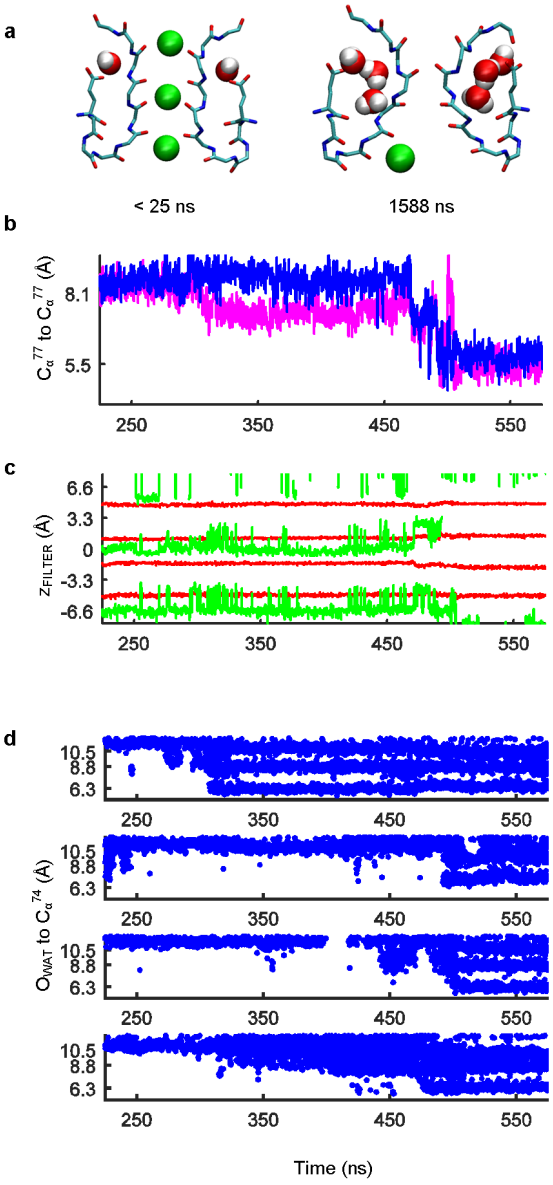

Figure 4.6: simulation of open channel starting with a conductive filter as in Fig. 4.5. Same outcome.

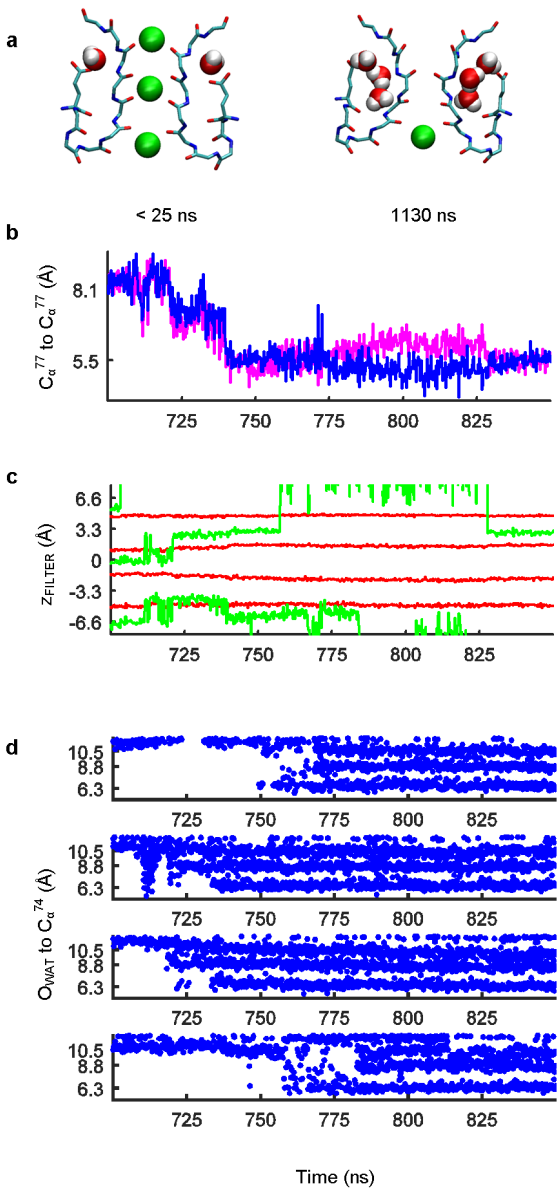

Figure 4.7: simulation of open channel starting with a conductive filter as in Fig. 4.5. Same outcome.

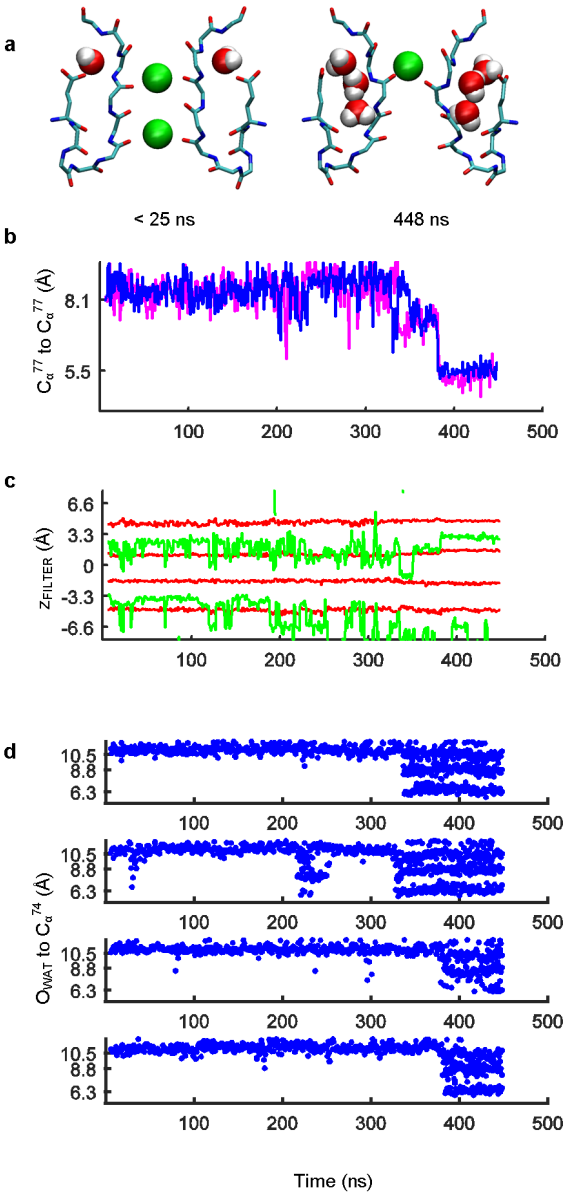

Figure 4.8: simulation of open channel starting with a conductive filter as in Fig. 4.5. Same outcome.

nates using the permeation pathway as a reference axis. After integrating out the angular coordinate and normalizing by shell volume, the units are converted to a free-energy scale by taking the negative log of the distribution. Water density profiles for the closed channel with conductive filter and open channel with the constricted filter serve as a reference for the analysis (Fig. 4.9a,b). In both of these cases, the filter is not expected to undergo a conformational transition. Results show that water molecules are absent behind the conductive filter, but present at their three specific binding sites behind the constricted filter. In contrast, the water density profiles calculated for KcsA under low-K^+ conditions, while the filter is conductive (Fig. 4.9c) or after it becomes constricted (Fig. 4.9d), appear markedly different. After excluding data collected during the transition process, the results show that water molecules enter behind the filter before it constricts, and remain there after the transition process is over. The situation is similar for the open channel: Water molecules are found behind the filter both before and after the transition (Fig. 4.9e,f). The presence of water molecules behind the filter appears to precede the collapse of the conductive state.

Because water molecules play a critical role in catalyzing the transition of the selectivity filter toward the constricted state, it is worth analyzing the pathway by which they enter the protein. Water molecules behind the filter always reach the same three specific binding sites behind the filter of each subunit, so the pathway can be determined by backtracking their movements from these sites. In 11 of the 12 water molecules that reached the bottom-most binding site, the water molecules first passed between residue Trp67 on one subunit and residues Asp80, Tyr82, and Arg82 of the neighboring subunit. The water molecules then slid down the pore-helix but were prevented from reaching the filter by the sidechains of residues Glu71 and Tyr78 (see Appendix 4.7, Fig. 4.15). Once the transition began the water molecules reached their specific sites directly behind the selectivity filter.

To test if the presence of water molecules behind the constricted selectivity filter are necessary to maintain its stability, the water molecules were removed in a simulation of the open channel (Fig. 4.10). The selectivity filter immediately makes a transition to a conductive state, despite the fact that the channel is in the activated conformation, which should destabilize the conductive filter. This test indicates that water molecules are required to keep the filter in a non-conductive state. The finding is confirmed by the free-energy landscape calculated using umbrella sampling along the transition pathway carried out with water molecules absent from behind the filter (see Appendix 4.7, Fig. 4.14). The free-energy landscape is plotted along the width of the filter measured by the average cross-subunit

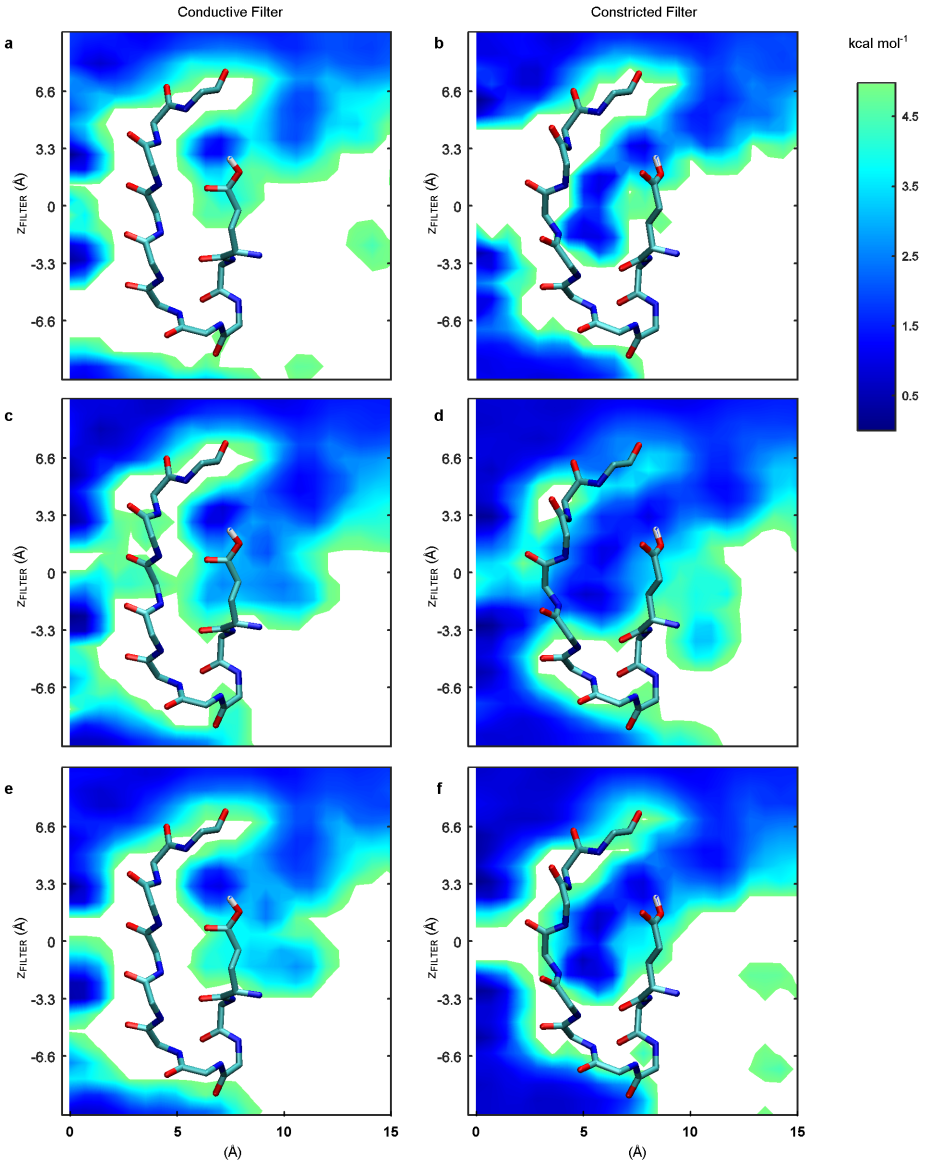

Figure 4.9: Distribution of water behind the selectivity filter plotted in cylindrical coordinates, averaged over the rotational axis θ, and scaled by the negative log of the probability (free energy profile). Data collected from long, unbiased MD simulations. a, Profile of waters around a conductive filter obtained by simulating KcsA with a closed activation gate. b, Profile of waters around a pinched filter obtained by simulating KcsA with an open activation gate. c, Profile of waters for KcsA under low-K^+ conditions before the filter began to undergo a conformational change. d, Profile of waters after the filter underwent the conformational change to a collapsed state. e, Profile of waters around the conductive filter with the activation gate open collected before the filter began to undergo a conformational change. f, Profile of waters after the filter underwent a conformational change to a pinched state.

distance between the central C_α atoms of the central glycine residues and the position of a K^+ ion from the center of the filter using the horizontal and vertical axes, respectively. See 4.6 for details on the bias used to prevent water molecules from entering behind filter. The free-energy landscape reveals that a K^+ ion from bulk must overcome a minor barrier (i) before entering the top of the filter (ii), after which the filter can make a transition to the conductive conformation (iii). Once the filter reaches a conductive state the K^+ ion at the top can permeate through (iv). Testing the importance of water in catalyzing the constricted conformation of the filter under a low-K^+ environment does not make sense because K^+ is presumably required to go from the constricted to the conductive conformation.

4.4 Discussion

In MD simulation of the Kcsa channel embedded in a solvated membrane, conditions designed to promote C-type inactivation in X-ray crystallographic structures of the potassium channel KcsA result in a constriction of the selectivity filter. Remarkably, starting from the conductive state of the filter and without any prior knowledge of the constricted conformation, the same outcome is systematically obtained. Just as important are results from the simulation where these conditions are absent: Here the filter is always observed to remain in a conductive state. The results favor the hypothesis that the constricted filter does indeed represent the C-type inactivated state observed in electrophysiological recordings of KcsA. While the transition is expected to occur when the activation gate is open, the process happens too fast in the current simulations. Entry into the inactivated state of the KcsA typically takes a few seconds, and yet the transition occurs within several hundred nanoseconds in each MD simulation [29]. Nonetheless, it is remarkable that the transition occurs only when the activation gate is open and not in an equivalent simulation of the closed channel (Fig. 4.3). That the MD simulations capture the expected behavior suggests the simulations are accurate but the structure used in the simulations is somehow preconditioned to push the selectivity filter into the constricted conformation.

Starting from the open structures, it takes on average less than half a microsecond for the selectivity filter to inactivate—a timescale that is several orders of magnitude shorter than what is observed in experiments. One possibility is that the constricted conformation is a flicker state, and that the simulations are not long enough to observe the transition to the conductive state. However, water molecules enter behind the filter after each transition,

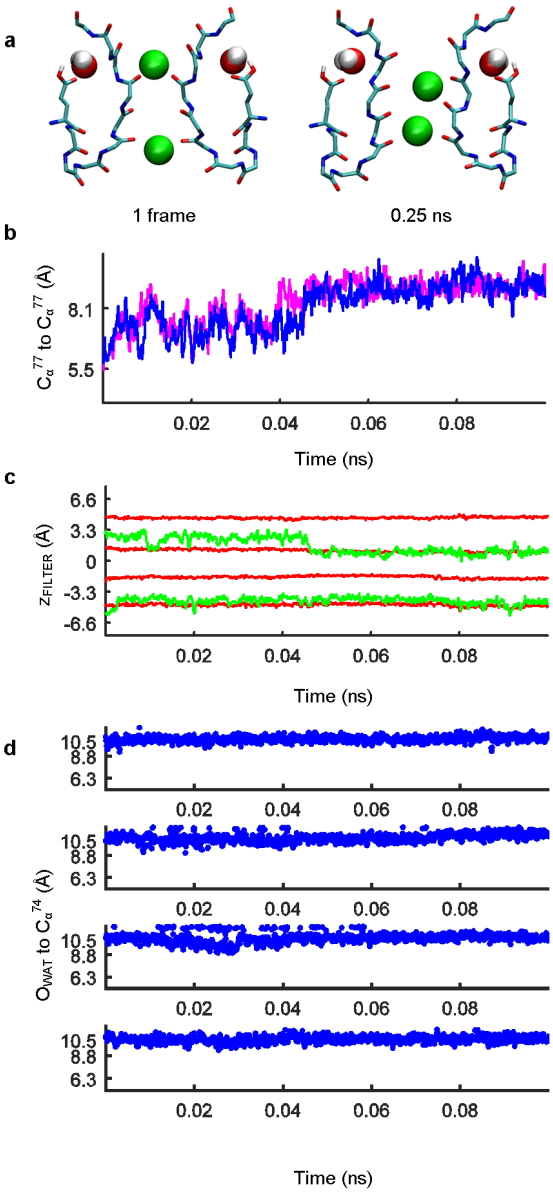

Figure 4.10: Simulation of open channel starting from a pinched filter but missing the the bottom two inactivating waters in each subunit. a, Snapshots of the filter at the beginning and end of the simulation. b, The width of the selectivity filter plotted along the reaction coordinates r_1, r_2 (see Fig. 4.11). The filter immediately returns to a conductive conformation. c, The position of the K^+ ions (green) in the selectivity filter plotted along the reaction coordinate z superimposed over the position of the carbonyl oxygen atoms that line the filter (red). The K^+ ion S1 transitions to S2. d, Water molecules never penetrate behind the filter.

which have been shown to trap the filter in the constricted conformation for several seconds [72]. A number of factors could be responsible for the acceleration of the entry into the constricted state. Studies have shown that truncating KcsA by removing the intracellular domain of the channel accelerates inactivation, which we were forced to do in our simulations. However, the experimentally measured rate constant of inactivation is only an order of magnitude faster after truncating the channel—no where near fast enough to explain the discrepancy [22]. Besides, the X-ray crystallographic structure used in these simulations (PDB ID 3F7V) is open to approximately the same extent as the full-length X-ray crystallographic structures (PDB ID 3PJS). Therefore, the extent of the structure opening may not be the cause of the problem. Another possibility is that an insufficient number of negative lipids bound to the KcsA channel, which is significant because studies have shown that an absence of negative lipids promotes C-type inactivation [113]. It is tempting to dismiss the simulations due to possible inaccuracies in the force field. Although some artifact in the MD simulations may be in part to blame, the sheer magnitude of the discrepancy seems too large to explain away as a problem of a computer simulation.

To explain the discrepancy in the inactivation rate, we propose that the activation gate is too open in our simulations, driving the selectivity filter to constrict much faster than it otherwise would. Nuclear magnetic resonance experiments on the full-length KcsA channel from the McDermott lab appear to support this hypothesis. They report that the X-ray crystal structures 3F7Y and 3FB8 best fit their solution state NMR data on the activated KcsA channel. The activation gate in these structures are several angstroms less open than the structure used in our simulations. If the activation gate in our simulations is too open, it would suggest that the conformation of the activation gate observed in many of the potassium channel X-ray crystallographic structures are also too open.

Water molecules buried behind the selectivity filter appear to play an indispensable role in stabilizing the constricted state. Before each transition to a constricted conformation, water molecules always enter first behind the selectivity filter of at least one subunit. Removing the water molecules behind the constricted conformation results in the reverse transition back to a conductive filter conformation. These results are reaffirmed by the free-energy landscape of the transition space calculated in the absence of water molecules behind the filter, which showed that the conductive state would remain more stable than the constricted state. Apparently, simply opening the channel is not enough to reach the constricted state—water molecules must be able to penetrate behind the filter.

The hypothesis that the selectivity filter undergoes a constriction during C-type inactivation remains controversial. The constricted conformation has never been observed in X-ray crystallographic structures of the potassium channels MthK, Kv1.2, and the Kv1.2/2.1 chimera under conditions designed to promote the C-type inactivated state [36, 37, 38]. However, in each structure, the filter was always observed to be in the conductive state, failing to provide an alternative conformation that could explain C-type inactivation. These structures therefore provide no evidence to either reinforce or refute the claim that the constricted conformation observed in KcsA represents the C-type inactivated state. A structure would be significant if an alternative filter conformation were identified for an open channel, but so far only the conductive and constricted filer conformations have been observed. Given that the sequence of amino acid residues in the selectivity filter is the same in all these channels, it remains reasonable to continue using the constricted filter conformation as a model of C-type inactivation.

4.5 Summary

Molecular Dynamic simulations reveal the selectivity filter of the bacterial potassium channel KcsA spontaneously transitioning from a conductive to a constricted conformation under conditions that promote C-type inactivation, closely matching the conformation observed in X-ray crystallographic structures. The simulations demonstrate the state is accessible in a lipid environment solvated in ionic solution on a timescale shorter than that of C-type inactivation.

4.6 Methods

Unless otherwise state, initial coordinates for the closed channel were taken from the X-ray crystal structure with Protein Date Bank (PDB) [114] ID 1K4C and initial coordinates for the open channel were taken from the X-ray crystal structure with PDB ID 3F7V. The X-ray crystal structures of the open channels are missing the tail ends of the activation gate and had to be modeled. The last few residues, which did not follow a helical structure, were removed and the α-helix of for the activation gate was extended to down to residues 22 and 124, where the closed channel ends. Hydrogen atoms and missing residues were added using the PSFGEN toolkit in Visual Molecular Dynamics (VMD). Except for Glu71 and the

residues protonated to keep the activation gate open, all residues were assigned standard protonation states at pH 7.0. Each channel was embedded into a lipid bilayer bathed in a solution of KCl using the web service CHARMMGUI. The total number of atoms per system varied between 40000 to 50000. All atom simulations were run using the CHARMM PARAM 27/36 for the protein and CHARMM PARAM 36 for the lipids without NB-Fix for the K^+—protein interactions [57]. Simulations were run at 310K and were carried out on either the special purpose super computer Anton on load at the Pittsburgh Computing Center (PSC) [58], or on the Midway Computing Cluster at the University of Chicago using NAMD 2.9 [59]. See Table 4.1 for further details.

All simulations were started with restraints applied to the protein. Restraints were gradually turned off over a period of time no shorter than 20 ns to ensure the surrounding water-ion-lipid environment relaxed to the conformation of the protein. To start the selectivity filter of the open channels in a conductive conformation, coordinates of the conductive filter conformation in the X-ray crystal structure 1K4C were used as the target coordinates for an additional set of restrains that were applied after the restraints on the whole protein were removed. Different restraints on the filter were tried in each simulation ranging from residues 71—80 to residues 65—82 but in each simulation the ions in the filter were restrained as well. The restraints on the filter were gradually turned off over a period of time no less than 20 ns, leaving the filter in an initial conductive conformation. Data collection did not begin until after removing all restraints on the system.

The density of water behind the selectivity filter was calculated by collecting the position of every water molecule around the filter at every frame in cylindrical coordinates. The radial component of the coordinates was integrated out and the position of the water molecules binned. Histograms were created after normalizing by shell volume. Final values were plotted on a negative log scaled by the Boltzmann machine constant multiplied by the temperature so that the water density maps could be expressed in units of kcal mol^{-1}.

The two-dimensional PMF (see Appendix 4.7, Fig. 4.14) was calculated using umbrella sampling (US). The region of interests along the reaction coordinates $r_{1,2} = \frac{r_1+r_2}{2}$ and z (see Appendix 4.7, Fig. 4.11a,b) was divided into a grid of equally spaced US windows spread 0.5 Å apart. A force constant of 20.0 kcal mol^{-1} was used to restrain each window. The initial windows were generated using coordinates from the equilibrate system of the open channel. Additional US windows were added one at a time using coordinates from the already existing windows by grabbing the nearest fluctuation [115]. To prevent water molecules from

Table 4.1: Conditions used in simulations for different channels

Structure	**Lipids**	**KCl (mM)**	**Force-Field (CHARMM PARAM)**	**NVT/ NVP**
1K4C	POPC	5mM (None in Filter)	27	NVT
1K4C	POPC	5mM	27	NVT
1K4C	POPC	(Started in Filter)	27	NVT
1K4C	3POPC:1POPG	200mM	36	NPT
3F7V	3POPC:1POPG	200mM	27 for protein,	NPT
3F7V	3POPC:1POPG	200mM	36 for lipids and ions	NPT
3F7V	3POPC:1POPG	150mM	27 for protein,	NPT
3F7V	3POPC:1POPG	150mM	36 for lipids and ions	NPT
3F7V	3POPC:1POPG	200mM	36	NPT

becoming buried behind the selectivity filter, dummy atoms were place behind the filter at the specific sites where the water molecules would bind. The dummy atoms were restrained in place by a series of bond, angle, and dihedral restrains that kept them from moving out of place. The dummy atoms had the VdW parameters of an oxygen atom to repel the water molecules, but all non-bonded interactions with the channel atoms were turned off. Each US window was equilibrated for 1.5 ns and ran for an additional 0.5 ns to use as part of the umbrella sampling procedure. Windows were unbiased using the Weighted Histogram Analysis Method (WHAM) [62].

4.7 Appendix: Supplementary Figures

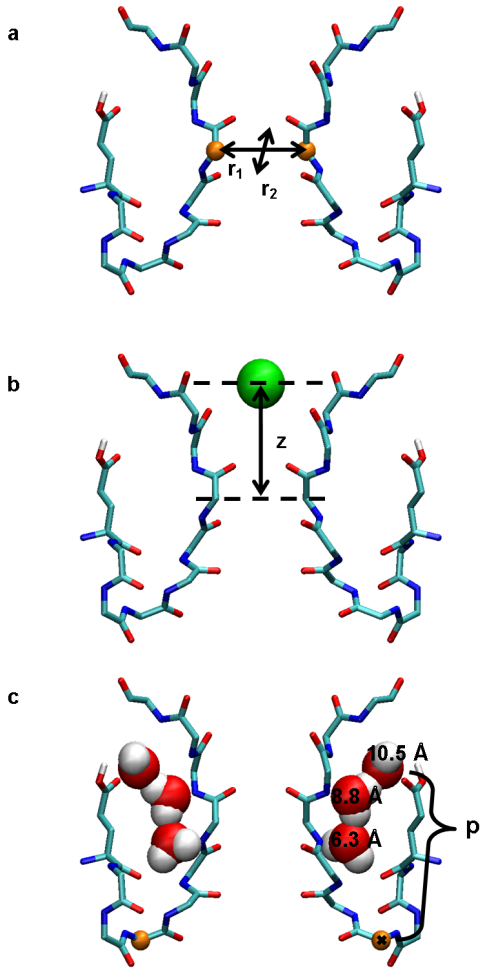

Figure 4.11: a, r_1 and r_2 reaction coordinates measure the distance between the C_α atoms of the central glycine residues on opposing subunits. The value r_1, r_2 for the conductive and pinched state are 8.1$\mathring{A}$ and 5.5$\mathring{A}$, respectively. b, z measures the height of a K^+ ion along the permeation pathway of the selectivity filter. The binding sites S0, S1, S2, S3, and S4 measure 6.6Å, 3.3Å, 0.0Å, -3.3Å, and -6.6Å, respectively. c, Reaction coordinate p measures penetration of water molecules behind the selectivity filter as the distance of each water molecule behind the filter to the C_α atom of residue 74. Three distinct water binding sites observed in the crystal structure 1K4D measure at 10.5Å, 8.8Å, and 6.3Å.

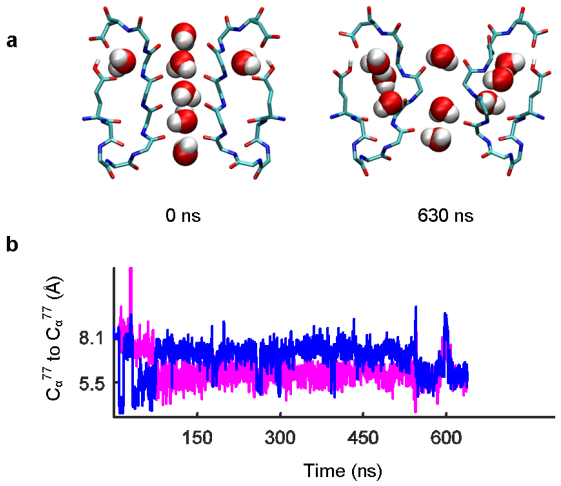

Figure 4.12: Simulation of the closed channel without K^+ in the selectivity filter. Initial coordinates taken from the crystal structure 1K4C. a, Snapshots of the filter at the beginning and end of the simulation. The carbonyl oxygen atoms of the valine residue underneath the central glycine residues is flipped about 180° out of place from the pinched state. b, Width of the selectivity filter plotted along the reaction coordinates r_1, r_2 (Fig. 4.11).

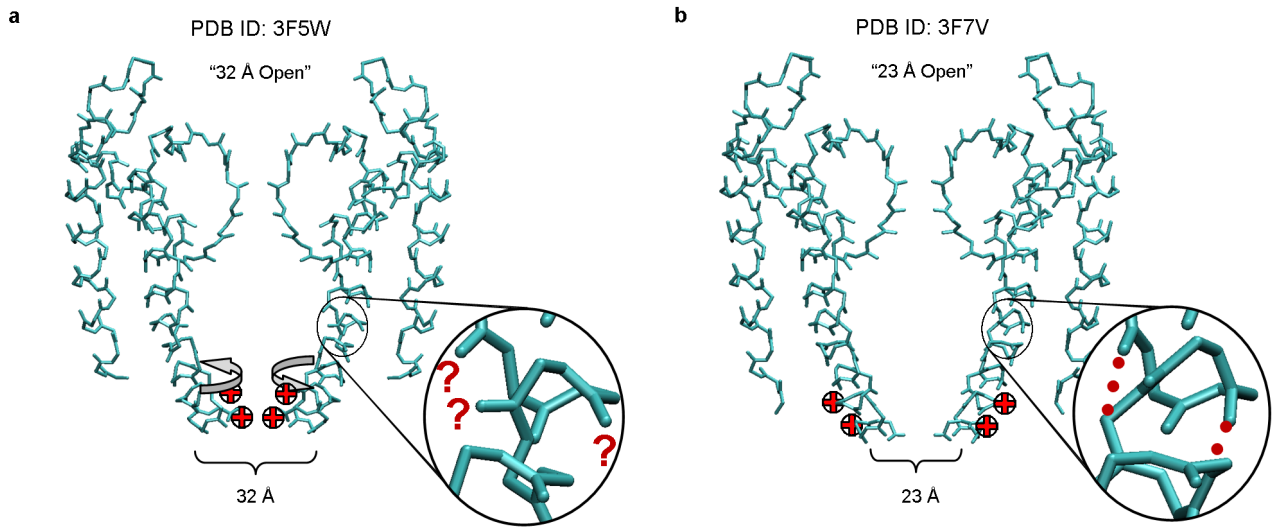

Figure 4.13: Comparison of published X-ray crystallographic structures of KcsA with the activation gate open. a, Crystal structure 3F5W, also known as the 32Å open structure. Magnified inlet shows that the α-helix is broken at Gly104, also known as the gating hinge. A turn in the α -helix is skipped, twisting the rest of the α-helix by approximate 120 °, leaving several positively charged arginine residues (+) pointing into the permeation pathway. b, Crystal structure 3F7V, also known as the 23Å open structure. Magnified inlet shows that although the hydrogen bond network of the α-helix is disrupted at residue Gly104, the helix does not skip a turn, and the positively charged arginines point outward capable of binding with negative lipids.

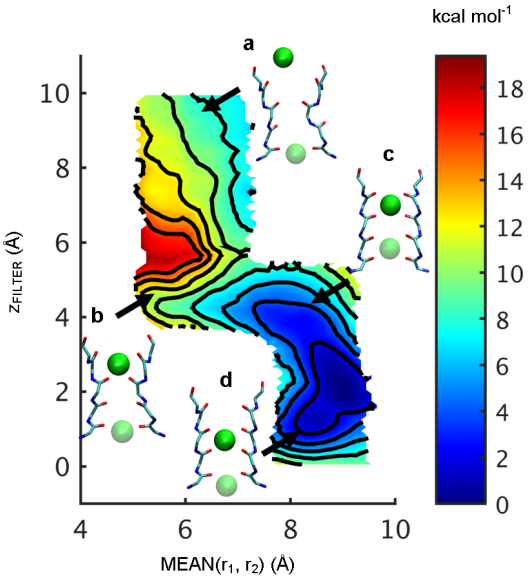

Figure 4.14: Free-energy landscape of the transition from the constricted to the conductive conformation calculated in the absence of water molecules behind the selectivity filter while the activation is open. The initial coordinates were taken from the crystal structure 3F7V. The reaction coordinate z represents an ion being brought down from bulk into the central binding site S2 of the selectivity filter and runs along the vertical axis of the plot. The reaction coordinate $Mean(r_1, r_2)$ represents the average cross-subunit distance across the selectivity filter measured at the central glycine residues and runs along the horizontal axis. The free-energy landscape shows that a K^+ ion can be brought from bulk (a) into the filter (b), at which point the filter can transition to a conductive conformation (c) and the K^+ ion can permeate through the filter (d). The transition is almost entirely downhill indicating the conductive conformation is more stable given that there are no water molecules behind the selectivity filter.

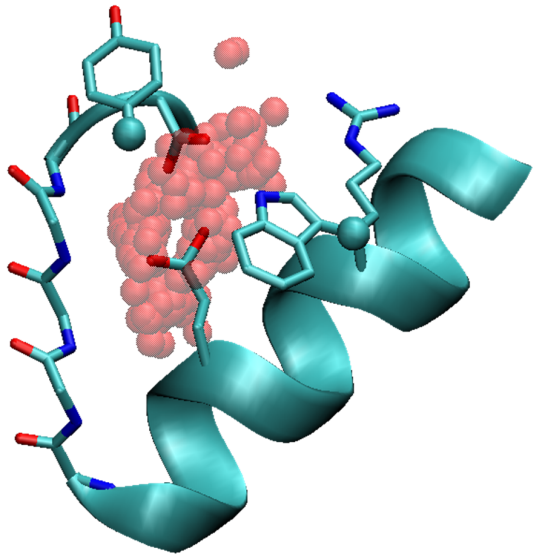

Figure 4.15: Pathway for water entry shown against the potassium channel selectivity filter. Water molecules pass by residues Asp80 and Tyr67 of the subunit shown and between Tyr82 and Arg89 of the neighboring subunit. Water molecules slide down the pore helix, stopping at Gly71 and Tyr78 (Not Shown). During the transition water molecules pass Gly71 and Tyr78 moving further down behind the selectivity filter.

CHAPTER 5
CONSTRICTED FILTER WITH THE D-ALANINE SUBSTITUTION

5.1 Abstract

The substitution of the central glycine residues by a D-alanine in the signature sequence TTVG*YGD is one of the few mutations tolerated in the potassium channel selectivity filter. Although the chemical modification is believed to prevent the selectivity filter from reaching a constricted conformation, electrical recordings have revealed the channel is still able to undergo C-type inactivation. Either the selectivity filter must adopt a yet unknown conformation during the inactivation process in contradiction of previous studies on the bacterial channel KcsA or the underlying assumption that the D-alanine substitution blocks the constricted conformation is invalid. To resolve this issue, MD simulations are used to investigate the effect of the D-alanine substitution on KcsA. Two candidate conformations are observed in both approaches: A partially pinched filter conformation and an asymmetric model where one pair of opposing filter units constrict while the other pair does not. Both models call into question the assertion that D-alanine substitution prevents the selectivity filter from pinching.

5.2 Introduction

The selectivity filter of potassium channels regulates ion flux across the cell membrane. It allows K^+ to pass through at a rate near the ion's diffusion limit while managing to restrict the flow of other ion species such as Na^+. X-ray crystallographic structures of the bacterial potassium channel KcsA provided a first glimpse of the molecular structure of the selectivity filter (Fig. 5.1a) [17]. Each of the four subunits of the channel contribute to one side of the filter, creating a narrow tunnel that allows K^+ ions to pass through in single file. Carbonyl oxygen atoms from the backbone of the protein line the passageway acting as surrogate water molecules to coordinate the penetrating K^+ ions. The carbonyl oxygen atoms create a series

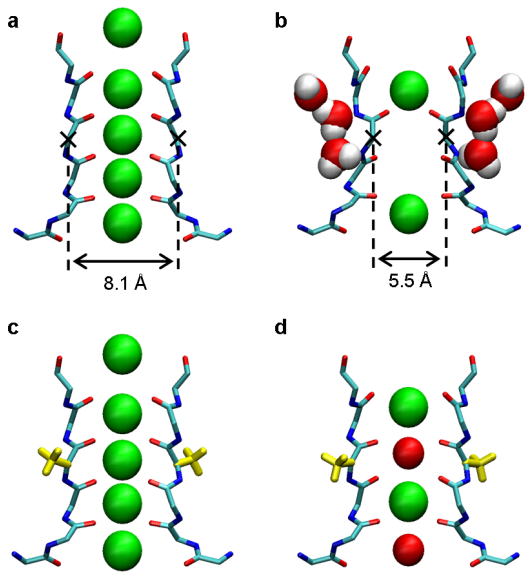

Figure 5.1: X-ray crystallographic structures of the KcsA selectivity filter. a, In the conductive conformation, K^+ is detected at each binding site. b, The constricted filter conformation observed under low-K^+ conditions or in some structures of the open channel. The pinching of the central glycine residues prevents K^+ from occupying the middle two binding sites. Hydrogen atoms of the crystallographic water molecules that stabilize the pinched conformation are modeled. c, Conformation of the filter after replacing each central glycine residue by D-alanine (Yellow) appears identical to the conductive conformation observed in wild-type channel. d, The filter does not constrict under the same low-K^+ conditions when the D-alanine substitution is present. Every other ion in the filter is depicted as Na^+ following the convention set forth by MacKinnon [44].

of cages for holding the K^+ ions, allowing K^+ ions to hop from one site to the next following a knock on mechanism [116]. Because the selectivity filter sequence—TTVGYGD—is highly conserved, it is expected that the conformational states of the selectivity filter are similar throughout most of the potassium channel family.

The conformation of the selectivity filter is allosterically coupled to the channel's intracellular activation gate [19]. After the application of an external stimulus opens the activation gate, the selectivity filter conducts ions for a period of time until it undergoes a conformational transition to a non-conductive state as part of a process called C-type inactivation. Although the molecular structure of the channel is known, the conformation of the selectivity filter during C-type inactivation remains a matter of debate. One of two hypotheses are possible: Either the selectivity filter becomes constricted, blocking the passage of K^+ ions through the channel, or the filter loses its ability to properly coordinate K^+ ions possibly

because it dilates. Separate lines of evidence would seem to support each hypothesis.

Yellen et al. first explored the idea that C-type inactivation is the result of a constriction in the selectivity filter [31]. Working on the Shaker potassium channel, they mutated the threonine residue located near the filter to a cysteine so that the channel could bind Cd^{2+}. Cd^{2+} bound weakly to the conductive state of the channel but its presence accelerated the transition to the C-type inactivated state, after which the binding affinity for Cd^{2+} increased by ∼45,000. To explain this effect, they proposed that Cd^{2+} could only bind to one cysteine at a time while the channel was conductive, but that after C-type inactivation the extracellular mouth of the channel constricted allowing Cd^{2+} to simultaneously interact with cysteines across multiple subunits. Later when X-ray crystallographic structures of the potassium channel KcsA became available, the filter was observed to exists in a constricted conformation under low-K^+ conditions or in some cases where the activation gate was open. Because these conditions promote C-type inactivation, the crystallographic structures would seem to support the hypothesis that the filter constricts during C-type inactivation (Fig. 5.1b) [23, 19]. The observed constricted conformation is characterized by a rotation of the Gly77–Val76 amide plane that moves the central glycine residues ∼1 Å closer to each other. The cross-subunit width of the filter measures 5.5 Å between the C_α atoms of the central glycine residues, which is less than the measurement of 8.1 Å for the conductive filter. Because the middle two K^+ binding sites are lost by this pinching motion, the conformation is believed to be non-conductive. Recently, we established that water molecules bound behind the constricted filter of KcsA stabilize the conformation, allowing the conformation to persists on a timescale comparable to that of C-type inactivation [72, 111].

The hypothesis that the selectivity filter loses its ability to coordinate K^+ during C-type inactivation gained traction after the discovery that the channel still inactivates when the filter's central glycine residues are substituted by a D-alanine [43]. The finding is significant because it is widely believed that the D-alanine substitution prevents the selectivity filter from constricting. The X-ray crystallographic structure of the KcsA D-ala77 channel revealed the selectivity filter to be in the same conductive conformation as wild-type channel (Fig. 5.1c). After soaking the crystals in Na^+ to reduce the K^+ concentration, a condition promoting the constricted conformation of the filter in a wild-type channel, the selectivity filter was found to remain in its conductive form (Fig. 5.1d) [44]. It was then proposed that the D-alanine sidechain blocked the rotation of the Val76-Gly77 amide plane, preventing the selectivity filter from making the transition to the constricted conformation. Based on

this evidence, it has been argued that the filter must enter a yet unidentified conformation during C-type inactivation [43]. To date, no structural evidence exists to indicating what this hypothetical conformation should look like.

5.3 Results

5.3.1 Modeling

To our knowledge, a molecular model of the KcsA D-ala77 in the constricted conformation has never been refined or simulated. Using the CHARMM force-fields, the coordinates of the pinched filter in Figure 4.1a,b are adjusted to minimize the structure's potential energy. The filter is observed to partially "un-pinch" during this process (Fig. 5.2c). The width of the selectivity filter measured as the cross-subunit distance between the C_α atoms of the central residues in the filter is 6.6 Å. Because water molecules buried behind the selectivity filter are important to the stability of the constricted conformation, we repeated the energy minimization procedure after including the buried water molecules. The final distance across the filter measured 6.0 Å. Although the filter remained pinched, the buried water molecules did not remain bound to their specific positions and failed to settle into a stable conformation (Fig. 5.2d). A visual inspection of the structure suggests that there is insufficient space behind the filter to accommodate both the D-alanine sidechain and three water molecules per subunit. Removing water molecules behind one pair of opposing filter units allows the filter to adopt an asymmetric conformation when the potential energy of the structure is again minimized (Fig. 5.2e). The two subunits with water molecules behind the filter remain stably pinched—the distance between the C_α atoms on the central glycine residues actually decreases to 5.3 Å—while the other two subunits without water molecules behind the filter "un-pinch". Given that the water molecules remained bound to their specific sites, we believe this model represent the best candidate for a stably pinched conformation for the G77dA substitution in KcsA.

5.3.2 Open Channel Simulations

Potassium channels with the D-alanine substitution introduced into the selectivity filer underwent C-type inactivation after opening the channel's activation gate in macroscopic electrophysiological recordings [43]. To mimic this experimental condition, the G77dA substitu-

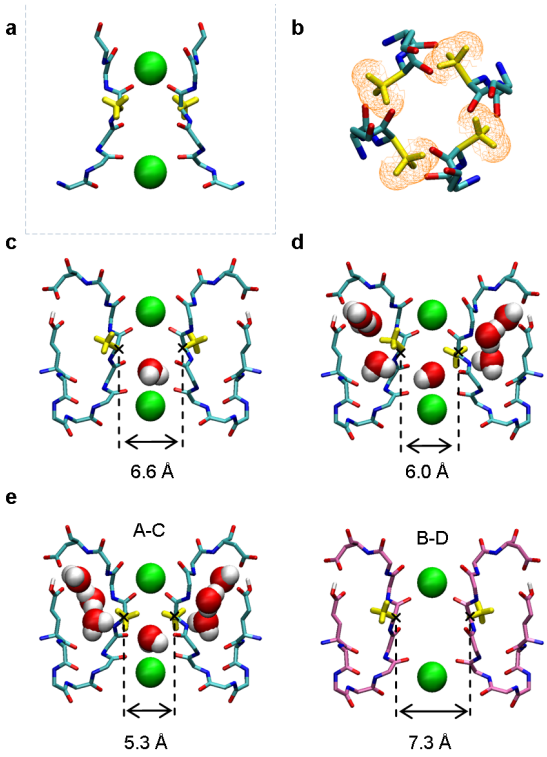

Figure 5.2: a, Model of the constricted filter with the D-alanine substitution. b, Top down view of the model. VdW spheres rendered as a wire-frame (Yellow) represent the volume of the D-alanine sidechain, which overlaps with the carbonyl oxygen atoms on the adjacent subunit. c, Conformation of the filter after energy minimization. Cross subunit width of the filter measured at the C_α atoms of the D-alanine residue is 6.6 Å when water molecules are not included behind the filter. d, Conformation of the filter after energy minimization when buried water molecules are included. The same cross-subunit distance measurement as before is 6.0 Å, however, the waters did not remain at their specific positions found in crystallographic structures of wild-type channel. e, Conformation of the filter after energy minimization when buried water molecules are only included behind the filter units A-C (Blue) but not B-D (Magenta). Subunits A, B, C D appear in clockwise fashion when viewed from the extracellular side. Cross-subunit distance measurements are 5.3 and 7.3 Å for the subunit pairs A-C and B-D, respectively.

tion is introduced onto an open structure of KcsA using the X-ray crystallographic structure 3F7V [19] published in the Protein Data Bank (PDB) [114].

Open Conductive MD1: The selectivity filter is initially placed in a conductive conformation with K^+ ions at every other binding site separated by water molecules. Plotting the cross-subunit distance between C_α atoms of opposing D-alanine residues reveals the width of the filter over the time-course of the simulation. The width of the selectivity filter remains around 8.1 Å for the first 80 ns, after which the width of the filter decreases to an average of 7.4 Å (Fig. 5.3a). At the end of the simulation, the molecular structure roughly resembles the conductive filter in appearance (Fig. 5.3b). The position of the K^+ ions in the filter plotted along the reaction coordinate reveals that K^+ ions occupied the filter throughout most of the simulation (Fig. 5.3c). It is interesting to note that water molecules entered behind the filter during the simulation, which is monitored by plotting their distance to the C_α atom of residue 74 at the bottom of the selectivity filter. The plots for each of the four subunits reveal water molecules entering behind the filter several times during the simulation, although the filter is never observed to constrict during these events (Fig. 5.3d).

Closed Conductive MD2 (WT): Because the width of the selectivity filter slightly decreased during the simulation, the closed channel is simulated to investigate what happens under conditions that do not promote C-type inactivation for wild-type channel. The filter starts in a conductive conformation using coordinates from the crystal structure with PDB ID 1K4C. The average width of the filter remains around 8.5 Å throughout the simulation, which is a full angstrom wider that what is observed in the mutant (see Appendix 5.7, Fig. 5.6a). Snapshots of the filter's molecular structure taken at the end of the simulation show the filter is still in a conductive conformation (see Appendix 5.7, Fig. 5.6b), and a plot of the K^+ ions along the permeation pathway reveals the filter is always in a conductive configuration (see Appendix 5.7, Fig. 5.6c). Unlike the simulation of the G77dA mutant, water molecules are almost never observed to enter behind the selectivity filter (see Appendix 5.7, Fig. 5.6d).

Open Constricted MD3: MD simulations can also be used to investigate what happens when the G77dA substitution is introduced onto the constricted filter conformation of the KcsA channel while the activation gate is open. To allow the protein to adapt to the presence of the D-ala side chain, a simulation is started with restraints holding the filter in the constricted conformation. Water molecules buried behind the filter are also restrained in place as the conformation would be unstable without them. After 25 ns, the restraints are

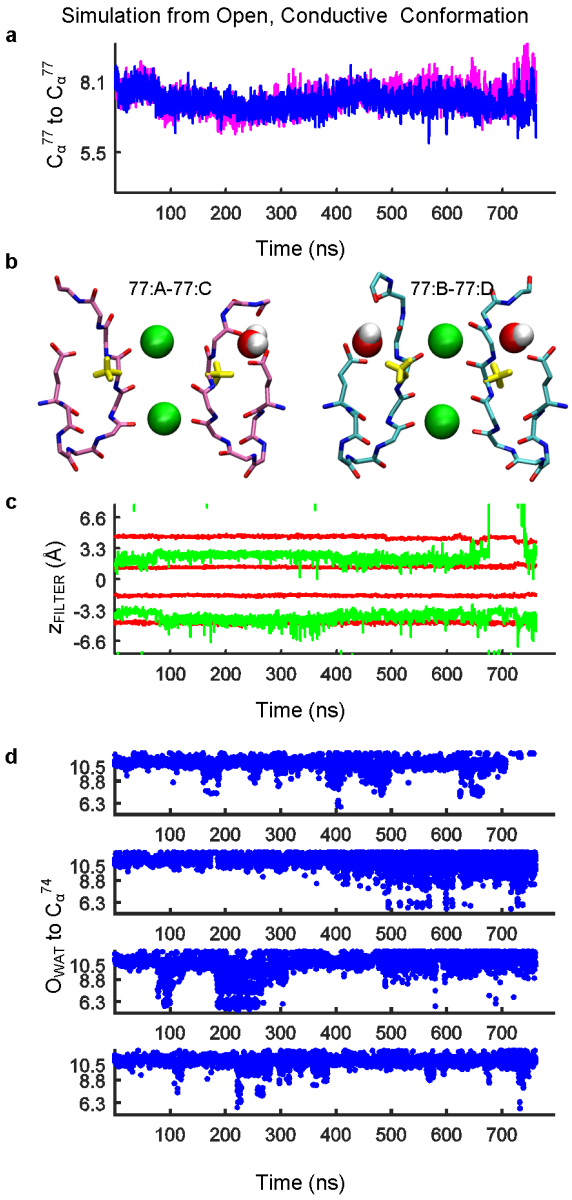

Figure 5.3: MD simulation of KcsA with the D-alanine substitution. The selectivity filter is initially conductive, and the activation gate is open to drive the C-type inactivation process. a, Cross-subunit distance between C_α atoms of the D-alanine residues plotted over time. The width decreases from 8.1 Å to 7.4 Å. b, Molecular structure of the filter at the end of the simulation shown for each pair of subunits. Colors correspond to the plot of the filter width (Top). c, Plot of K^+ ions along the permeation pathway showing ions present in the filter over the entire simulation. d, Plot showing the penetration of water molecules behind the filter of all four subunits by measuring the distance of the buried waters to the C_α atom of residue 74. Water molecules remain buried behind the filter for extended periods of time.

slowly removed to allow the equilibrated system to run without any artificial biases. While removing the restraints, the selectivity filter relaxes to a partially pinched conformation with the D-alanine sidechains occluding the permeation pathway. Plotting the cross-subunit distance between the C_α atoms of opposing D-alanine residues reveals the width of the filter over the time-course of the unbiased simulation. Gradually the filter transitions away from a symmetric conformation where all four units of the filter are partially pinched to an asymmetric conformation where one pair of opposing filter units are completely constricted and the other two filter units spread apart to the width of a conductive filter (Fig. 5.4a). The molecular structure of the filter after 300 ns resembles the appearance of the asymmetric model noted earlier (Fig. 5.2b). Even though only one pair of opposing filter units are constricted, no permeation events are observed during the simulation, as shown in a plot of the K^+ ions along the permeation pathway of the filter (Fig. 5.2c). Water molecules remain bound to their three specific sites behind the pair of constricted filter units throughout the entire simulation, which may act to stabilize the conformation (Fig. 5.4d).

Because only one pair of opposing filter units remains constricted, the selectivity filter has been further analyzed to verify that it is indeed too narrow for K^+ ions to permeate through. Using VdW spheres to model the atomic radii of each protein atom, the diameter of the largest particle that can fit in the filter along the permeation pathway is computed (Fig. 5.5a). Only a particle with a diameter ≥ 0.9 Å can pass between the central D-alanine residues. The permeation pathway is actually wider for wild-type channel with all four subunits in the constricted conformation, which can accommodate a particle as wide as 1.1 Å (Fig. 5.5b). The presence of the D-alanine substitution creates a narrower passageway because the sidechain partially occludes the permeation pathway. In contrast, the conductive filter conformation allows for a particle as wide as 1.7 Å in diameter to pass through (Fig. 5.5c).

5.4 Discussion

Using a space filling model that shows the D-alanine side chains sterically clashing into one another, it has been argued that this substitution prevents the selectivity filter from reaching a constricted conformation [44]. The hypothesis fit with existing experimental data at the time it was proposed. Replacing Na^+ for K^+ promotes C-type inactivation in the wild-type channel, but because the D-alanine substitution has been shown to remain conductive to Na^+

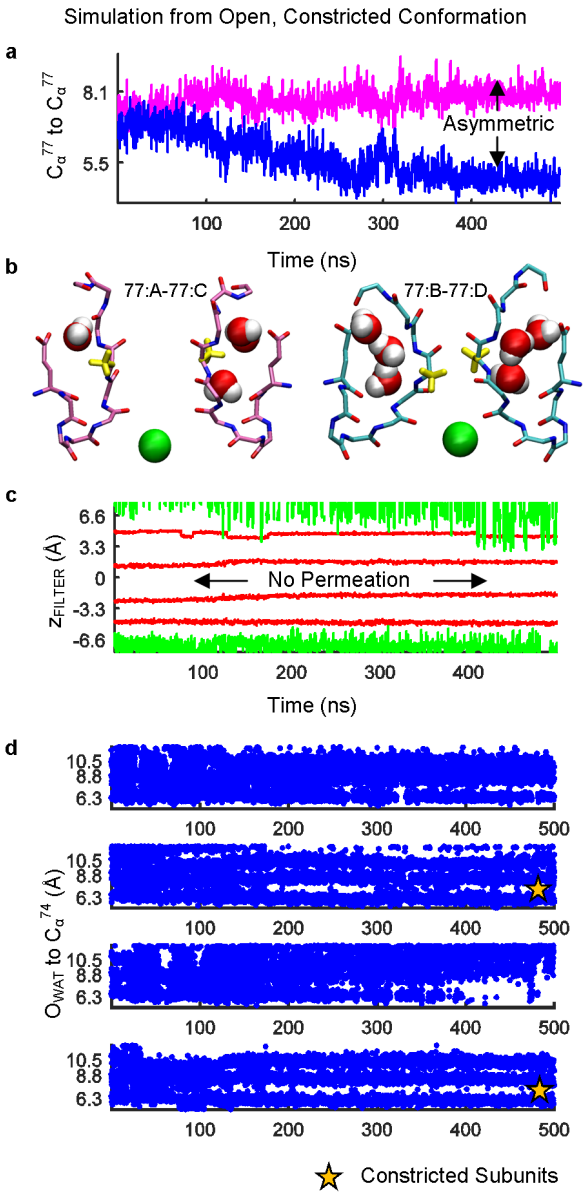

Figure 5.4: MD simulation of the D-alanine substitution in KcsA. Restraints used to start the filter in the constricted conformation are removed after 25 ns. a, Cross-subunit distance between C_α atoms of the D-alanine residues plotted over time reveals the filter becomes asymmetric. b, Molecular structure of the filter at the end of the simulation shown for each pair of subunits. Colors correspond to the plot of the filter width (Top). One pair of filter units is constricted, the other is not. c, Plot of K^+ ions along the permeation pathway shows that no permeation events occurred. d, Plot showing the penetration of water molecules behind the filter of all four subunits by measuring the distance of the buried waters to the C_α atom of residue 74. Water molecules always present behind the constricted filter units (B, D) but leave behind the other pair of subunits by the end of the simulation (A, C).

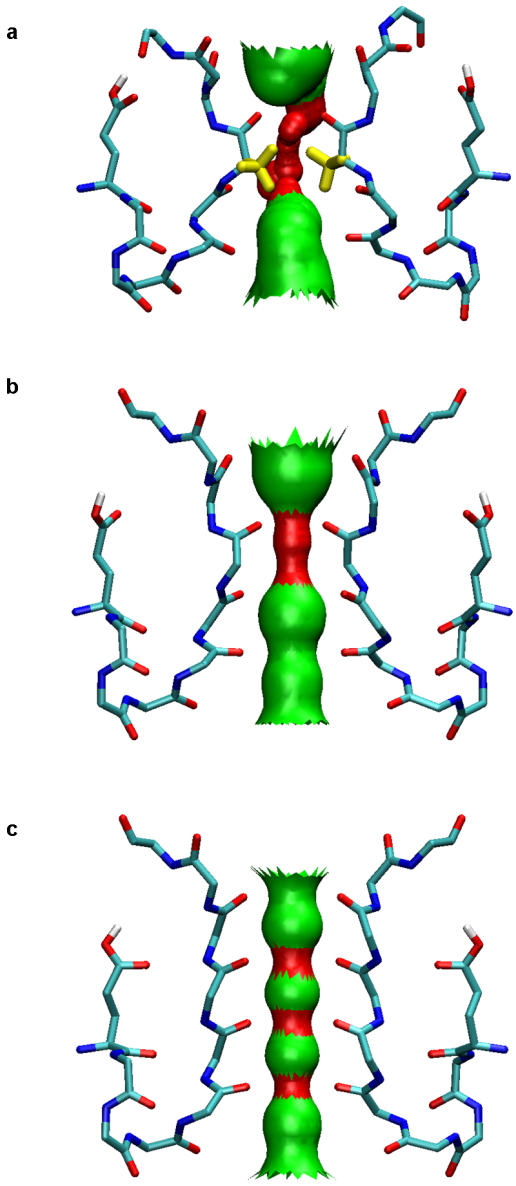

Figure 5.5: Width of the permeation pathway plotted along the selectivity filter. Funnel size represents the diameter of the largest particle able to pass through at that point. a, Width shown for asymmetric conformation of the filter taken from the last frame of MD simulation in Fig. 5.4. The pathway narrows considerably around the D-alanine residues even though only one pair of filter units are constricted. b, Same rendering shown for the pinched conformation and c, conductive conformations of wild-type channel.

in the complete absence of K^+, it was reasoned that the substitution prohibits a transition to the low-K^+ conformation. Structures obtained by X-ray crystallography seemed to fit with this understanding. The filter of the G77dA substitution did not pinch when the crystal were soaked in a bath of Na^+ solution. However, the structures do not show what happens when the activation gate is open, which is the only condition that has been shown to promote the C-type inactivated state with the D-alanine substitution present. To demonstrate that the D-alanine substitution blocks the constricted filter conformation during C-type inactivation would require an X-ray crystallographic structure of the channel with the activation gate open, and to date no such structure is available.

Refining the model of the D-alanine substitution on the pinched KcsA filter lead to the identification of two new conformations: A partially pinched symmetric conformation and an asymmetric conformation where the filter completely constricts on two subunits. The partially pinched conformation can be obtained simply by refining the model to minimize its internal energy. The filter also partially pinches during a MD simulations of the open channel starting from a conductive filter conformation. After 80 ns, the selectivity filter constricts by approximately half an angstrom (Fig. 5.3a) in contrast to the control simulation where the filter widens by approximately half an angstrom (Fig. 5.6a). During the simulation, water molecules are observed to enter behind the selectivity filter over extended periods of time, which could represent the first step in a transition toward a constricted filter conformation.

The selectivity filter adopts the asymmetric conformation during the energy minimization of the mutant channel when buried water molecules are included behind the filter of one pair of opposing subunits. The same conformation spontaneously appears again during an MD simulation starting from pinched filter in a symmetric conformation, suggesting that the asymmetric conformation is more stable. The asymmetric conformation is actually narrower than the pinched conformation because the D-alanine sidechain ends up protruding into the permeation pathway where it compensates for the two filter units that are not pinched. The discovery of this stable, asymmetric conformation undermines the assertion that the D-alanine substitution prevents the filter from constricting, and the implications that would follow.

We propose the following model for C-type inactivation for the special case of the D-alanine substitution. The initial step of opening the activation gate destabilizes the conductive filter, driving the filter towards a partially pinched conformation. From here, the filter can reach the asymmetric conformation where two filter units completely pinch. The confor-

Table 5.1: Data on filter conformation during C-type inactivation

Evidence	Outcome	Ref.
MacKinnon Model of D-ala mutant	Alternative Conformation	[44]
Model of D-ala mutant using MD	Constriction	-
Cd^{2+} binding	Constriction	[31]
NMR of KcsA	Constriction	[34, 35, 67]
X-ray structures of WT KcsA	Constriction	[23, 19]
X-ray structures of KvAP and MthK	NULL	[117, 118, 36]
X-ray structures KcsA with D-ala mutation	NULL	[44]
Na^{+} permeation during C-type inactivation	Alternative Conformation	[108]

mation is stabilized after water molecules become buried behind the pair of constricted filter units. At this point it is unclear if the asymmetric conformation can remain stable over the long timescales associated with C-type inactivation. The recovery time in wild-type channel is believed to be drawn out into the range of tens of seconds because water molecules become trapped behind the filter of all four subunits. Only when the water molecules spontaneously leave all four subunits, a rare event, may the channel return to a conductive conformation. But if the D-alanine sidechain only allows two filter units to constrict then it would suggest that the conformation will be shorter lived—only half the number of water molecules need to spontaneously leave from behind the filter before it can return to a conductive conformation. One possible explanation is that the D-alanine sidechain could hinder the transition between states. In this way, the barrier posed by the sidechain would compensate for fact that there are fewer buried water molecules that must spontaneously leave.

Given our findings that the D-alanine substitution does not forbid the pinched filter conformation, it would seem important to examine the evidence against the hypothesis that the filter constricts during C-type inactivation (Table 5.1). Crystallographic structures of several potassium channels and of the D-alanine substitution have been obtained under conditions that are expected to favor the C-type inactivated state, and yet the filter is always found to exist in a conductive conformation. This has been used as evidence that the pinched conformation is not the C-type inactivated state [43]. However, these results are a null finding because the filter was never observed to exist in an alternative conformation that could represent an inactivated state. To date, existence of an alternative conformation to the constricted filter observed in 1K4D and 3F7V remains hypothetical. No such conformation

has ever been observed in any crystallographic structure. The only evidence left that supports a non-constricted filter conformation for the C-type inactivated state is the observation that Na^+ can permeate through the inactivated filter. The argument is that partially solvated Na^+ is going through a dilated filter. We speculate that Na^+ could pass through a partially pinched filter as opposed to the alternative hypothesis that has been suggested by others that partially hydrated Na^+ ions are passing through a dilated filter conformation [108].

5.5 Conclusion

A space filling model has been used to argue that the D-alanine blocks the constricted filter conformation in potassium channels. After refining the models two candidate conformations of a constricted filter are identified. The models are supported by MD simulations that show the filter spontaneously adopting similar conformations. These results cast doubt on the claim that the discovery of C-type inactivation in channels with the D-alanine substitution would imply that the filter of the wild-type channels does not constrict during C-type inactivation.

5.6 Methods

We constructed an ideal CMAP for D-alanine . All X-ray crystallographic structures came from the Protein Data Bank (PDB) and are referenced by their ID values [114]. Space filling models of the D-alanine substitution on a pinched filter are based off of the crystal structure with PDB ID 1K4D. The D-alanine substitution is introduced using the PSFGEN package in VMD to orient the D-alanine sidechain according to the default bond, angle, and dihedral parameters. Additional models are created by by minimizing the energy of the space filling model in vacuo using NAMD. The minimization procedure follows three steps. First, only the position of the hydrogen atoms on water molecules are adjusted during the first 500 steps of minimization followed by another 500 steps of minimization on all the hydrogen atoms in the system.Finally, the positions of the water molecules, hydrogen atoms, and all the atoms on residues 74 to 80 of the selectivity filter are adjusted during the last 5000 steps of minimization. The ions are left fixed throughout the minimization procedure.

The crystal structure of KcsA with PDB ID 3F7V is used for all simulations of the D-alanine substitution [19]. The structure is missing the tail ends of the activation gate,

which is in the open conformation. The last few residues, which do not follow a helical structure, are removed and the α-helix of the activation is extended down to residues 22 and 124. Hydrogen atoms and missing sidechains are added using the PSFGEN toolkit in VMD. All residues are assigned their standard protonation state at pH 7.0, except for His25, Glu71, Glu118, and His124, which are protonated to keep the activation gate open during the simulation. The channel is embedded in a lipid bilayer bathed in a solution of 200 mM KCl using the web service CHARMMGUI. The total number of atoms is $\sim$41000. All atom simulation are run using the CHARMM PARAM36 force fields at a temperature of 310K.

To start the filter in the desired conformation, positional restraints are used. To place the filter in the conductive conformation, the filter atoms (residues 71–80) are restrained to the coordinates found in the X-ray crystallographic structure 1K4C. The restraints are then gradually turned off over a period of time lasting for 20 ns. To place the filter in a symmetric pinched conformation, the filter along with the water molecules buried behind it are restrained to the coordinates found in the X-ray crystallographic structure 1K4D. The restraints on the protein are turned off over a period of 10 ns in a stepwise fashion by first removing the bias on the hydrogen atoms, then the sidechains, and finally the backbone atoms. The restraints on the water molecules are left on for an additional 10 ns before being gradually turned off over an additional 5 ns. Data collection for the figures begins only after all restraints are removed.

5.7 Appendix: Supplementary Figures

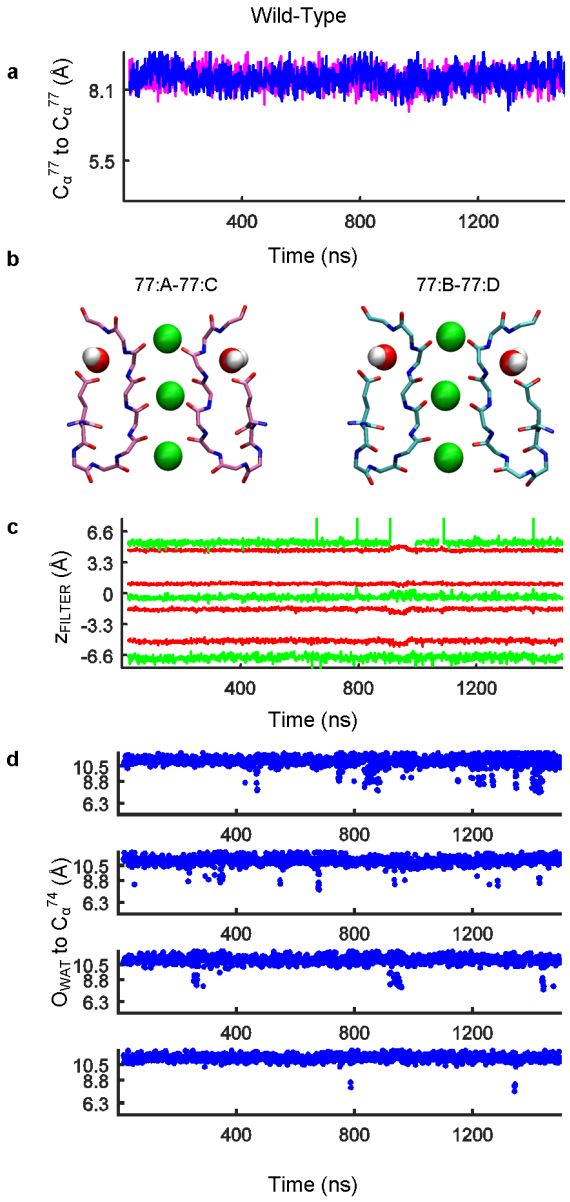

Figure 5.6: MD simulation of the wild-type KcsA. The activation gate is closed to stabilize the conductive conformation of the selectivity filter. a, Cross subunit distance between C_α atoms of the central glycine residues plotted over time. The width increases from 8.1 Å to 8.5 Å. b, Molecular structure of the filter at the end of the simulation shown for each pair of subunits. Colors correspond to the plot of the filter width (Top). c, Plot of K^+ ions along the permeation pathway showing ions present in the filter over the entire simulation. d, Plot showing penetration of water molecules behind the filter of all four subunits by measuring the distance of the buried water molecules to the C_α atom of residue 74. Water molecules almost never enter behind the selectivity filter.

CHAPTER 6
CONCLUDING REMARKS

6.1 Abstract

In addition to the C-type inactivated state, the conductance of potassium channels exhibits a host of dynamical states that appear to be modulated by the selectivity filter. The most pervasive ones are flicker states, which are brief interruptions of current that are observed during ion conduction. The bacterial channel KcsA exhibits at least three distinct flicker states, and presumably each is associated with a different conformation of the filter [48]. On the other hand, a long-lived non-conductive state called the "defunct state" has been observed in some K_v channels in the complete absence of K^+. The state takes several minutes to recover from, making it kinetically distinct from C-type inactivation [41]. The existence of these alternative states complicates the study of C-type inactivation because the conditions used to promote their occurrences are the same in some cases. Capturing the filter in the constricted conformation under conditions expected to promote C-type inactivation, as has been done using X-ray crystallography [23, 19], does not seem sufficient to link the constricted conformation to the inactivated state. It must be shown (i) that the filter can reach the constricted filter conformation within the timescales associated with C-type inactivation and (ii) the constricted filter conformation can remain non-conductive over a stretch of time comparable to that of the recovery process. Molecular Dynamic (MD) simulations of the bacterial channel KcsA proved useful in addressing these two concerns. The latter was answered first—it is far easier conceptually to simulate the conditions associated with recovery from C-type inactivation because the process occurs in the absence of ion conduction. The discoveries provided the necessary insight to begin to understand entry into C-type inactivation.

6.2 Results

An initial side-by-side comparison of the constricted and conductive filter conformations uncovered nothing that could explain the long timescales associated with C-type inactiva-

tion. So the observation that the constricted filter remained stable throughout a multiple microsecond MD simulation of the KcsA channel came as a surprise. Upon analyzing the simulation, three water molecules bound in place behind the constricted filter on each of the four subunits were identified. A space-filling atomic representation indicated that the constricted filter could not transition to a conductive conformation without the buried water molecules first moving out of the way. To test if the water molecules trap the filter in the constricted conformation, simulations were run with the water molecules removed. In a majority of these tests, the filter made an immediate transition from the constricted to the conductive conformation, confirming that buried water molecules trap the filter in the constricted conformation. To quantify the size of the barrier imposed by the buried water molecules, free-energy landscapes were calculated using umbrella sampling MD simulations. With the buried water molecules included behind the filter, a large barrier appeared (≥ 20 kcal mol^{-1}) that both prevented the filter from "un-pinching" and that blocked the passage of K^+ ions through the filter. When the water molecules were removed from the calculation, the process of "un-pinching the filter and bringing a K^+ ion down through the filter became an energetically downhill process that would be driven spontaneously (See Chap. 4, Fig. 3). The calculated free-energy landscapes therefore confirmed that the buried water molecules present a large barrier that prevent the filter from making an immediate recovery to the conductive conformation [72].

The long timescales associated with recovery from C-type inactivation can also be understood using a kinetic model. Results from MD simulations indicated that the filter cannot transition to a conductive conformation until all or most of the buried water molecules leave. Only after water molecules leave from behind the filter of each subunit may a K^+ ion bind to the filter forcing it to "un-pinch". MD simulations were used to obtain initial estimates of how long it takes for water molecules to clear one of the four subunits, and how quickly the water molecules can return. Because it is rare for the buried waters molecules to spontaneously leave and favorable for water molecules to return, the forward rate constant (1/79 ns) is much smaller than the backward rate constant (1/11 μs). Considering that this process has to occur on all four subunits of the channel, it is easy to understand the multi-second timescales associated with recovery from C-type inactivation. Simulating the kinetic model correctly predicts the recovery time of KcsA given the extracellular K^+ concentration (See Chap. 4, Fig. 1c) [72].

To experimentally test if buried water molecules regulate recovery from C-type inactiva-

tion, the KcsA channel was subject to 2M extracellular sucrose. Adding sucrose increases the viscosity, which in general is expected to slow down any molecular processes. But the pocket for the buried water molecules acts as an osmotic filter allowing only water molecules through. Adding sucrose (the osmolite) to the extracellular side of the channel decreases the probability of water molecules spontaneously entering the pocket behind the filter. As predicted by the model, adding sucrose accelerated recovery from C-type inactivation, thereby confirming that buried water molecules regulate recovery from C-type inactivation [72].

After showing that the timescale associated with the transition from the constricted to the conductive conformation is on par with that of C-type inactivation, it remained to be shown that the filter can reach the constricted conformation within the timescale associated with entry into C-type inactivation. C-type inactivation occurs over a timescale of hundreds of milliseconds, which is well beyond the reach of an unbiased MD simulation using currently available computer hardware. However, simulations of KcsA with its activation gate open somehow managed to capture the filter transitioning from the conductive to the constricted conformation in less than half a microsecond. The outcome was the same for each of the three additional times the simulation was repeated. Although the timescale associated with the transition process is orders of magnitude too fast, it does demonstrate the filter can constrict within (less than) the timescales associated with entry into the C-type inactivated state.

Each time the selectivity filter made a spontaneous transition from the conductive to the constricted conformation, water molecules first entered the space behind the selectivity filter. When the water molecules behind the filter were removed, the selectivity filter made an immediate transition back to the conductive conformation. This indicates that the water molecules play a role in initiating the transition and are essential to the stability of the constricted filter conformation, even when the activation gate is open. The importance of the water molecules was reaffirmed by a calculation of the free-energy landscape. With the activation gate open and the water molecules removed from behind the filter, the transition from the constricted to the conductive conformation was found to be energetically downhill. The free-energy landscape reveals that the conductive conformation is $\sim$8 kcal mol^{-1} more stable than the constricted conformation.

During the course of this research, a study was published showing that the selectivity filter still undergoes C-type inactivation even when the central glycine residues of the filter are replaced by D-alanines [43]. The discovery is significant because it is widely believed

that the D-alanine substitution prevents the filter from constricting, which if true would imply the filter does not constrict during C-type inactivation. However, the only evidence that the substitution blocks the filter from constricting is a space filling model that shows the D-alanine sidechains sterically clashing with the rest of the protein [44].

We decided to refine the picture offered by the space filling model by minimizing the internal energy of the complete atomic structure and by running MD simulations. Two candidate conformations of a constricted filter with the D-alanine substitution emerged: A partially pinched filter conformation and an asymmetric filter conformation with only one pair of opposing filter units pinched. In each case, no steric clashes are observed. These results show that the filter can still constrict even after introducing the D-alanine substitution into the channel. Therefore, the D-alanine substitution may not provide a clear-cut unambiguous argument about C-type inactivation, as was originally believed.

Descriptions of additional MD simulations of the potassium channel KcsA are listed in Table 6.1. Simulations of the KcsA with the mutations E71A, E71Q, Y82A, F103A, W67F, W67Y, T75S, and Y78F have also been simulated, and may be found in Tables 6.2, 6.3, 6.4, 6.5, 6.6, 6.7, 6.8, and 6.9, respectively. Descriptions of the simulations for the D-alanine substitution are in Table 6.10, .

6.3 Inactivation in Other Potassium Channels

Throughout this thesis, the bacterial potassium channel KcsA has been used a model to study C-type inactivation—no other channels were studied. To gauge if the mechanism of C-type inactivation generalizes other potassium channels, it is worth examining the similarity of KcsA to other channels. Out of all the eukaryotic channels, KcsA most closely resembles the central pore domain of the voltage-gated potassium (K_v) channels. Not only do these channels share the same selectivity filter sequence TTVGYG, but X-ray crystallographic structures reveal that the conductive conformation of the filters are the same [36, 37, 38]. Moreover, several aspects of C-type inactivation observed in voltage-gate potassium channels also appear to be reproduced by the KcsA channel. The common properties of C-type inactivation are (i) a dependence on the external potassium concentration, (ii) a slow rate of inactivation accompanied by an even slower rate of recovery, and (iii) mutations can be found around the filter that disrupt inactivation. These similarities suggests that KcsA is a meaningful model system for studying inactivation in the K_v channels.

Unfortunately, the constricted filter conformation has never been observed in any X-ray crystallographic structure outside that of KcsA. This point has been used to argue that the filter does not constrict during C-type inactivation [108, 43]. However, the absence of a crystal structure capturing a specific conformational state cannot be used to argue that such as state does not exist. Furthermore, the filter has never been found to exist in an alternative conformation that could serve as an alternative explanation for the inactivated state. Even when the channels are crystallized under conditions expected to promote C-type inactivation, the filter is still found to exist in the conductive conformation. These crystallographic structures are therefore a null result. With no alternative conformation to use, the constricted conformation observed with the KcsA channel remains the only option available for modeling the inactivated state of the selectivity filter.

Using the constricted filter of KcsA as a template, models of the K_v 1.2, Shaker, and MthK channels reveal that the filter can exist in the same constricted conformation (Fig. 6.1). No steric clashes are observed in these molecular models. The models also reveal that the same pocket for holding water molecules behind the KcsA filter can exist in these channels as well. Once lodged behind the filter, the water molecules could form a network of hydrogen bonds between themselves and the protein backbone in much the same way as it happens in KcsA (The hydrogen bond network in KcsA filter is only between backbone atoms, so the specific sidechains are irrelevant). Therefore, it would seem that the constricted filter conformation is possible in these channels as well. That said, even if the filter of a channel can constrict, it does not mean that the channel will under C-type inactivation. The propensity for a channel to inactivate depends on two independent values: The forward and backward rates to the inactivated state. While the backward rate depends on water molecules spontaneously leaving from behind the filter, the rate limiting factors on the forward rate remain unclear. In other words, C-type inactivation could theoretically be possible in any potassium channel—it is just that the forward rate is too small for the transition to occur in some channels. A difference in the forward rate constant might explain why Shaker can undergo C-type inactivation while K_v 1.2 does not.

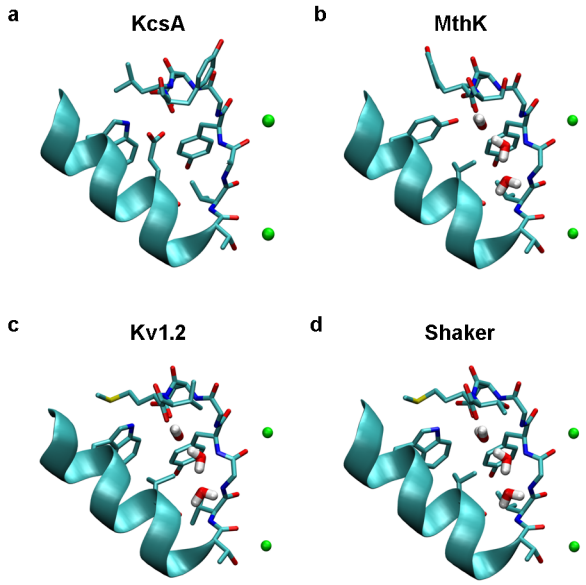

Figure 6.1: n
a. Pinched conformation observed in the KcsA selectivity filter. Pinched conformations modeled for MthK (panel b), K_v 1.2 (panel c), and Shaker (panel d).

6.4 What Potassium Channels Teaches Us About Structural Biology

Compared to other proteins, the molecular structure of the potassium channel selectivity filter can best be described as singular. While most proteins comprise common elements of secondary structures observed such as helices, sheets, and turns, the conformation of the selectivity filter allows the backbone carbonyl oxygen atoms of ∼5 residues to point toward the permeation pathway along a central axis (Fig. 6.2a). Such a conformation would normally be forbidden because the phi/psi dihedral angles lie in unfavorable regions (Fig. 6.2b). However, the segment from each subunit contains two glycine residues, which lack a sidechain allowing the protein backbone to visit a wider range of phi/psi dihedral angles than what would not otherwise be possible (Fig. 6.2c).

The presence of the glycine residues removes constraints that would otherwise limit the flexibility of the protein backbone. With few constraints acting on the structure's conformations, it should not be surprising if it is eventually discovered that the selectivity filter can adopt numerous alternative conformations in addition to the constricted and conductive conformations that have already been observed. Already, some evidence exists to support the view that the filter's conformation is degenerate. Using NMR the McDermott lab found

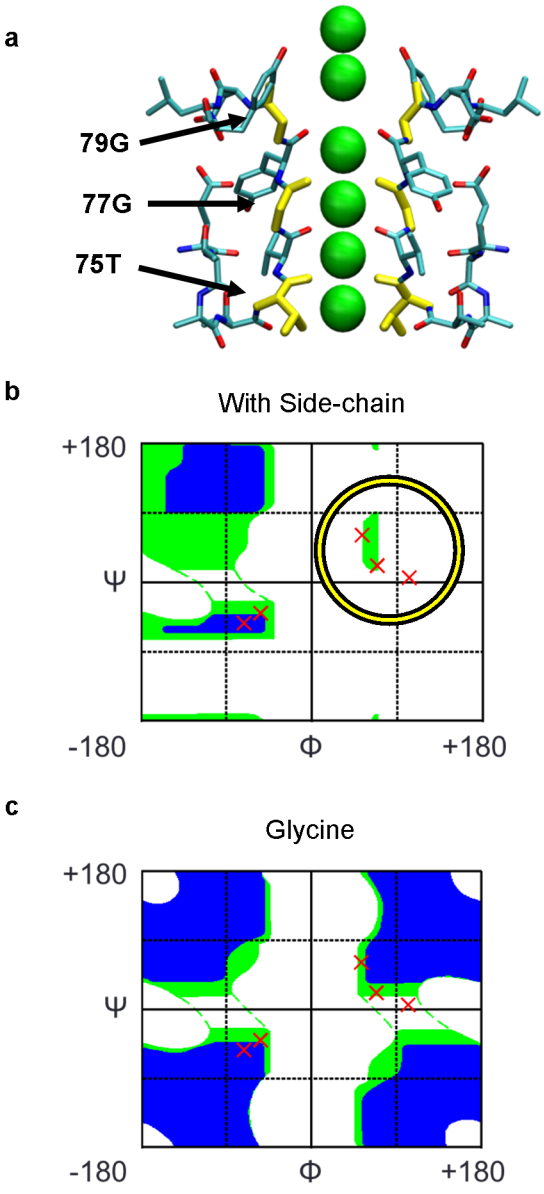

Figure 6.2: a, Structure of the potassium channel selectivity filter from KcsA. The backbone carbonyl oxygen atoms of the selectivity filter point in the same direction (toward the permeation pathway), an unusual conformation for a protein. The conformation places structural constraints on residues 75, 77, and 79 (Yellow). b, Ramachandran plot of the phi/psi dihedral angles for the backbone atoms of the selectivity filter. The color map indicates favorable regions averaged over all residues with a sidechain. Residues 77 and 79 are not a good fit (Yellow circle). c, Same plot for glycine residues. Almost all phi/psi dihedral angles are permitted because glycine lacks a sidechain.

that the selectivity filter exists in a "disordered" state when the E71A mutation is made to KcsA [35]. The E71A mutation is a particularly interesting case because the mutant channel may better represent the K_v channels. Like the E71A mutation, the K_v channels lack a glutamic acid at this position, which acts to stabilize the structure of the filter [47]. That said, even the wild-type KcsA filter has been observed to alternative between different gating modes [48]. Presumably each mode represents a different set of conformational states in which the selectivity filter can exists. The existence of disordered conformations of the potassium channel selectivity filter may prove problematic for MD simulations. The latter will need to be extremely sample all of the filter's possible configurations. Many of the enhanced sampling methods that have been devised will be of little value unless all the possible states are identified.

A key question is to identify the factors that control the conformational stability of the selectivity filter. Typically, the secondary structure of the protein backbone forms either an α-helix or a β-sheet. These types of secondary structures represent stable configurations of the protein allowing the backbone to form a hydrogen bond network with other backbone atoms. But the potassium channel selectivity has no recognizable secondary structure, and the hydrogen bond network between the protein atoms of the filter is sparse. This indicates that we should look for ligands that will stabilize the filter's conformation. For the case of the constricted filter of KcsA, it has become apparent that water molecules stabilize the conformation. For the conductive filter conformation, the permeable ion probably plays a major role in shaping the filter's conformation. For other potassium channels, the mechanism is probably similar, although the details may vary. There is no reason to believe that the same number of ligands, waters, or ions will bind to the same sites as they do in KcsA. These lessons may also carry over to other types of ion channels. Sodium channels, calcium channels, and chloride channels are all gated membrane proteins with a filter region. In cases where the filter regions lack a clear secondary structure, the conformation of the filter region may be controlled by external ligands. Again, the general story may be the same but the details will almost certainly be different for each type of channel.

6.5 Final Remarks

Potassium channels now are among the best-characterized systems in biophysics, with a wealth of structural and functional data. Yet, these are very complex systems and the task

of assigning specific sets of structural conformations to observable functional states remains largely incomplete. Efforts in this direction represents cutting edge scientific research. The computational approaches used in the present thesis will hopefully prove useful in the study of other protein systems. Furthermore, the challenges that were encountered highlight the difficulties associated the treatment of complex protein systems. In the case of potassium channels, this complexity does not necessarily stem from the large number of atoms, but from its design. Like all biological systems, the design of a potassium channel is the outcome of an evolutionary process. As a process, Evolution has no regard for simplicity or even consistency. Simplicity is not one of the objectives of this process. There are no guarantees that the mechanism underlying the function of a protein is designed such that it can be explained in simple terms, or that there is a one-to-one correspondence between its functional states and its underlying structural conformations. Whenever a simple mechanism is discovered that can explain the functional behavior of a protein, it might just be that Natural selection happened to randomly favor a simple mechanism.

6.6 Appendix: List of Simulations

Table 6.1 (Continues on next page): Simulations of wild-type KCSA channel

Gate	Filter	KCl	#	Goal	Outcome	
Intracellular Gate Closed	Pinched Filter	200 mM / 1M	x 3	Long, unbiased MD simulation designed to test if the pinched filter is stable. In an attempt to favor the conductive filter, a bath solution with a high external potassium concentration was used. Crystallographic water molecules behind the pinched filter were included.	The pinched filter remained stable throughout the entire simulation despite the high K^+ concentration. No ion permeation events observed.	1
		1M	x 26	Determine what happens when the water molecules behind the filter are absent.	In 10 out of the 26 trials, the selectivity filter became conductive. The conductive state matched conformations seen in crystallographic structures.	2
		1M	x 33	Determine what happens when water molecules are absent behind the selectivity filer in all but one subunit.	In 32 of the trials, the selectivity filter remained pinched, and water molecules entered into the empty spaces behind the selectivity filter. In one trial, the filter recovered to a conductive state.	3
		1M	x 6	Determine what happens when water molecules are absent behind two subunits (leaving water molecules behind the other two subunits).	In each trial, the selectivity filter remained pinched, and water molecules entered into the empty spaces behind the filter.	4
		1M	x 25	Determine what happens when water molecules are absent behind only one subunit (leaving water molecules behind the other three subunits).	In each trial, the selectivity filter remained pinched, and water molecules filled the space behind the empty subunit. The mean time it took for the water molecules to re-enter and stably bind to their specific positions was ~ 90 ns. This value was important in constructing a Markov model of the recovery process.	5
		1M	x 4	Determine what happens when all but the top-most water molecules behind the filter are removed, leaving one water molecule per subunit.	The filter failed to reach a conductive state. The top-most water molecule behind the filter tumbled down inhibiting the transition from the pinched to the conductive state. Eventually water molecules filled all the empty spaces behind the filter.	6

Table 6.1 (Continued from previous page, Continues on next page): Simulations of wild-type KCSA channel

Gate	Filter	KCl	#	Goal	Outcome	
		5mM	x 1	Determine if the pinched filter with water molecules behind it remains stable with no K^+ ions in it. The three free K^+ ions are restrained to prevent them from entering the filter.	The pinched conformation remains stable throughout the simulation, which is greater than 1μs in length.	7
		5mM	x 15	Determine if recovery can happen without free K^+ ions. To allow the filter to transition to a conductive state, all the water molecules behind the filter were removed.	The filter did not recover. Water molecules entered into the space behind the filter acting to stabilize the pinched conformation.	8
	Conductive Filter	200 mM / 1M	x 2	Long unbiased MD simulation to determine if the conductive filter is stable. Simulations conducted at 200mM KCl and 1M KCl.	The selectivity filter remained in a conductive state. The ions in the filter rarely exchanged with ions in bulk solution.	9
		5mM	x 1	Long unbiased MD simulation of the conductive filter under conditions of low-K^+. The simulation was started without ions in the filter to counter-balance the carbonyl oxygen atoms.	The filter collapsed shut to a conformation resembling the pinched state with one major exception. The carbonyl oxygen atoms of residue 77 pointed 180° in the wrong direction. Consequently, the hydrogen bond network that stabilizes the water molecules behind the filter did not always match each inactivating water molecule with two donors and an acceptor.	10
		200 mM	x 1	Long unbiased MD simulation of the conductive filter under conditions of low-K^+. The filter started with started with ions in positions S0-S2-S4.	The selectivity filter collapsed shut after the ions disassociated from it. By the end of the simulation, two of the four subunits precisely matched the pinched state seen in the crystal structures.	11
	N / A	1M	x 226	Replica Exchange Molecular Dynamics simulations to compute the free-energy landscape of the inactivation process when water molecules are absent behind the selectivity filter.	The recovery process is energetically downhill, indicating that the pinched filter will spontaneously transition to a conductive conformation when all the water molecules behind the filter are absent.	12

Table 6.1 (Continued from previous page, Continues on next page): Simulations of wild-type KCSA channel

Gate	Filter	KCl	#	Goal	Outcome	
		1M	x 137	Replica Exchange Molecular Dynamics simulations to compute the free-energy landscape of the inactivation process when water molecules are present behind the selectivity filter.	The transition of the conductive conformation is forbidden. K^+ ions cannot permeate through the selectivity filter because it is too narrow, and the filter cannot "un-pinch" because water molecules are buried behind it.	13
Intracellular Gate Partially Closed	Pinched Filter	200 mM	x 1	Test if the partially closed activation gate is stable using an unbiased MD simulation. The initial coordinates were taken from the X-ray structure 3FB5, which is open by 14.5Å. Residue His25 was protonated.	After 200ns, the activation gate had remained stable at a width hovering around 14.5Å. In addition, the pinched conformation of the selectivity filter remained stable.	14
	Conductive Filter	200 mM	x 1	Test if the partially closed activation gate is stable using an unbiased MD simulation. The initial coordinates were taken from the X-ray structure 3FB5, which is open by 14.5Å. Residue His25 was protonated.	After 400ns, the activation gate had remained stable at a width hovering around 14.5Å. In addition, the conductive state of the selectivity filter remained stable.	15
Intracellular Gate Partially Open	Pinched Filter	200 mM	x 1	Test if the partially open activation gate is stable using an unbiased MD simulation. The initial coordinates were taken from the X-ray structure 3FB6, which is open by 16Å. Residue Glu118 was protonated.	The activation gate was stable, and the selectivity filter remained pinched. That said, the simulation was only 85ns long, which may have been too short.	16
		200 mM	x 1	Test if the partially open activation gate is stable using an unbiased MD simulation. The initial coordinates were taken from the X-ray structure 3FB6, which is open by 16Å. Residue His25 was protonated.	After 100ns, the selectivity filter was still pinched. However, two opposing subunits of the activation gate began to close up.	17
		200 mM	x 1	Test if the partially open activation gate is stable using an unbiased MD simulation. The initial coordinates were taken from the X-ray structure 3FB6, which is open by 16Å. Residues His25 and Glu118 were protonated.	After 100ns, the selectivity filter was still pinched. However, the two opposing subunits of the activation gate began to open up.	18

Table 6.1 (Continued from previous page, Continues on next page): Simulations of wild-type KCSA channel

Gate	Filter	KCl	#	Goal	Outcome	
	Conductive Filter	200 mM	x 1	Test if the partially open activation gate is stable using an unbiased MD simulation. The initial coordinates were taken from the X-ray structure 3FB6, which is open by 16Å. Residue Glu118 was protonated.	After 85ns, the selectivity filter was still conductive. The conformation of the activation gate had remained stable, but the simulation may have been too short.	19
		200 mM	x 1	Test if the partially open activation gate is stable using an unbiased MD simulation. The initial coordinates were taken from the X-ray structure 3FB6, which is open by 16Å. Residue His25 was protonated.	After 100ns, the selectivity filter remained conductive. However, two opposing subunits of the activation gate began to close up.	20
		200 mM	x 1	Test if the partially open activation gate is stable using an unbiased MD simulation. The initial coordinates were taken from the X-ray structure 3FB6, which is open by 16Å. Residues His25 and Glu118 were protonated.	After 100ns, the selectivity filter remained conductive. However, two opposing subunits of the activation gate began to open.	21
Intracellular Gate Open	N/A	150 mM	x 1	Test if the open activation gate is stable using an unbiased MD simulation. The initial coordinates were taken from the X-ray structure 3F7V, which is open by 23Å. Residues His25 and His118 were protonated.	The activation gate remained stable.	22
		150 mM	x 1	Test if the open activation gate is stable using an unbiased MD simulation. The initial coordinates were taken from the X-ray structure 3F7V, which is open by 23Å. Residues His25 and His124 were protonated.	The activation gate remained stable.	23
		150 mM	x 1	Test if the open activation gate is stable using an unbiased MD simulation. The initial coordinates were taken from the X-ray structure 3F7V, which is open by 23Å. Residues His25, Glu120, & His124 were protonated.	After a lengthy period of equilibration, the position of the TM2 segment on one subunit shifted out of place.	24

Table 6.1 (Continued from previous page): Simulations of wild-type KCSA channel

x 1	Test if the open activation gate is stable using an unbiased MD simulation. The initial coordinates were taken from the X-ray structure 3F7V, which is open by 23Å. Residues His25, Glu118, & His124 were protonated.	The activation gate remained stable.	25
x 2	Long unbiased MD simulation starting with water molecules behind the pinched filter.	The pinched state of the selectivity filter remained stable.	26
x 1	Test if the pinched filter is stable without water molecules behind it. In each subunit, the bottom two inactivating water molecules were removed, leaving only the water molecules at the top sites behind the filter.	The filter immediately transitioned from the pinched state to the conductive state.	27
x 4	Long unbiased MD simulations starting with the selectivity filter in a conductive conformation.	The selectivity filter transitioned from the pinched to the conductive state in each simulation.	28
x 1	MD simulation starting with the selectivity filter in a conductive conformation. The ion at the center of the selectivity filter (position S2) was restrained in place to trap the filter in a conductive conformation.	The selectivity filter remained in a conductive conformation as intended. Water molecules could be observed entering behind the selectivity filter, although the presence of the water molecules behind the filter was transient.	29
x 1	Test if the open activation gate is stable using an unbiased MD simulation. The initial coordinates were taken from the X-ray structure 3F5W, which is open by 32Å. Residues His25 and Glu118 were protonated.	The activation gate is unstable.	30
x 1	Test if the open activation gate is stable using an unbiased MD simulation. The initial coordinates were taken from the X-ray structure 3F5W, which is open by 32Å. Residues His25, Glu118, and His125 were protonated.	The activation gate is unstable.	31

Table 6.2: Simulations of KcsA with E71A mutation (Non-inactivating)

Gate	Filter	KCl	#	Goal	Outcome	
Intra. Gate Closed	Pinched Filter	1M	x 1	Long unbiased MD simulation starting with the filter in a pinched conformation. A bath solution with a high external potassium concentration was used.	The filter remains pinched for several microseconds and then denatures (the rest of the channel remains stable). The selectivity filter enters into a dilated state, and then later reforms back into a pinched-like conformation.	32
Intra. Gate Open	Pinched Filter	200 mM	x 1	Long unbiased MD simulation starting with the filter in a pinched conformation.	The pinched conformation remains stable throughout the entire 1.4 μs long simulation.	33
	Conductive Filter	200 mM	x 1	Long unbiased MD simulation starting with the filter in a conductive conformation.	The selectivity gradually constricts shut. However, the final pinched conformation was badly deformed when compared to the pinched state observed in crystallographic structures.	34

Table 6.3: Simulations of KcsA with E71Q mutation (Flicker)

Gate	Filter	KCl	#	Goal	Outcome	
Intra. Gate Closed	Pinched Filter	1M	x 1	Long unbiased MD simulation starting with the selectivity filter in a pinched conformation. A bath solution with a high external potassium concentration was used.	The selectivity filter remained pinched shut. Nothing interesting happened in the 600ns simulation.	35

Table 6.4: Simulations of KcsA with Y82A mutation (Accelerated)

Gate	Filter		#	Goal	Outcome	
Intra. Gate Closed	Pinched Filter	1M	x 1	Long unbiased MD simulation starting with the selectivity filter in a pinched conformation. A bath solution with a high external potassium concentration was used.	The selectivity filter remained pinched shut. Mutating tyrosine to an alanine at position 82 effectively removed a lid that separated water molecules behind the filter from the bulk solution. As a result, water molecules behind the filter were able to readily exchange with bulk.	36
		1M	x 22	Determine what happens when water molecules are absent behind only one subunit, leaving water molecules behind the other three subunits.	In each trial, the selectivity filter remained pinched, and water molecules entered into the empty spaces behind the selectivity filter. The mean time it took for the water molecules to re-enter and stably bind to their specific positions was only ~ 15 ns, which is considerably shorter than what was observed in WT channel.	37
Intra. Gate Open	Pinched Filter	200 mM	x 1	Long unbiased MD simulation starting with the selectivity filter in a pinched conformation.	The selectivity filter remained pinched shut.	38
	Conductive Filter	150 / 200 mM	x 5	Unbiased MD simulation starting with the selectivity filter in a conductive conformation. Each simulation was less than 250 ns.	In two simulations the selectivity filter rapidly transitioned to the pinched state. In the other simulations, the filter collapsed but did not reach the pinched state by the end of the trajectory.	39

Table 6.5: Simulations of KcsA with F103A mutation (Non-inactivating)

Gate	Filter		#	Goal	Outcome	
Intra. Gate Open	Pinched Filter	200 mM	x 1	Long unbiased MD simulation starting with the selectivity filter in a pinched conformation.	Selectivity filter remains pinched shut.	40
	Conductive Filter	200 mM	x 3	Long Unbiased MD simulation starting with the selectivity filter in a conductive conformation.	At the end of the simulation, the selectivity filter had pinched shut.	41

Table 6.6: Simulations of KcsA with W67F mutation (Non-inactivating)

Gate	Filter	KCl	#	Goal	Outcome	
Intra. Gate Open	Pinched Filter	200 mM	x 1	Long unbiased MD simulation starting with the selectivity filter in a pinched state.	The selectivity filter remained pinched. A few events were observed where three negative lipids were found bound on the extracellular side between the subunits.	42
	Conductive Filter	200 mM	x 1	Long unbiased MD simulation starting with the selectivity filter in a conductive state.	Over the course of the 800ns simulation, the selectivity filter remained conductive. It was very rare to see water molecules enter behind the selectivity filter, which may explain why the filter did not collapse. The simulation was long enough to observe up to three negative lipids bind to the extracellular side between the subunits; however, the lipids did not stick.	43

Table 6.7: Simulations of KcsA with W67Y mutation (Inactivating)

Gate	Filter	KCl	#	Goal	Outcome	
Intra. Gate Open	Pinched Filter	200 mM	x 1	Long unbiased MD simulation starting with the selectivity filter in a pinched state.	The selectivity filter remained pinched.	44
	Conductive Filter	200 mM	x 1	Long unbiased MD simulation starting with the selectivity filter in a conductive state.	Over the course of the 800ns simulation, the selectivity filter remained conductive. It was very rare to see water molecules enter behind the selectivity filter, which may explain why the filter did not collapse.	45

Table 6.8: Simulations of KcsA with T75S mutation

Gate	Filter	KCl	#	Goal	Outcome	
Intra. Gate Open	Pinched Filter	200 mM	x 1	Long unbiased MD simulation starting with the selectivity filter in a pinched state.	Filter remained pinched. A few events were observed where three negative lipids were found bound on the extracellular side between the subunits.	46
	Conductive Filter	200 mM	x 1	Long unbiased MD simulation starting with the selectivity filter in a conductive state.	The selectivity filter spontaneously pinched shut.	47

Table: 6.9: Simulations of KcsA with Y78F mutation

Gate	Filter	KCl	#	Goal	Outcome	
Intra. Gate Open	Pinched Filter	200 mM	x 1	Long unbiased MD simulation starting with the selectivity filter in a pinched state.	The selectivity filter remained pinched shut. A few events were observed where three negative lipids were found bound on the extracellular side between the subunits.	48
	Conductive Filter	200 mM	x 1	Long unbiased MD simulation starting with the selectivity filter in a conductive state.	The selectivity filter collapsed. The selectivity filter from only three subunits reached the pinched state by the end of the 800ns simulation.	49

Table: 6.10: Simulations of KcsA with G77dA mutation (Presumably cannot pinch shut)

Gate	Filter	KCl	#	Goal	Outcome	
Intra. Gate Open	Pinched Filter	200 mM	x 1	Long unbiased MD simulation starting with the selectivity filter in a pinched state. Restraints holding the filter in the pinched state were gradually released. After that, restraints holding the water molecules behind the filter were turned off.	The selectivity filter remains halfway pinched. Because of the mutation, the permeation pathway through the filter remained blocked even though the filter was not fully pinched. Water molecules were observed to fill the space behind the selectivity filter throughout the whole simulation.	50
	Conductive Filter	200 mM	x 1	Long unbiased MD simulation starting with the selectivity filter in a conductive state.	The selectivity filter remained conductive. However, water molecules are observed entering behind the filter in a manner that suggests that it will pinch shut soon.	51

REFERENCES

[1] Christopher Miller et al. An overview of the potassium channel family. Genome biol, 1(4):1–5, 2000.

[2] Christian Biervert, Björn C Schroeder, Christian Kubisch, Samuel F Berkovic, Peter Propping, Thomas J Jentsch, and Ortrud K Steinlein. A potassium channel mutation in neonatal human epilepsy. Science, 279(5349):403–406, 1998.

[3] Bernd A Neubauer, S Waldegger, J Heinzinger, A Hahn, G Kurlemann, B Fiedler, F Eberhard, H Muhle, U Stephani, S Garkisch, et al. Kcnq2 and kcnq3 mutations contribute to different idiopathic epilepsy syndromes. Neurology, 71(3):177–183, 2008.

[4] David L Browne, Stephen T Gancher, John G Nutt, Ewout RP Brunt, Eric A Smith, Patricia Kramer, and Michael Litt. Episodic ataxia/myokymia syndrome is associated with point mutations in the human potassium channel gene, kcna1. Nature genetics, 8(2):136–140, 1994.

[5] Christian Kubisch, Björn C Schroeder, Thomas Friedrich, Björn Lütjohann, Aziz El-Amraoui, Sandrine Marlin, Christine Petit, and Thomas J Jentsch. Kcnq4, a novel potassium channel expressed in sensory outer hair cells, is mutated in dominant deafness. Cell, 96(3):437–446, 1999.

[6] Paula L Hedley, Poul Jørgensen, Sarah Schlamowitz, Romilda Wangari, Johanna Moolman-Smook, Paul A Brink, Jørgen K Kanters, Valerie A Corfield, and Michael Christiansen. The genetic basis of long qt and short qt syndromes: a mutation update. Human mutation, 30(11):1486–1511, 2009.

[7] David B Simon, Fiona E Karet, Juan Rodriguez-Soriano, Jahed H Hamdan, Antonio DiPietro, Howard Trachtman, Sami A Sanjad, and Richard P Lifton. Genetic heterogeneity of barter's syndrome revealed by mutations in the K^+ channel, romk. Nature genetics, 14(2):152–156, 1996.

[8] Anna L Gloyn, Ewan R Pearson, Jennifer F Antcliff, Peter Proks, G Jan Bruining, Annabelle S Slingerland, Neville Howard, Shubha Srinivasan, José MCL Silva, Janne Molnes, et al. Activating mutations in the gene encoding the atp-sensitive potassium-channel subunit kir6. 2 and permanent neonatal diabetes. New England Journal of Medicine, 350(18):1838–1849, 2004.

[9] Carol Deutsch and Li-Qiong Chen. Heterologous expression of specific K^+ channels in t lymphocytes: functional consequences for volume regulation. Proceedings of the National Academy of Sciences, 90(21):10036–10040, 1993.

[10] Christine Beeton, Heike Wulff, Nathan E Standifer, Philippe Azam, Katherine M Mullen, Michael W Pennington, Aaron Kolski-Andreaco, Eric Wei, Alexandra Grino, Debra R Counts, et al. Kv1. 3 channels are a therapeutic target for t cell-mediated autoimmune diseases. Proceedings of the National Academy of Sciences, 103(46):17414–17419, 2006.

[11] Steve AN Goldstein, Detlef Bockenhauer, Ita O'Kelly, and Noam Zilberberg. Potassium leak channels and the kcnk family of two-p-domain subunits. Nature Reviews Neuroscience, 2(3):175–184, 2001.

[12] Jim Boulter, Karen Evans, Dan Goldman, Gary Martin, Doug Treco, Steve Heinemann, and Jim Patrick. Isolation of a cdna clone coding for a possible neural nicotinic acetylcholine receptor alpha-subunit. Nature, 319(6052):368–374, 1985.

[13] Alan L Hodgkin and Andrew F Huxley. A quantitative description of membrane current and its application to conduction and excitation in nerve. The Journal of physiology, 117(4):500–544, 1952.

[14] AL Hodgkin and AF Huxley. Propagation of electrical signals along giant nerve fibres. Proceedings of the Royal Society of London. Series B, Biological Sciences, pages 177–183, 1952.

[15] Erwin Neher, Bert Sakmann, and Joe Henry Steinbach. The extracellular patch clamp: a method for resolving currents through individual open channels in biological membranes. Pflügers Archiv, 375(2):219–228, 1978.

[16] Bertil Hille et al. Ion channels of excitable membranes, volume 507. Sinauer Sunderland, MA, 2001.

[17] Declan A Doyle, Joao Morais Cabral, Richard A Pfuetzner, Anling Kuo, Jacqueline M Gulbis, Steven L Cohen, Brian T Chait, and Roderick MacKinnon. The structure of the potassium channel: molecular basis of K^+ conduction and selectivity. science, 280(5360):69–77, 1998.

[18] Youxing Jiang, Alice Lee, Jiayun Chen, Martine Cadene, Brian T Chait, and Roderick MacKinnon. The open pore conformation of potassium channels. Nature, 417(6888):523–526, 2002.

[19] Luis G Cuello, Vishwanath Jogini, D Marien Cortes, and Eduardo Perozo. Structural mechanism of c-type inactivation in K^+ channels. Nature, 466(7303):203–208, 2010.

[20] Luis G Cuello, Vishwanath Jogini, D Marien Cortes, Albert C Pan, Dominique G Gagnon, Olivier Dalmas, Julio F Cordero-Morales, Sudha Chakrapani, Benoît Roux, and Eduardo Perozo. Structural basis for the coupling between activation and inactivation gates in K^+ channels. Nature, 466(7303):272–275, 2010.

[21] Sudha Chakrapani and Eduardo Perozo. How to gate an ion channel: lessons from mthk. Nature structural & molecular biology, 14(3):180–182, 2007.

[22] Serdar Uysal, Luis G Cuello, D Marien Cortes, Shohei Koide, Anthony A Kossiakoff, and Eduardo Perozo. Mechanism of activation gating in the full-length kcsa K^+ channel. Proceedings of the National Academy of Sciences, 108(29):11896–11899, 2011.

[23] Yufeng Zhou, Joao H Morais-Cabral, Amelia Kaufman, and Roderick MacKinnon. Chemistry of ion coordination and hydration revealed by a K^+; channel–fab complex at 2.0 åresolution. Nature, 414(6859):43–48, 2001.

[24] Francis I Valiyaveetil, Matthew Sekedat, Roderick MacKinnon, and Tom W Muir. Glycine as a d-amino acid surrogate in the K^+-selectivity filter. Proceedings of the National Academy of Sciences of the United States of America, 101(49):17045–17049, 2004.

[25] Toshinori Hosm, WN Zagotta, and Richard W Aldrich. Biophysical and molecular mechanisms of shaker potassium channel inactivation. Science, 250:533–538, 1990.

[26] Clay M Armstrong and Francisco Bezanilla. Inactivation of the sodium channel. ii. gating current experiments. The Journal of General Physiology, 70(5):567–590, 1977.

[27] Toshinori Hoshi, William N Zagotta, and Richard W Aldrich. Two types of inactivation in shaker K^+ channels: effects of alterations in the carboxy-terminal region. Neuron, 7(4):547–556, 1991.

[28] J Lopez-Barneo, T Hoshi, SH Heinemann, and RW Aldrich. Effects of external cations and mutations in the pore region on c-type inactivation of shaker potassium channels. Receptors & channels, 1(1):61–71, 1992.

[29] Sudha Chakrapani, Julio F Cordero-Morales, and Eduardo Perozo. A quantitative description of kcsa gating i: macroscopic currents. The Journal of general physiology, 130(5):465–478, 2007.

[30] Julio F Cordero-Morales, Luis G Cuello, Yanxiang Zhao, Vishwanath Jogini, D Marien Cortes, Benoît Roux, and Eduardo Perozo. Molecular determinants of gating at the potassium-channel selectivity filter. Nature structural & molecular biology, 13(4):311–318, 2006.

[31] Gary Yellen, Deborah Sodickson, Tsung-Yu Chen, and Mark E Jurman. An engineered cysteine in the external mouth of a K^+ channel allows inactivation to be modulated by metal binding. Biophysical Journal, 66(4):1068, 1994.

[32] H Raghuraman, Julio F Cordero-Morales, Vishwanath Jogini, Albert C Pan, Astrid Kollewe, Benoît Roux, and Eduardo Perozo. Mechanism of cd 2+ coordination during slow inactivation in potassium channels. Structure, 20(8):1332–1342, 2012.

[33] Wayland WL Cheng, Jason G McCoy, Ameer N Thompson, Colin G Nichols, and Crina M Nimigean. Mechanism for selectivity-inactivation coupling in kcsa potassium channels. Proceedings of the National Academy of Sciences, 108(13):5272–5277, 2011.

[34] Shunsuke Imai, Masanori Osawa, Koh Takeuchi, and Ichio Shimada. Structural basis underlying the dual gate properties of kcsa. Proceedings of the National Academy of Sciences, 107(14):6216–6221, 2010.

[35] Manasi P Bhate and Ann E McDermott. Protonation state of e71 in kcsa and its role for channel collapse and inactivation. Proceedings of the National Academy of Sciences, 109(38):15265–15270, 2012.

[36] Sheng Ye, Yang Li, and Youxing Jiang. Novel insights into K^+ selectivity from high-resolution structures of an open K^+ channel pore. Nature structural & molecular biology, 17(8):1019–1023, 2010.

[37] Stephen B Long, Ernest B Campbell, and Roderick MacKinnon. Crystal structure of a mammalian voltage-dependent shaker family K^+ channel. Science, 309(5736):897–903, 2005.

[38] Stephen B Long, Xiao Tao, Ernest B Campbell, and Roderick MacKinnon. Atomic structure of a voltage-dependent K^+ channel in a lipid membrane-like environment. Nature, 450(7168):376–382, 2007.

[39] John G Starkus, Lioba Kuschel, Martin D Rayner, and Stefan H Heinemann. Ion conduction through c-type inactivated shaker channels. The Journal of general physiology, 110(5):539–550, 1997.

[40] Froylan Gomez-Lagunas. Shaker b K^+ conductance in na+ solutions lacking kK^+ ions: a remarkably stable non-conducting state produced by membrane depolarizations. The Journal of physiology, 499(1):3–15, 1997.

[41] Alexey Melishchuk, Andrey Loboda, and Clay M Armstrong. Loss of shaker k channel conductance in $0K^+$ solutions: role of the voltage sensor. Biophysical journal, 75(4):1828–1835, 1998.

[42] Andrey Loboda, Alexey Melishchuk, and Clay Armstrong. Dilated and defunct k channels in the absence of K^+. Biophysical journal, 80(6):2704–2714, 2001.

[43] Prasanna K Devaraneni, Alexander G Komarov, Corey A Costantino, Jordan J Devereaux, Kimberly Matulef, and Francis I Valiyaveetil. Semisynthetic K^+ channels show that the constricted conformation of the selectivity filter is not the c-type inactivated state. Proceedings of the National Academy of Sciences, 110(39):15698–15703, 2013.

[44] Francis I Valiyaveetil, Manuel Leonetti, Tom W Muir, and Roderick MacKinnon. Ion selectivity in a semisynthetic K^+ channel locked in the conductive conformation. science, 314(5801):1004–1007, 2006.

[45] Kurt Wuthrich. NMR of proteins and nucleic acids. Wiley, 1986.

[46] Sudha Chakrapani, Julio F Cordero-Morales, and Eduardo Perozo. A quantitative description of kcsa gating ii: single-channel currents. The Journal of general physiology, 130(5):479–496, 2007.

[47] Julio F Cordero-Morales, Vishwanath Jogini, Anthony Lewis, Valeria Vásquez, D Marien Cortes, Benoît Roux, and Eduardo Perozo. Molecular driving forces determining potassium channel slow inactivation. Nature structural & molecular biology, 14(11):1062–1069, 2007.

[48] Sudha Chakrapani, Julio F Cordero-Morales, Vishwanath Jogini, Albert C Pan, D Marien Cortes, Benoît Roux, and Eduardo Perozo. On the structural basis of modal gating behavior in K^+ channels. Nature structural & molecular biology, 18(1):67–74, 2011.

[49] Julio F Cordero-Morales, Vishwanath Jogini, Sudha Chakrapani, and Eduardo Perozo. A multipoint hydrogen-bond network underlying kcsa c-type inactivation. Biophysical Journal, 100(10):2387–2393, 2011.

[50] Daniel I Levy and Carol Deutsch. Recovery from c-type inactivation is modulated by extracellular potassium. Biophysical Journal, 70(2):798, 1996.

[51] Benoit Roux and Martin Karplus. Ion transport in a gramicidin-like channel: dynamics and mobility. The Journal of Physical Chemistry, 95(12):4856–4868, 1991.

[52] Manasi P Bhate, Benjamin J Wylie, Lin Tian, and Ann E McDermott. Conformational dynamics in the selectivity filter of kcsa in response to potassium ion concentration. Journal of molecular biology, 401(2):155–166, 2010.

[53] Roman Meyer and Stefan H Heinemann. Temperature and pressure dependence of shaker K^+ channel n-and c-type inactivation. European biophysics journal, 26(6):433–445, 1997.

[54] VA Parsegian, RP Rand, NL Fuller, and DC Rau. [29] osmotic stress for the direct measurement of intermolecular forces. Methods in enzymology, 127:400–416, 1986.

[55] KD Rector, Jianwen Jiang, Mark A Berg, and MD Fayer. Effects of solvent viscosity on protein dynamics: infrared vibrational echo experiments and theory. The Journal of Physical Chemistry B, 105(5):1081–1092, 2001.

[56] Albert C Pan, Luis G Cuello, Eduardo Perozo, and Benoît Roux. Thermodynamic coupling between activation and inactivation gating in potassium channels revealed by free energy molecular dynamics simulations. The Journal of general physiology, 138(6):571–580, 2011.

[57] Alexander D MacKerell, Donald Bashford, MLDR Bellott, RL Dunbrack, Jeffrey D Evanseck, Martin J Field, Stefan Fischer, Jiali Gao, H Guo, Sookhee Ha, et al. All-atom empirical potential for molecular modeling and dynamics studies of proteins. The Journal of Physical Chemistry B, 102(18):3586–3616, 1998.

[58] David E Shaw, Ron O Dror, John K Salmon, JP Grossman, Kenneth M Mackenzie, Joseph A Bank, Cliff Young, Martin M Deneroff, Brannon Batson, Kevin J Bowers, et al. Millisecond-scale molecular dynamics simulations on anton. In High Performance

Computing Networking, Storage and Analysis, Proceedings of the Conference on, pages 1–11. IEEE, 2009.

[59] James C Phillips, Rosemary Braun, Wei Wang, James Gumbart, Emad Tajkhorshid, Elizabeth Villa, Christophe Chipot, Robert D Skeel, Laxmikant Kale, and Klaus Schulten. Scalable molecular dynamics with namd. Journal of computational chemistry, 26(16):1781–1802, 2005.

[60] Wei Jiang, Yun Luo, Luca Maragliano, and Benoît Roux. Calculation of free energy landscape in multi-dimensions with hamiltonian-exchange umbrella sampling on petascale supercomputer. Journal of Chemical Theory and Computation, 8(11):4672–4680, 2012.

[61] Shankar Kumar, John M Rosenberg, Djamal Bouzida, Robert H Swendsen, and Peter A Kollman. The weighted histogram analysis method for free-energy calculations on biomolecules. i. the method. Journal of computational chemistry, 13(8):1011–1021, 1992.

[62] Benoît Roux. The calculation of the potential of mean force using computer simulations. Computer Physics Communications, 91(1):275–282, 1995.

[63] AH Delcour, B Martinac, J Adler, and C Kung. Modified reconstitution method used in patch-clamp studies of escherichia coli ion channels. Biophysical Journal, 56(3):631, 1989.

[64] D Marien Cortes, Luis G Cuello, and Eduardo Perozo. Molecular architecture of full-length kcsa role of cytoplasmic domains in ion permeation and activation gating. The Journal of general physiology, 117(2):165–180, 2001.

[65] Gary Yellen. The voltage-gated potassium channels and their relatives. Nature, 419(6902):35–42, 2002.

[66] Hirofumi Shimizu, Masayuki Iwamoto, Takashi Konno, Amiko Nihei, Yuji C Sasaki, and Shigetoshi Oiki. Global twisting motion of single molecular kcsa potassium channel upon gating. Cell, 132(1):67–78, 2008.

[67] Christian Ader, Robert Schneider, Sönke Hornig, Phanindra Velisetty, Vitya Vardanyan, Karin Giller, Iris Ohmert, Stefan Becker, Olaf Pongs, and Marc Baldus. Coupling of activation and inactivation gate in a K^+-channel: potassium and ligand sensitivity. The EMBO journal, 28(18):2825–2834, 2009.

[68] Christian Ader, Robert Schneider, Sönke Hornig, Phanindra Velisetty, Erica M Wilson, Adam Lange, Karin Giller, Iris Ohmert, Marie-France Martin-Eauclaire, Dirk Trauner, et al. A structural link between inactivation and block of a K^+ channel. Nature structural & molecular biology, 15(6):605–612, 2008.

[69] Julio F Cordero-Morales, Luis G Cuello, and Eduardo Perozo. Voltage-dependent gating at the kcsa selectivity filter. Nature structural & molecular biology, 13(4):319–322, 2006.

[70] Elwin AW van der Cruijsen, Deepak Nand, Markus Weingarth, Alexander Prokofyev, Sönke Hornig, Abhishek Arun Cukkemane, Alexandre MJJ Bonvin, Stefan Becker, Raymond E Hulse, Eduardo Perozo, et al. Importance of lipid–pore loop interface for potassium channel structure and function. Proceedings of the National Academy of Sciences, 110(32):13008–13013, 2013.

[71] Carmen Domene, Michael L Klein, Davide Branduardi, Francesco L Gervasio, and Michele Parrinello. Conformational changes and gating at the selectivity filter of potassium channels. Journal of the American Chemical Society, 130(29):9474–9480, 2008.

[72] Jared Ostmeyer, Sudha Chakrapani, Albert C Pan, Eduardo Perozo, and Benoît Roux. Recovery from slow inactivation in K^+ channels is controlled by water molecules. Nature, 501(7465):121–124, 2013.

[73] Adam Lange, Karsten Seidel, Laurent Verdier, Sorin Luca, and Marc Baldus. Analysis of proton-proton transfer dynamics in rotating solids and their use for 3d structure determination. Journal of the American Chemical Society, 125(41):12640–12648, 2003.

[74] Robert Schneider, Christian Ader, Adam Lange, Karin Giller, Sönke Hornig, Olaf Pongs, Stefan Becker, and Marc Baldus. Solid-state nmr spectroscopy applied to a chimeric potassium channel in lipid bilayers. Journal of the American Chemical Society, 130(23):7427–7435, 2008.

[75] Markus Weingarth, Dan E Demco, Geoffrey Bodenhausen, and Piotr Tekely. Improved magnetization transfer in solid-state nmr with fast magic angle spinning. Chemical Physics Letters, 469(4):342–348, 2009.

[76] Markus Weingarth, Geoffrey Bodenhausen, and Piotr Tekely. Broadband carbon-13 correlation spectra of microcrystalline proteins in very high magnetic fields. Journal of the American Chemical Society, 131(39):13937–13939, 2009.

[77] Benoıt Roux and Roderick MacKinnon. The cavity and pore helices in the kcsa K^+ channel: electrostatic stabilization of monovalent cations. Science, 285(5424):100–102, 1999.

[78] Yufeng Zhou and Roderick MacKinnon. Ion binding affinity in the cavity of the kcsa potassium channel. Biochemistry, 43(17):4978–4982, 2004.

[79] Sudhakar Parthasarathy, Yusuke Nishiyama, and Yoshitaka Ishii. Sensitivity and resolution enhanced solid-state nmr for paramagnetic systems and biomolecules under very fast magic angle spinning. Accounts of chemical research, 46(9):2127–2135, 2013.

[80] Donghua H Zhou and Chad M Rienstra. Rapid analysis of organic compounds by proton-detected heteronuclear correlation nmr spectroscopy with 40 khz magic-angle spinning. Angewandte Chemie International Edition, 47(38):7328–7331, 2008.

[81] AE McDermott, FJ Creuzet, AC Kolbert, and RG Griffin. High-resolution magic-angle-spinning nmr spectra of protons in deuterated solids. Journal of Magnetic Resonance (1969), 98(2):408–413, 1992.

[82] Veniamin Chevelkov, Kristina Rehbein, Anne Diehl, and Bernd Reif. Ultrahigh resolution in proton solid-state nmr spectroscopy at high levels of deuteration. Angewandte Chemie International Edition, 45(23):3878–3881, 2006.

[83] Lichi Shi, Izuru Kawamura, Kwang-Hwan Jung, Leonid S Brown, and Vladimir Ladizhansky. Conformation of a seven-helical transmembrane photosensor in the lipid environment. Angewandte Chemie International Edition, 50(6):1302–1305, 2011.

[84] Donghua H Zhou, Andrew J Nieuwkoop, Deborah A Berthold, Gemma Comellas, Lindsay J Sperling, Ming Tang, Gautam J Shah, Elliott J Brea, Luisel R Lemkau, and Chad M Rienstra. Solid-state nmr analysis of membrane proteins and protein aggregates by proton detected spectroscopy. Journal of biomolecular NMR, 54(3):291–305, 2012.

[85] Alessandro Marchetti, Stefan Jehle, Michele Felletti, Michael J Knight, Yao Wang, Zhi-Qiang Xu, Ah Young Park, Gottfried Otting, Anne Lesage, Lyndon Emsley, et al. Backbone assignment of fully protonated solid proteins by 1h detection and ultrafast magic-angle-spinning nmr spectroscopy. Angewandte Chemie, 124(43):10914–10917, 2012.

[86] Christiane Ritter, Marie-Lise Maddelein, Ansgar B Siemer, Thorsten Lührs, Matthias Ernst, Beat H Meier, Sven J Saupe, and Roland Riek. Correlation of structural elements and infectivity of the het-s prion. Nature, 435(7043):844–848, 2005.

[87] Hélène Van Melckebeke, Paul Schanda, Julia Gath, Christian Wasmer, René Verel, Adam Lange, Beat H Meier, and Anja Böckmann. Probing water accessibility in het-s (218–289) amyloid fibrils by solid-state nmr. Journal of molecular biology, 405(3):765–772, 2011.

[88] Gabriela K Popescu. Modes of glutamate receptor gating. The Journal of physiology, 590(1):73–91, 2012.

[89] Markus Weingarth, Alexander Prokofyev, Elwin AW van der Cruijsen, Deepak Nand, Alexandre MJJ Bonvin, Olaf Pongs, and Marc Baldus. Structural determinants of specific lipid binding to potassium channels. Journal of the American Chemical Society, 135(10):3983–3988, 2013.

[90] Marie Renault, Ria Tommassen-van Boxtel, Martine P Bos, Jan Andries Post, Jan Tommassen, and Marc Baldus. Cellular solid-state nuclear magnetic resonance spectroscopy. Proceedings of the National Academy of Sciences, 109(13):4863–4868, 2012.

[91] Li-Wei Hung, Iris Xiaoyan Wang, Kishiko Nikaido, Pei-Qi Liu, Giovanna Ferro-Luzzi Ames, and Sung-Hou Kim. Crystal structure of the atp-binding subunit of an abc transporter. Nature, 396(6712):703–707, 1998.

[92] Thomas E Angel, Mark R Chance, and Krzysztof Palczewski. Conserved waters mediate structural and functional activation of family a (rhodopsin-like) g protein-coupled receptors. Proceedings of the National Academy of Sciences, 106(21):8555–8560, 2009.

[93] Bryan Schmidt, John McCracken, and Shelagh Ferguson-Miller. A discrete water exit pathway in the membrane protein cytochrome c oxidase. Proceedings of the National Academy of Sciences, 100(26):15539–15542, 2003.

[94] Vladimir P Denisov, Jörg Peters, Hans Dietrich Hörlein, and Bertil Halle. Using buried water molecules to explore the energy landscape of proteins. Nature structural biology, 3(6):505–509, 1996.

[95] Filip Persson and Bertil Halle. Transient access to the protein interior: simulation versus nmr. Journal of the American Chemical Society, 135(23):8735–8748, 2013.

[96] Christian Ader, Olaf Pongs, Stefan Becker, and Marc Baldus. Protein dynamics detected in a membrane-embedded potassium channel using two-dimensional solid-state nmr spectroscopy. Biochimica et Biophysica Acta (BBA)-Biomembranes, 1798(2):286–290, 2010.

[97] Wenbin Luo and Mei Hong. Conformational changes of an ion channel detected through water- protein interactions using solid-state nmr spectroscopy. Journal of the American Chemical Society, 132(7):2378–2384, 2010.

[98] Kristin K Kumashiro, Klaus Schmidt-Rohr, Owen J Murphy, Kerry L Ouellette, William A Cramer, and Lynmarie K Thompson. A novel tool for probing membrane protein structure: solid-state nmr with proton spin diffusion and x-nucleus detection. Journal of the American Chemical Society, 120(20):5043–5051, 1998.

[99] Markus Weingarth, Piotr Tekely, and Geoffrey Bodenhausen. Efficient heteronuclear decoupling by quenching rotary resonance in solid-state nmr. Chemical Physics Letters, 466(4):247–251, 2008.

[100] Markus Weingarth, Geoffrey Bodenhausen, and Piotr Tekely. Low-power decoupling at high spinning frequencies in high static fields. Journal of Magnetic Resonance, 199(2):238–241, 2009.

[101] Donghua H Zhou and Chad M Rienstra. High-performance solvent suppression for proton detected solid-state nmr. Journal of Magnetic Resonance, 192(1):167–172, 2008.

[102] Adam Lange, Karin Giller, Sönke Hornig, Marie-France Martin-Eauclaire, Olaf Pongs, Stefan Becker, and Marc Baldus. Toxin-induced conformational changes in a potassium channel revealed by solid-state nmr. Nature, 440(7086):959–962, 2006.

[103] Robin T Shealy, Anuradha D Murphy, Rampriya Ramarathnam, Eric Jakobsson, and Shankar Subramaniam. Sequence-function analysis of the K^+-selective family of ion channels using a comprehensive alignment and the kcsa channel structure. Biophysical journal, 84(5):2929–2942, 2003.

[104] Luis G Cuello, Jesus G Romero, D Marien Cortes, and Eduardo Perozo. ph-dependent gating in the streptomyces lividans K^+ channel. Biochemistry, 37(10):3229–3236, 1998.

[105] Lise Heginbotham, Meredith LeMasurier, Ludmilla Kolmakova-Partensky, and Christopher Miller. Single streptomyces lividans K^+ channels functional asymmetries and sidedness of proton activation. The Journal of general physiology, 114(4):551–560, 1999.

[106] Laszlo Kiss and Stephen J Korn. Modulation of c-type inactivation by K^+ at the potassium channel selectivity filter. Biophysical Journal, 74(4):1840–1849, 1998.

[107] Morais JH Cabral, A Kaufman, R Mackinnon, et al. Chemistry of ion coordination and hydration revealed by a K^+ channel-fab complex at 2.0åresolution. Nature, 414:43–48, 2001.

[108] Toshinori Hoshi and Clay M Armstrong. C-type inactivation of voltage-gated K^+ channels: Pore constriction or dilation? The Journal of general physiology, 141(2):151–160, 2013.

[109] Carmen Domene and Simone Furini. Dynamics, energetics, and selectivity of the low-K^+ kcsa channel structure. Journal of molecular biology, 389(3):637–645, 2009.

[110] Céline Boiteux and Simon Bernèche. Absence of ion-binding affinity in the putatively inactivated low-[K^+] structure of the kcsa potassium channel. Structure, 19(1):70–79, 2011.

[111] Markus Weingarth, Elwin AW Van Der Cruijsen, Jared Ostmeyer, Sylke Lievestro, Benoît Roux, and Marc Baldus. Quantitative analysis of the water occupancy around the selectivity filter of a K^+ channel in different gating modes. Journal of the American Chemical Society, 136(5):2000–2007, 2014.

[112] Luis G Cuello, D Marien Cortes, Vishwanath Jogini, Amornrat Sompornpisut, and Eduardo Perozo. A molecular mechanism for proton-dependent gating in kcsa. FEBS letters, 584(6):1126–1132, 2010.

[113] Phedra Marius, Michele Zagnoni, Mairi E Sandison, J Malcolm East, Hywel Morgan, and Anthony G Lee. Binding of anionic lipids to at least three nonannular sites on the potassium channel kcsa is required for channel opening. Biophysical journal, 94(5):1689–1698, 2008.

[114] Helen M Berman, John Westbrook, Zukang Feng, Gary Gilliland, TN Bhat, Helge Weissig, Ilya N Shindyalov, and Philip E Bourne. The protein data bank. Nucleic acids research, 28(1):235–242, 2000.

[115] Wojciech Wojtas-Niziurski, Yilin Meng, Benoıt Roux, and Simon Berneche. Self-learning adaptive umbrella sampling method for the determination of free energy landscapes in multiple dimensions. Journal of chemical theory and computation, 9(4):1885–1895, 2013.

[116] Simon Berneche and Benoit Roux. Energetics of ion conduction through the k+ channel. Nature, 414(6859):73–77, 2001.

[117] Youxing Jiang, Alice Lee, Jiayun Chen, Vanessa Ruta, Martine Cadene, Brian T Chait, and Roderick MacKinnon. X-ray structure of a voltage-dependent K^+ channel. Nature, 423(6935):33–41, 2003.

[118] Seok-Yong Lee, Alice Lee, Jiayun Chen, and Roderick MacKinnon. Structure of the kvap voltage-dependent K^+ channel and its dependence on the lipid membrane. Proceedings of the National Academy of Sciences, 102(43):15441–15446, 2005.